1

New Insights From The Jülich Ozone-Sonde Intercomparison Experiments: Calibration Functions Traceable To One Ozone Reference Instrument

Herman G.J. Smit[1], Deniz Poyraz[2], Roeland Van Malderen[2], Anne M. Thompson[3,4], David W. Tarasick[5], Ryan M. Stauffer[3], Bryan J. Johnson[6], Debra E. Kollonige[3,7]

[1]Forschungszentrum Jülich, Institute of Energy and Climate Research, IEK-8: Troposphere, Jülich, 52425, Germany

[2]Royal Meteorological Institute of Belgium & Solar-Terrestrial Centre of Excellence, Uccle, Belgium

[3]Atmospheric Chemistry and Dynamics Laboratory, NASA/GSFC, Greenbelt, MD, USA

[4]University of Maryland Baltimore County, Baltimore, MD, USA,

[5]Environment and Climate Change Canada, Downsview, ON, Canada

[6]Global Monitoring Laboratory, NOAA Earth System Research Laboratory, Boulder, CO, USA

[7]Science Systems and Applications, Inc, Lanham, MD, USA

Correspondence to: Herman G.J. Smit (h.smit@fz-juelich.de)

Abstract

Although in principle the ECC (Electrochemical Concentration Cell) ozonesonde is an absolute measuring device, in practice it has several "artefacts" which change over the course of a flight. Most of the artefacts have been corrected in the recommendations of the Assessment of Standard Operating Procedures for Ozone Sondes Report (GAW Report No. 268), giving an overall uncertainty of 5-10% throughout the profile. However, the conversion of the measured cell current into the sampled ozone concentration still needs to be quantified better, using time-varying background current and more appropriate pump efficiencies. We describe an updated methodology for ECC sonde data processing that is based on JOSIE 2009/2010 and JOSIE 2017-SHADOZ test chamber data. The methodology resolves the slow and fast time responses of the ECC ozonesonde and in addition apply calibration functions to make the sonde data traceable to the JOSIE ozone reference UV-photometer (OPM). The stoichiometry (O_3/I_2) factors and their uncertainties along with fast and slow reaction pathways for the different sensing solution types used in the global ozonesonde network are determined. Experimental evidence is given for treating the background current of the ECC-sensor as the superposition of a constant ozone independent component (I_{B0}, measured before ozone exposure in the sonde preparation protocol) and a slow time-variant ozone-dependent current determined from the initial measured ozone current using a first-order numerical convolution. The fast sensor current is refined using the time response determined in sonde preparation with a first order deconvolution scheme. Practical procedures for initializing the numerical deconvolution and convolution schemes to determine the slow and fast ECC currents are given. Calibration functions for specific ozonesondes and sensing solution type combinations were determined by comparing JOSIE 2009/2010 and JOSIE-2017-SHADOZ profiles with the JOSIE-OPM. With fast and slow currents resolved and the new calibration functions, a full uncertainty budget is obtained. The time responses correction methodology makes every ozonesonde record traceable to one standard, i.e. the OPM of JOSIE, enabling the goal of a 5% relative uncertainty to be met throughout the global ozone network.

1 Introduction

Although it is a minor trace gas constituent of the Earth's atmosphere, ozone plays several essential roles in its chemistry and physics. In the stratosphere, where about 90% of the total ozone amount resides, ozone protects life on Earth by absorbing the harmful ultraviolet (UV) radiation from the sun, adding heat to the stratosphere. In the upper troposphere, ozone is an important absorber of infrared radiation, acting as a powerful greenhouse gas (IPCC-Climate Change, 2013, 2023). Ozone is the primary source of the hydroxyl (OH) radical in the troposphere, controlling the lifetime of hundreds of pollutants (Seinfeld and Pandis, 2016), and determining its oxidizing capacity (Thompson, 1992). The stratosphere is a natural source of tropospheric ozone but approximately half of the ozone in the troposphere is formed photochemically when combustion (vehicular, industrial or pyrogenic) processes release NO_x, ($NO + NO_2 = NO_x$), carbon monoxide (CO) and hydrocarbons (also referred to as volatile organic compounds (VOC)) that react through free radical cycles in the presence of UV. VOC may also originate from combustion or natural sources, the latter predominantly from vegetation and to a lesser extent from the ocean. Surface ozone is considered a pollutant with adverse impacts on human and animal health (e.g., respiratory problems) and on vegetation (Mills et al., 2018) and is a primary marker for "Air Quality," setting the scale for Good, Fair, and Unhealthy definitions used by local Air Quality agencies (Garner and Thompson, 2013). The photochemistry of ozone pollution or "smog" was first identified by Haagen-Smit (1952) in the early 1950s and was found to typically occurs at very high concentrations of VOC and NO_X, whereby organic particles also playing an important role (e.g. Seinfeld and Pandis, 2016); surface ozone measurements became widespread as regions or nations enacted regulations to mitigate episodes of high ozone.

Measurements of stratospheric ozone gained attention in the 1960s and 1970s when it was recognized that natural levels of ozone were regulated by catalytic cycles involving nitrogen oxides (NO_x, N_2O_5, NO_3 and HNO_3), hydrogen oxides (with H_2O vapor a source of OH and HO_2, $HO_x = OH+HO_2$) and halogens (XO and XO_2, where X was Cl or Br derived from oceanic methyl chloride and methyl bromide). Anthropogenic perturbations of these cycles were investigated when it was recognized that emissions of N- and Cl-containing compounds by rockets and high-altitude aircraft could threaten stratospheric ozone (Crutzen, 1970; Stolarski and Cicerone, 1974). A worse threat was hypothesized when it was realized that chlorofluorocarbons (CFCs) present in the atmosphere (Lovelock et al., 1973), but relatively inert in the troposphere could enter the stratosphere and destroy ozone photochemically there (Molina and Rowland, 1974). Perturbed stratospheric ozone chemistry by CFCs was a cause for alarm, leading to first regulations in CFC usage in the 1970s. However, it was not until ground-based total ozone monitoring (Farman et al., 1985) discovered catastrophic springtime ozone loss over Antarctica in 1984-1985 that international action was taken to phase out Ozone Depleting Substances through the 1987 signing of the Montreal Protocol (UNEP-Ozone Secretariat,14th edition, 2020). Implementation of the Montreal Protocol and its follow-on Amendments require governments to monitor ozone, reporting every four years to the World Meteorological Organization (WMO) and United Nations Environment Programme (UNEP) in Scientific Assessments on total column ozone, its vertical distribution and attribution of long-term. Since 1991 there have been nine UNEP/WMO Scientific Assessments, with the most recent report released in 2022 (WMO/UNEP, 2023).

Global monitoring of total ozone has relied on satellite instruments since the 1970s but ground-based instrumentation deployed on all continents still provides ground-truth. In particular, ozonesondes are essential for satellite algorithms and validation of satellite-derived profiles and reanalysis products (Wang et al., 2020; Thompson et al., 2022). Balloon-borne ozonesondes, flown together with radiosondes, make relatively inexpensive, accurate, all-weather measurements of the ozone concentrations from the ground to 30 km or higher, with ~100 m vertical resolution (Smit, 2014). The electrochemical concentration cell (ECC) ozonesonde has been deployed for more than 50 years with approximately 60 stations currently launching on all continents (global ozonesonde network shown in figure 1-2 in GAW Report No.268, 2021; Thompson et al., 2022; Stauffer et al., 2022). Ozonesonde data constitute the most important record for deriving ozone trends throughout both

83   the stratosphere and troposphere, particularly in the climate-sensitive altitude region near the tropopause where satellite

84   measurements are most uncertain. Strategic ozonesonde networks like MATCH and IONS (Intensive Ozonesonde Network

85   Studies) have been organized to support aircraft campaigns in characterizing photochemical and dynamical interactions

86   affecting vertical and regional ozone distributions (Thompson et al., 2007a and 2011; Tarasick et al., 2010).

1.1 Establishing Quality Assurance/Quality Control (QA/QC) practices for ozonesondes (1996-2021)

88   Despite the advantages of ozonesonde profiles, there is a challenge in that each ozonesonde instrument is unique, typically

89   launched only once, and it must be carefully prepared prior to launch in order to obtain accurate data. Processing of the final

90   measurement is carried out using certain parameters determined pre-launch. In addition, there are two manufacturers of

91   ozonesondes that show systematic offsets relative to each other. Further biases in ozonesonde datasets can occur because

92   three variants of the sensing solution that produce the ECC current signal from the ozone are currently in use. The

93   ozonesonde community has created guidelines for operations and data processing applicable to the range of instrument and

94   sensing solution types used in the global ECC-sonde network. When the guidelines are followed it is possible for

95   consistently high-quality data to be collected across the global network.

96   The creation of guidelines or "best practices" has evolved over the past 20 years in a process referred to as the Assessment of

97   Standard Operating Procedures (SOP) for Ozonesondes (ASOPOS) and organized through the WMO Global Atmosphere

98   Watch (GAW). The key element of ASOPOS was the establishment of the World Calibration Centre for Ozone Sondes

99   (WCCOS) with a custom-designed Environmental Simulation Facility (ESF) at the Research Centre in Jülich, Germany, in

100   1995 (GAW Report No.104, 1994; Smit et al., 2000). The ESF consists of an absolute ozone measuring reference, a fast

101   response (2s), accurate (2-3%), dual beam UV-absorption ozone photometer (OPM) (Proffitt and McLaughlin, 1983)

102   attached to the chamber that enables control of pressure, temperature and ozone concentration simulating flight conditions of

103   an ozone sounding up to 35 km over ~ 2 hours (Smit et al., 2007). Up to four ozonesonde instruments at once can be

104   intercompared through this process. Simulations in the ESF included conditions of polar, midlatitude, subtropical and

105   tropical sonde launches. Other aspects of sonde operations, e.g., response times to rapid changes in ozone concentration, are

106   also tested in the ESF. Since 1996, nine Jülich OzoneSonde Intercomparison Experiment (JOSIE) campaigns have been

107   conducted at WCCOS and documented in a series of publications (Smit and Kley, GAW Report No. 130, 1998) for JOSIE-

108   1996; JOSIE-1998 (Smit and Sträter, GAW Report No. 157, 2004a), JOSIE-2000 (Smit and Sträter, GAW Report No. 158,

109   2004b; Smit et al., 2007; Thompson et al., 2007b); JOSIE-2009/2010; JOSIE-2017 (Thompson et al., 2019). The first three

110   JOSIEs, which tested several non-ECC instruments as well as Science Pump Corporation (SPC) and ENSCI ECC

111   instruments, showed the ECC-sonde to be more accurate. After JOSIE-2000 only ECC-sondes were tested in the WCCOS.

112   In 2004 a the WMO/BESOS (Balloon Experiment on Standards for OzoneSondes) field campaign, carried out in Laramie

113   (Wyoming, USA) deployed a large gondola with 18 ozonesondes and the OPM of WCCOS (Deshler et al., 2008) with results

114   similar to JOSIE-2000. These early experiments demonstrated that high precision and accuracy depend not only on sonde

115   manufacturer and sensing solution strength, but also on pre-launch preparation details. Smit et al. (2007) concluded that

116   standardisation of operating procedures for ECC sondes yields a precision better than $\pm$ (3-5) % and an accuracy of about

117   $\pm(5\text{-}10)\%$ up to 30 km altitude.

118   In 2004 an expert team of ozonesonde operators, data providers and manufacturers formally instituted the ASOPOS to

119   analyse the results of BESOS and the JOSIE campaigns up to that time. The ASOPOS goal was to ensure consistency of data

120   quality across stations and within individual station time series by specifying how to prepare and operate the ozonesonde

121   instrument and to accurately process and report profile data. The first set of SOP recommended by ASOPOS, based on the

122   JOSIE campaigns from 1996 to 2000 and BESOS, was published online in 2012 and as GAW Report No. 201 in 2014 (Smit

123   and ASOPOS 1.0 Panel). To make (historical) ozonesonde time series records compliant with the ASOPOS standards, an

OzoneSonde Data Quality Assessment (O3S-DQA) activity was initiated in 2011 within the framework of SI2N[1], resulting in procedures for "homogenizing" data and estimating uncertainties (Smit and O3S-DQA Panel, 2012; https://www.wccos-josie.org/o3s-dqa); transfer functions in support of the guidelines were documented in Deshler et al. (2017). Within several years roughly half of the global network stations had reprocessed their data (Tarasick et al., 2016; Van Malderen et al., 2016; Thompson et al., 2017; Sterling et al., 2018; Witte et al., 2017, 2018, 2019; Ancellet et al., 2022). Comparisons between original and homogenized data allowed elimination of significant systematic errors, particularly where changes in technique and/or equipment had been made.

The homogenised time series were based on having raw currents from the ozonesonde cells, a prerequisite for the analysis and processing methods of the present paper. However, the ozonesonde community agreed that several issues were unresolved. These included the complexity of the so-called "background current" characterized during the preparation and the lack of traceability of the archived ozone profile to an absolute standard. A JOSIE-2017 campaign was designed to address these concerns. In addition to the tests of prior JOSIEs, the 2017 tests focused on a single regime, tropical profiles, to gather a larger set of statistics. A special challenge of tropical soundings is that near the tropopause the ozone concentrations can be very low such that the signal to noise is very small (Thompson et al., 2007b), causing large relative uncertainties in the ozonesonde readings (Smit et al. 2007). JOSIE-2017 (also called JOSIE-SHADOZ) was carried out with eight SHADOZ operators who supplied their home-prepared sensing solutions, following their own preparation procedures for half the simulations (Thompson et al., 2019). The other half of the simulations tested a lower-buffer variant of the sensing solution with the WMO/GAW SOP. The overall results of JOSIE-2017 resembled those of the 1996-2000 JOSIE and BESOS. In other words, the offsets of the various instrument-sensing solution types (SST) from the OPM reference and associated biases of ECC sonde instruments and SST had not changed over more than 20 years.

An ASOPOS 2.0 Panel formed in 2018 to review the JOSIE-2017 campaign data along with lessons learned from reprocessed datasets and the JOSIE 2009/2010 results. ASOPOS 2.0 published GAW Report No. 268, "Ozonesonde Measurement Principles and Best Operational Practices" (Smit, Thompson and ASOPOS, 2021; hereafter referred to as GAW Report No. 268) as an update to GAW Report No. 201. The newer report gives the same recommendations as GAW Report No. 201 on sonde manufacturer-SST combinations, but stricter and more unified SOP. The latter consist of more detailed recommendations based on physical principles of the ozonesonde measurement. More explicit procedures are given for data quality indicators, hardware usage and maintenance and metadata. GAW Report No. 268 also specified for the first time how to report ozone profiles traceable to the standard OPM. However, the issues of a time-varying background current, specification of uncertainties in the ozone measurement (and related pump efficiencies) required analysis beyond GAW Report No. 268 before consensus could be reached on data-processing recommendations. That is the scope of this paper.

1.2 Addressing residual ozonesonde QA/QC issues from WMO/GAW 268. Outline of paper

Chapter 3 of GAW Report No. 268 draws on the Tarasick et al. (2021) review of ozonesonde performance characteristics. Both documents point out that the greatest barriers to reducing uncertainties in the final ozone measurement derive from (1) the use of improper pump efficiencies and (2) a background current that varies with ozone exposure (hence with time) over the course of the balloon ascent. The current paper revisits fundamentals of the ozonesonde measurement to overcome these two shortcomings. The here reported methodology to resolve the fast and slow time responses builds on an earlier study by Imai et al. (2013), and more recently on the work by Tarasick et al. (2021) and Vömel et al. (2020). We first give a more detailed description of the physical and chemical origin of the ECC ozonesonde signal (Section 2), illustrated with laboratory

---

[1] This is a joint initiative under the auspices of SPARC (Stratosphere–troposphere Processes And their Role in Climate), the International Ozone Commission (IO3C), the ozone focus area of the Integrated Global Atmospheric Chemistry Observations (IGACO-O3) programme, and the Network for Detection of Atmospheric Composition Change (NDACC). For simplicity, an acronym of acronyms, SI2N, was adopted.

measurements from the Uccle, Belgium, ozonesonde station. Section 3 first corrects for the background signal composed of (i) a constant physical component (I_{B0}) and (ii) a small and slow varying (time constant 25 min) chemical component that varies with ozone exposure. The remaining fast component of the signal is then corrected by deconvolution with an exponential decay with a time constant between 20 and 30s. Although the approach is similar to Vömel et al. (2020), an advantage of our updated method is that it is developed from and applied to dedicated JOSIE chamber data (JOSIE 2009/2010) that used consistently prepared ozonesondes, with detailed in-flight and post-flight measurements and metadata. Second, the simultaneous OPM measurements in the simulation chamber serve as reference data for determining key parameters of the method, e.g. the contribution of the slow component to the overall signal. In Section 4, the OPM reference data are used to evaluate the updated method with comparisons to the conventional method. For these analyses, measurements from all JOSIE campaigns, covering a range of simulated environments are used. Comparing residuals of the corrected ozonesonde profiles to the OPM profiles allows us to determine a set of the calibration functions for each instrument-SST combination (Section 5) and to estimate uncertainties of the updated time response correction (TRC) method (Section 6). The TRC method is implemented with actual sounding data in Section 7 for ascent and descent profiles at tropical, mid-latitude and polar (Antarctic) stations and improvements with respect to the conventional approach are quantified. A summary and outlook appear in Section 8.

2 Physical and Chemical Origins of the ECC Ozonesonde Signal

2.1 Principle of Operation

The ECC (=Electrochemical Concentration Cell) ozonesonde, developed by Komhyr (1969), uses an electrochemical method to measure ozone which is based on the titration of ozone in a neutral buffered potassium iodide (NBKI) sensing solution according to the redox reaction (R1):

$$2\,KI \;+\; O_3 \;+\; H_2O \quad \rightarrow \quad I_2 \qquad + \quad O_2 \;+\; 2\,KOH \tag{R1}$$

A neutral pH$\approx$7 is obtained through the addition of a phosphate buffer ($NaH_2PO_4.H_2O$ and $Na_2HPO_4.12H_2O$) The titration involves a coulometric method employing electrochemical cells to determine the amount of generated "free" iodine (I_2) per unit time through conversion into an electrical current at a depolarizing cathode electrode. The actual ECC component of the ozone sensor, made of Teflon or molded plastic, consists of two chambers. Each chamber contains a platinum (Pt) mesh electrode that serves as cathode or anode. The chambers are immersed in a KI-solution of different concentrations and linked together to provide an ion pathway and to prevent mixing of the cathode and anode concentrations.

Continuous operation is achieved by a small nonreactive gas sampling pump (Komhyr 1967) forcing ozone in ambient air through the cathode cell that contains a lower-concentration KI-sensing solution, causing an increase of "free iodine" (I_2) according to the redox reaction (1). Transported by the stirring action of the air bubbles, the free I_2 contacts the Pt-cathode and is converted to 2 I^- through the uptake of two electrons. At the Pt-anode surface, I^- is converted to I_2 through the release of two electrons. The overall cell reaction is:

$$3\,I^- \qquad + \quad I_2 \quad \rightarrow \quad I_3^- \;+\; 2\,I^- \tag{R2}$$

The electrical current I_M (μA) generated in the external circuit of the electrochemical cell is directly related to the uptake rate of ozone in the sensing solution. By knowing the gas volume flow rate Φ_{P0} [cm^{3}s^{-1}] of the air sampling pump and its

temperature T_P (K), the electrical cell current I_M (µA), after subtracting a background current I_B (µA), is converted to the ozone partial pressure P_{O3} (in mPa) (Komhyr 1969):

$$P_{O3} = 0.043085 * \frac{T_P}{(\eta_P * \eta_A * \eta_C * \Phi_{P0})} * (I_M - I_B) \tag{1}$$

The constant 0.043085 is determined by the ratio of the universal gas constant, R, to twice the Faraday constant, F, (because two electrons flow in the electrical circuit from reaction (R2) (Komhyr 1969).

The overall efficiency of conversion consists of:

a) Pump efficiency, η_P, that declines at lower pressures. At reduced air pressures (< 100 hPa), the pump efficiency declines due to pump leakage, dead volume in the piston of the pump, and the back pressure exerted on the pump by the cathode cell (Komhyr 1967, Steinbrecht et al., 1998, Nakano and Morofuji, 2023).

b) Absorption (i.e capture) efficiency, η_A, for the transfer of the sampled gaseous ozone into the liquid phase. Although evaporation reduces the amount of the sensing solution available for ozone uptake, η_A is not significantly affected (Komhyr, 1971). This was confirmed by Davies et al. (2003), who determined experimentally at different pressures in a vacuum tank the absorption efficiency η_A from the responses of two ECC-sondes connected in series. Thus, η_A remains at 1.0, with an uncertainty of $< \pm 1\%$ (Tarasick et al., 2021; Davies et al., 2003).

c) Conversion efficiency, η_C, of the absorbed ozone in the cathode solution creating iodine that leads to the measured cell current I_M. Historically, it has been assumed that η_C is unity at neutral pH (Saltzman and Gilbert, 1959; Komhyr, 1969; Komhyr, 1986). However, there is now a great deal of evidence that this is not quite the case, as will be discussed below.

Currently, there are two manufacturers of ECC ozonesondes, Science Pump Corporation and Environmental Science Corporation, most recently producing the SPC-6A and EN-SCI-Z ozonesonde series, respectively. The designs of both ECC types are similar but differences include: (i) the material of the electrochemical cell (Teflon for SPC-6A and molded plastic for EN-SCI-Z); (ii) ion bridges (details are not known due to manufacturer proprietary issues); (iii) layout of the metal frame. Since 2014, a modified ECC-type ozonesonde manufactured at the Institute of Atmospheric Physics (IAP), Beijing, has been produced (Zhang et al., 2014a,b) but to date, few comparisons of the Chinese instrument with the well-characterized SPC-6A and EN-SCI models have been carried out. Thus, profiles from Chinese instruments are not included in the current study.

Three different aqueous sensing solution types (SST) are commonly used in the ECC-sonde cathode cells: (i) SST1.0: 1.0% KI & full buffer; (ii) SST0.5: 0.5% KI & half buffer; (iii) SST0.1: 1.0% KI & 1/10th buffer (GAW Report No. 268), respectively. In all cases a KI saturated cathode solution is employed in the anode cell. Laboratory studies by Johnson et al. (2002) found that, depending on the concentration of the cathode sensing solution, the stoichiometric ratio of the ozone to iodine conversion reaction (1) can increase from 1.00 up to 1.05-1.20. Johnson et al. (2002) determined that this increase is caused primarily by the phosphate buffer and to a lesser extent depends on the KI concentration. No significant influence of KBr-concentration was observed, although its role is not well understood. From JOSIE 2000 (Smit et al., 2007), BESOS 2004 (Deshler et al., 2008) and multiple other sounding tests (e.g. Deshler et al., 2016) it is known that there is a significant difference in the ozone readings when sondes of the same type are operated with different sensing solutions, e.g. STT0.5 and SST1.0. Both sonde types exhibit a systematic change of sensitivity, about 5-10% over the entire profile, when the sensing solution is changed from SST0.5 to SST1.0. Johnson et al. (2002) demonstrated that this offset is mostly caused by the phosphate buffer with a minor contribution from the KI- concentration. In addition, the EN-SCI sonde tends to measure about 4-5 % more ozone than the SPC-sonde when operated with the same SST for reasons that are not understood.

2.2 Impact of Pump efficiency and Conversion Efficiency (Stoichiometry)

The accuracy of the ECC ozonesonde depends on the extent of the ozone-iodide reaction in the cathode cell and the efficiency of the reduction of the iodine produced, which can be expressed primarily in the overall uncertainty based on the contribution of the individual uncertainties of each parameter expressed in Eq. (1). Tarasick et al. (2021) quantified and reviewed the uncertainty budget of the measured partial pressure of ozone, confirming that the most critical parameters are the (background) current for the tropospheric part of the ozone profile and the pump and conversion efficiencies used in the post flight data processing for the stratospheric part of the ozone profile.

Since JOSIE 1996 (Smit and Kley, 1998) it was recognized that, if the preparation and data correction procedures prescribed by Komhyr (1986) are used, an increase of the stoichiometric factor, presumably due to evaporation of the cathode sensing solution in the course of the sounding, may be compensated by a too low pump flow correction in the stratosphere above 20-25 km altitude. With new pump flow calibrations and stoichiometry investigations, Johnson et al. (2002) demonstrated that the pump efficiency tables reported by Komhyr (1986) and Komhyr et al. (1995) indeed compensate for the increase of the stoichiometric factor, i.e. the conversion efficiency. Commonly used pump efficiencies and their uncertainties recommended by ASOPOS 2.0 (GAW Report No. 268) are listed in Table 1.

Table 1: Pump efficiencies (η_P) as a function of air pressure for ECC ozonesondes reported by (i) Komhyr (1986), referred as empirical effective K86-efficiency; (ii) Komhyr et al. (1995), referred as empirical effective K95-efficiency; (iii) Johnson et al. (2002), referred as NOAA/CMDL & UWYO at Univ.Wyoming; (iv) Nakano and Morofuji, 2023, at JMA.

Pressure [hPa]	ECC (SPC-6a) *Komhyr,*1986 K86-Efficiency	ECC (ENSCI) *Komhyr et al.,* 1995 K95-Efficiency	ECC (CMDL) *Johnson et al.,* 2002	ECC (UWYO) *Johnson et al.,* 2002	ECC (JMA) *Nakano and Morofuji,* 2023
1000	1	1	1	1	1
100	0.989 ± 0.005	0.993 ± 0.005	0.968 ± 0.009	0.978 ± 0.011	0.978 ± 0.009
50	0.985 ± 0.006	0.982 ± 0.005	0.951 ± 0.011	0.964 ± 0.012	0.964 ± 0.011
30	0.978 ± 0.008	0.972 ± 0.008	0.935 ± 0.011	0.953 ± 0.015	0.948 ± 0.013
20	0.969 ± 0.008	0.961 ± 0.011	0.918 ± 0.012	0.938 ± 0.018	0.929± 0.014
10	0.948 ± 0.009	0.938 ± 0.021	0.873 ± 0.015	0.893 ± 0.026	0.883 ± 0.017
7	0.935 ± 0.010	0.920 ± 0.022	0.837 ± 0.019	0.858 ± 0.029	0.848 ± 0.020
5	0.916 ± 0.012	0.889 ± 0.021	0.794 ± 0.023	0.817 ± 0.034	0.807 ± 0.023

The pump efficiency tables reported by Johnson et al. (2002) and more recently by Nakano and Morofuji (2023) are both based on a large number of pump calibrations using complementary and well-established methods and can therefore be classified as true pump efficiencies. Both tables are generally consistent within statistical uncertainty but diverge significantly from the older Komhyr (1986) and Komhyr et al. (1995) tables. Although the Komhyr tables (K86 and K95) have historically been called "pump efficiencies", the Komhyr values in Table 1 are now recognized as empirical efficiencies, which combine decreasing pump efficiency, increasing conversion efficiency, and typical memory effects in the background current for the standard buffered solutions SST1.0 and SST0.5 (Tarasick et al., 2021). For consistency with long-term data records, the values reported by Komhyr (1986) and Komhyr et al. (1995) are recommended by ASOPOS 2.0

274 (GAW Report No. 268) for SPC-6A & SST1.0 and EN-SCI & SST0.5, but now referred as empirical effective K86-
275 Efficiency and K95-Efficiency, respectively.
276
277 Normally, in the pH = 7 buffered KI sensing cathode the stoichiometry of the conversion (R1) of ozone into iodine is
278 assumed to be 1.00 with an uncertainty of about ±0.03 (Dietz et al., 1973), while the initial absorption efficiency of gaseous
279 ozone into the sensing solution will be 1.00 with an uncertainty of 0.01. These values for η_A and η_C are used in the
280 conventional method of ozonesonde data processing as recommended by ASOPOS in GAW Report No. 268 and before in
281 GAW Report No. 201.
282

283 **2.3 Perspectives on the Background Current**

284 **2.3.1 I_{B0} and I_{B1} Conventions for Background Currents**

285 The ECC sensor background current, I_B, is defined as the residual current output by the cell when sampling ozone free air.
286 Since the 1990s during the preparation of the ECC sensor at the day of flight, two background currents, I_{B0} and I_{B1},
287 respectively, are measured: before and after exposure of a certain amount of ozone, usually about 5μA ozone equivalent for
288 about 10 minutes. Both background currents are measured after flushing the cell for 10 minutes with ozone free air. (GAW
289 Report No. 201 and GAW Report No. 268). Although small (typically < 0.1 μA), the ECC sensor background current may be
290 of appreciable magnitude compared to the ozone current when there is very low ozone such as in the tropical upper
291 troposphere or in the stratosphere above 5 hPa but also during ozone hole conditions in polar regions.
292

293 Background measurements of SPC-5A sondes operated with the SST 1.0 using ozone-free air, showed before about 1993,
294 typical values of I_{B0} = 0.06±0.02 μA and I_{B1} = 0.09±0.02 μA, respectively (Smit, 2004c). After 1993 I_{B0} dropped to values of
295 0.00-0.03 μA and at the same time I_{B1} dropped by about 0.06 μA. This may mean that the manufacturer made changes, most
296 likely cleaning or conditioning the electrodes or ion bridge (e.g. less leakage of I_2 into the cathode solution). In the past thirty
297 years, both SPC-6A and EN-SCI sondes have shown similar low I_{B0} and I_{B1} values when a high-quality gas filter flushes the
298 cells with ozone free "zero" air. However, the difference of I_{B1}-I_{B0} of ~ 0.03-0.04 μA has stayed the same over decades. This
299 is actually the "chemical" contribution of the overall O_3 + KI chemistry in the cathode cell to the measured background
300 current after zero-air flushing, whereas I_{B0} is independent of ozone exposure and assumed to be an inherent property of the
301 ECC-sensor. The latter has been demonstrated in several laboratory experiments (Smit et al., 2007; Vömel and Diaz, 2010),
302 and in this study (Sect.2.3.3).
303

304 Theoretically, an ECC sensor in electrochemical equilibrium will produce no current; any current in the absence of ozone or
305 other oxidants must be due to an imbalance of tri-iodide between the anode and cathode cells (Komhyr, 1969). Possible
306 causes of such an imbalance include (i) a leaky ion bridge, (ii) limited mass transfer of residual tri-iodide (I_3^-) in the cathode
307 solution (Thornton & Niazy, 1982), (iii) limited electron transfer at the cathode surface, (iv) an imbalance resulting from cell
308 conditioning or contamination, or (v) previous exposure to ozone. The first three cases represent a background current that
309 may be expected to remain roughly constant and should therefore be subtracted as a best approximation; however, the last
310 two cases, (iv) and (v), should decline according to the response time of the cell (Tarasick et al., 2021).
311

312 **2.3.2 Constant Background Current?**

313 In the early days of the ECC there was no clear distinction between I_{B0} or I_{B1} to apply for I_B in Eq. (1). Komhyr (1969)
314 suggested that I_B resulted largely from a residual sensitivity of the ECC sensor to oxygen, and that I_B decreased with air

315 pressure in proportion to the rate at which oxygen entered the sensor. Thornton and Niazy (1982) showed in a laboratory

316 study that the primary source of the background current is from the removal of residual tri-iodide, normally present in the

317 cathode solution and not from the reaction of oxygen with iodide to produce tri-iodide nor from the direct reduction of

318 oxygen. Since 1975 the manufacturer (Science Pump Corporation) has preconditioned the ECC electrodes with iodide such

319 that the oxygen dependence has become vanishingly small and can be neglected (Thornton and Niazy, 1982).

320

321 **2.3.3 Past Ozone Dependent Background Current**

322 Based on simulation chamber experiments Smit et al. (1994) recommended using I_{B0} for the constant I_B subtraction, which

323 was confirmed in a field experiment by Reid et al. (1996). However, the results could not be confirmed in later JOSIE

324 experiments which demonstrated that the background current most likely varies with the past ozone measured, implying that

325 two background currents operate over the sonde operation (Smit and Sträter, 2004a,b; Smit et al., 2007): (i) one background

326 current I_{B0}, which is independent of ozone exposure and (ii) a second past ozone dependent background current that will vary

327 in the course of the sounding. This time variant ECC background current is assumed to result from a minor, but still slowly

328 decaying, contribution to the measured cell current. Based on laboratory experiments Johnson et al. (2002) and Vömel and

329 Diaz (2010) suggested that its origin is related to the ECC-chemistry having a fast (20-30 s) and an additional minor pathway

330 (reaction time constant ~20-30 min) that causes a memory effect, probably due to slow side reactions in the oxidation of

331 iodide by O_3 in the cathode sensing solution. In equilibrium this can lead to an overall stoichiometry factor, O_3/I_2, larger than

332 1.0 as observed by Johnson et al. (2002). The magnitude of the excess stoichiometry depends strongly on the phosphate

333 buffer concentration in the cathode sensing solution. Vömel and Diaz (2010) suggested that, instead of a measured

334 background current, it would be better to use an appropriate solution-dependent conversion efficiency and background

335 current values in the basic ECC-formula Eq. (1). For improved data processing the contributions of the slow (20-30 min) and

336 fast (20-30 s) responses to the overall measured ECC ozone signal need to be considered simultaneously using an

337 appropriate response (memory) function.

338

339 Such a possible methodology may be the deconvolution of the measured ozone profile after determining the overall

340 frequency response of the combined sensor and air sampling system (De Muer and Malcorps, 1984). However, the method is

341 complicated and not practical to apply to the global ozonesonde network. More accessible are first order numerical schemes

342 that deconvolve the fast response which were developed and tested by Imai et al. (2013) and Huang et al. (2015). Tarasick et

343 al. (2021) further developed one simple first order numerical scheme to resolve both the fast and slow time responses of the

344 ECC-sensor. Vömel et al. (2020) developed the methodology for quantifying the fast and slow currents in more detail but

345 several aspects were not fully considered, and their methodology was not assessed with the most comprehensive data base

346 and for various pairs of sonde types and SSTs. This study remedies these gaps.

347

348 To investigate the chemical origins of the slow current, laboratory response-time tests for hundreds of ECC-ozone sensors

349 (EN-SCI, SST0.5) were made at the Uccle (Belgium) sounding station since August 2017 during every routine day-of-launch

350 preparation to measure the two-time constants in the ECC signal. In this experiment, the following steps were taken to record

351 the ECC sensor current as function of time:

352   a. Before ozone exposure, flush the ECC-cell for 10 min with zero air: Record I_{B0}.

353   b. Expose the ECC-cell for 10 min to 5 μA ozone equivalent.

354   c. Flush the ECC-cell for 10 min with zero air: Record I_{B1} and stop flushing (pump inactive, short-circuit sensor leads)

355   d. No Flushing until t= 55 min, then flush 5 min. zero air**:** Record I_{B60} and then stop flushing.

356   e. No Flushing until t=115 min, then flush 5 min with zero air: Record I_{B120}.

357   The steps (a) to (c) follow exactly GAW Report No. 201 and GAW Report No. 268 SOPs. However, after these steps, most

358   of the time between t=10 and 120 min., flushing with ozone-free air has stopped except for the 5-minute periods at t=55 min

359   and t= 115 min. During the 5 minutes of flushing a short current increase was observed but it declined rapidly with a typical

360   "fast" 1/e response time of 25 seconds. The 120-min timing was chosen because this is the typical duration of the ascent of

361   an ozone sounding. Summaries of the observations for the fast and slow currents appear in Figure 1.

362
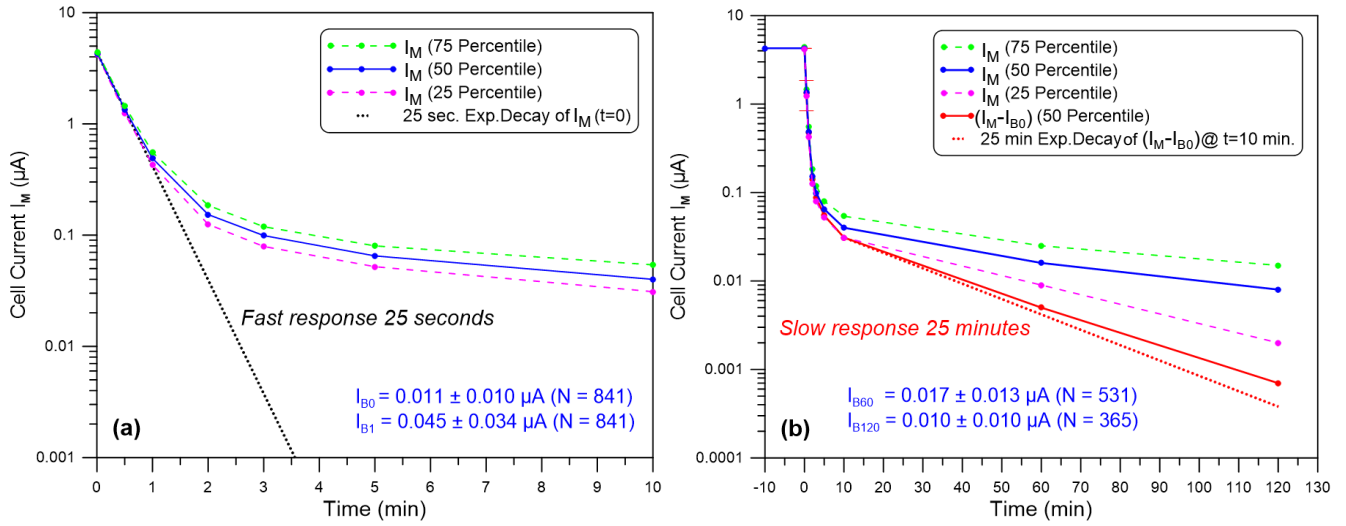
Figure 1.   Relaxation of the measured ECC-cell current $I_M(t)$ (logarithmic scale) flushed with purified ozone free air as a
function of time after the cells have been exposed for 10 minutes with 5 µA ozone. The sequence: (i) No flushing t=10-55
min.; (ii) Flushing t=55-60 min.; (iii) No flushing t=60-115 min; (iv) Flushing t= 115-120 min. Displayed are the medians of
$I_M(t)$ (blue solid line) and its 25 and 75 percentiles (green and pink dashed lines, respectively). Left diagram: first 10
minutes relaxation of $I_M(t)$; grey dotted line: 1/e decay of $I_M(t = 0$ min) with 25 s. time constant. Right diagram: full two
hours of relaxation of $I_M(t)$; red solid line: median of $I_M(t)-I_{B0}$; red dotted line: 1/e decay of $I_{B1}-I_{B0}$ ($t = 10$ min.) with 25
min. time constant.

370

371   The observed relaxations in Figure 1 follow a typical superposition of two first order exponential decays of the fast and the

372   slow component which can be expressed here as:

$$I_M(t) = I_{F0} Exp\left[\frac{-t}{\tau_F}\right] + I_{S0} Exp\left[\frac{-t}{\tau_S}\right] + I_{B0} \qquad (2)$$

374   where I_{F0} and I_{S0} are the fast and slow sensor current contributions, respectively, at the start of the response test at t=0.

375

376   Although, after t=10 min. until t=120 min. for only two short periods of 5 minutes the cathode cell was flushed with ozone

377   free air, the results are consistent with the observations of Vömel and Diaz (2010), who flushed the cathode cell over the

378   entire 120 minutes relaxation period. Clearly the relaxation of the slow component of the background is independent of the

379   flushing, i.e. no stirring action in the cathode sensing solution, and therefore most likely has a chemical origin from a slow

380   reaction pathway. The I_{B0} and I_{B1} shown in Fig.1 are typical of present-day ECC sondes (e.g. GAW Report No. 268). Further,

381   the characteristic difference of I_{B1} and I_{B0} of about 0.03-0.04 µA has been observed over a large number of sondes ($\cong$800)

382   and is most likely the residual of the slow reaction pathway.

383

384   In contrast to Vömel and Diaz (2010), based on around 25 runs, in the more than 350 Uccle experiments the cell current does

385   stabilize after 1-2 hours decay time to the background current before exposure to ozone, I_{B0}. As a matter of fact, assuming a

386   25 min 1/e-decay from the mean $I_{B1} = 0.045$ µA at t=10 min, the I_{B60} and I_{B120} would decay on average down to 0.006 µA

387   and 0.00055 µA, after 60 and 120 minutes, respectively. Actually, we recorded mean values of 0.017 µA and 0.010 µA,

11

388 respectively. The average differences of I_{B60}-I_{B0} and I_{B120}-I_{B0} are 0.008 µA and < 0.001 µA, respectively. This indicates that

389 after correcting the measured cell current $I_M(t)$ for the constant background current I_{B0}, the residual current $I_M(t)$-I_{B0} (Fig.1:

390 red solid line) fits very well with the 25 min. 1/e-decay of the mean I_{B1}- I_{B0} starting at t=10 min. (Fig.1: Red dotted line).

391 Similar observations were made in 1993 in the simulation chamber at WCCOS, whereby four ECC sondes were flushed for

392 more than 90 minutes with zero ozone air during the simulation of a tropical descent pressure profile. After a relaxation time

393 of about 70 minutes the cell currents approximate constant values which are very close to the corresponding recorded I_{B0} (for

394 details see Fig. S1 in the supplementary material). This means that after 1-2 hour of flushing the ECC-sensor with zero

395 ozone, the remaining current is identical to I_{B0}, so that during the typical duration of the ascent of an ozone sounding, the

396 remaining current (I_{B0}) persists, which is not the result of a 25 min decay but has another origin. This inherent I_{B0} of the

397 ECC-sensor, possibly caused by a small leakage of iodine (I_2) from the ion bridge into the cathode solution or by a mass-

398 transfer limit in the solution or electron transfer at the cathode surface (Thornton and Niazy, 1982, 1983), appears to be

399 constant over the 2 hours of an ozonesounding.

400

401 To understand the KI+O_3 chemistry and the impact of the phosphate buffer on the stoichiometry of the conversion of the

402 sampled ozone into "free" iodine, Tarasick et al. (2019, 2021) reviewed many studies in which a variety of KI-solution

403 strengths with different pH-buffers were investigated. The reaction mechanism of KI+O_3 in aqueous solution in presence of a

404 phosphate buffer as investigated by Saltzman and Gilbert (1959) may explain the observations made here and are discussed in

405 detail in Appendix A. In short, they proposed two reaction pathways: a primary reaction pathway without a buffer and the

406 secondary pathway with a buffer. Experimentally, Saltzman and Gilbert (1959) showed that the impact of the slow reactions

407 increases with the buffer concentration, whereas buffered solutions with no KI showed no evidence of any O_3 reactions. This

408 means that the additional reactions with O_3 are secondary reactions after the initial O_3 + KI reaction. Saltzman and Gilbert

409 further demonstrated that the secondary pathway could form additional free iodine, half of it reacting very fast (<< than 1 sec,

410 i.e. residence time of air sample in the cathode cell), the other half more slowly (~25 min). This means that the secondary

411 reaction pathway can contribute both to the fast and slow ECC current, respectively. However, loss mechanisms may occur

412 too. In summary, we do not know exactly the stoichiometry of the fast and slow reaction pathways leading to "free" iodine."

413 Therefore, we can only indirectly quantify these two stoichiometries that lead to the fast and slow cell current components

414 observed, respectively. In other words, the measured cell current $I_M(t)$ is the superposition of

415

416    $$I_M(t) = I_{P,F}(t) + I_{S,F}(t) + I_S(t) + I_{B0} \qquad\qquad\qquad (3)$$

417 where

418 $I_{P,F}$ = sensor current contribution from fast primary reaction pathway.

419 $I_{S,F}$ = sensor current contribution from fast secondary reaction pathway.

420 I_S = sensor current contribution from slow secondary reaction pathway with a typical 20-25 min time response.

421 The contribution of the fast reaction pathways that form iodine fast is lumped together in the total fast sensor current

422 component $I_F(t)$ with a typical time response of 20-30 s. The measured sensor current $I_M(t)$ is then expressed as:

423    $$I_M(t) = I_F(t) + I_S(t) + I_{B0} \qquad\qquad\qquad (4)$$

424 The overall stoichiometry S_T of the chemical conversion of O_3 into I_2 is the sum of the stoichiometry factors S_F and S_S of the

425 fast and slow reaction pathways, respectively.

426

427 **2.4 Formulating New Fast and Slow Components of the ECC Current**

428 From the response tests (fast decay from 5µA down to 0.1-0.5µA within less than 1 minute) it can be concluded that S_F is

429 close to one (0.9-1.1) and at least a factor 10-20 larger than S_S, which is small (0.01-0.10). The time scale of the slow current

430   component (τ_S=25 min) is about a factor of 60 slower than the dominating fast current component. This means that the slow

431   current acts as a slowly time-varying background current. The latter can be treated as a superposition with the ozone-

432   independent background I_{B0} to constitute the total background but given now as the time varying $I_B(t)$ in Eq. (1).

433       $I_B(t) = I_{B0} + I_S(t)$ (5)

434   By substituting $I_M(t)$-$I_B(t)$ into Eq. (1) the partial pressure of ozone is now expressed as Eq. (6):

435       $P_{O3} = 0.043085 * \frac{T_P}{(\eta_P * \eta_A * \eta_C * \Phi_{P0})} * I_F(t)$ (6)

436   where the fast sensor current is expressed as:

437       $I_F(t) = I_M(t) - I_S(t) - I_{B0}$ (7)

438   The conversion efficiency may depend on sonde type and sensing solution type. It is largely related to the stoichiometry of

439   the conversion of O_3 into I_2 from the primary fast reaction pathway and to a lesser degree on the secondary reaction pathway.

440   The partial ozone pressure can be determined from equation Eqs. (6)-(7) in two steps:

     a.   Determine the slow current as a function of time. Because the past ozone exposure-dependent slow current

442   component $I_S(t)$ is much slower and smaller than the fast current component $I_F(t)$, the slow current can be

443   determined from the convolution of the measured current $I_M(t)$ with the slow time constant τ_S=25 min.

     b.   Calculate the fast current $I_F(t)$ and then through deconvolution of $I_F(t)$, resolve the time delay of the relatively fast

445   time constant τ_F=20-30 seconds.

446   The fast as well as the slow reaction path are determined by a first order time response and can therefore be separated in a

447   convolution part to determine $I_S(t)$ and a deconvolution part to obtain the fast current component, $I_{F,D}(t)$, respectively. The

448   mathematical techniques used here to resolve the impacts of the slow and fast time constants, τ_S and τ_F, respectively, are

449   based on the numerical scheme described by Miloshevich et al. (2004) and were first applied by Imai et al (2013) to resolve

450   the time delay effects caused by the ECC fast response time. A first order response of a measured sensor signal U (here ECC

451   ozone sensor current) that is approximately proportional to a change in time of U, is described by the common "growth law

452   equation":

453       $\frac{dU_m}{dt} = \frac{1}{\tau} * (U_a - U_m)$ (8)

454   where U_m is the instantaneous measured signal, U_a is the ambient ("true") signal that is driving the change in U_m, and τ is the

455   time constant of the signal.

456   Integrating Eq.(8) over a small time step $\Delta t_k = t_{k-1} - t_k$ gives the measured signal as a function of time:

457       $U_m(t_k) = U_a(t_k) - \{U_a(t_k) - U_m(t_{k-1})\} * Exp\left(-\frac{\Delta t_k}{\tau}\right)$ (9)

458   In case the time step Δt_k is chosen small relative to the response time τ it can be assumed that the "true" (ambient) signal U_a

459   is quasi-stationary during time step Δt_k such that $U_a(t_k) = U_a(t_{k-1})$. The exponential term is the response function.

460   Eq. (9) can be expressed in a numerical convolution or de-convolution scheme. From Eq. (9) we can obtain $I_S(t)$ and $I_{F,D}(t)$,

461   as follows:

462   ***Case 1:*** *Slow current component derived from convolution (time constant* τ_S*) of the ambient sensor current I_a:*

463   To obtain the slow current component (I_S), U_m in Eq. (9) is substituted by the slow fraction of I_a, represented here by the

464   stoichiometry S_S multiplied with the ambient ("true") ozone sensor current I_a. Eq. (9) can now be re-written into the

465   integrating form:

466       $I_S(t_k) = S_S * I_a(t_k) - \{S_S * I_a(t_k) - I_S(t_k - 1)\} * X_S$ (10)

467   whereby the slow response function X_S is:

468       $X_S = Exp\left(-\frac{\Delta t_k}{\tau_S}\right)$ (11)

469

470   *Case 2*: *Deconvolution (time constant* τ_F*) of the fast signal* I_F *with* τ_F*:*

471   To obtain the deconvolved fast current component $I_{F,D}$, Eq. (9) should be solved to obtain U_a (=$I_{F,D}$), and U_m is substituted by

472   the fast fraction I_F. Eq. (9) can then be re-written into the differentiating form:

473
$$I_{F,D}(t_k) = \frac{I_F(t_k) - I_F(t_{k-1}) * X_F}{(1 - X_F)} \qquad (12)$$

474   where the fast response function X_F is:

475
$$X_F = Exp\left(-\frac{\Delta t_k}{\tau_F}\right) \qquad (13)$$

476

477   Compared to Vömel et al. (2020), the recursive numerical convolution scheme proposed here (Eq.11) is the same, while the

478   deconvolution scheme (Eq.12) differs through the inclusion of the exponential fast response function X_F (Eq. 13) itself,

479   rather than its first order approximation. The latter allows larger time steps Δt_k, which may become significant for older

480   ozone sounding records that had data with resolution of 10 seconds or more.

481   **3 Resolving Slow- and Fast-Response Signals using JOSIE 2009/2010**

482   To resolve the slow and fast time responses of the measured ECC sensor current, the JOSIE measurements conducted in

483   several campaigns between 1996 and 2017 form an ideal dataset, because of several reasons. Firstly, all the ozonesonde

484   preparations and the measurements were carried out in a controlled environment. Secondly, the availability of simultaneous

485   reference measurements from a fast-response photometer OPM with high precision and accuracy provides an absolute

486   reference for the derived ozone profiles. Further, in the course of the simulation several response tests are performed in

487   which the ozonesondes and the OPM are exposed to zero-ozone air for a five minute period (see Fig. 2). These response tests

488   enable us to determine the stoichiometry of the slow reaction pathway and subsequently the slow sensor current $I_S(t)$ as a

489   function of time. In this sense, the JOSIE 2009 and 2010 campaigns dataset is of particular interest, because all experiments

490   included four of those response tests in the simulation profiles themselves.

491

492   For the sake of clarity, it is to be noted that the here reported ozone readings of the OPM are already based on the new UV-

493   absorption cross-section, referred to as the CCQM.O3.2019 (BIPM, 2022; Hodges et al., 2019) value that is about 1.23%

494   lower than the former cross-section (Hearn et al., 1961) that was mostly used before in the global ozone ground based

495   monitoring networks. In 2024-2025 the new cross-section will be introduced into the global ozone observation networks

496   using UV-photometry (BIPM, 2022). Consequently, all P_{O3} measurements of the OPM reported here are about 1.23% larger

497   than the values reported before in earlier JOSIE-publications.

498   **3.1 JOSIE 2009/2010**

499   The JOSIE 2009 and 2010 protocols are similar to the JOSIE 1998 campaign (Smit and Sträter, 2004a; Smit et al., 2007). In

500   2009 a set of 40 brand new ECC sondes (20 SPC6A and 20 ENSCI) were tested; in 2010 the same set of ECC sondes, re-

501   furbished and tested under the same conditions, were evaluated against the same OPM reference. One aim of these

502   campaigns was to test the performance of brand new and refurbished ozonesondes. It was found that the re-used sondes

503   agree within 1%–2% with brand new sondes, although with a slightly lower precision of ~5% (see Fig. 3.1 in GAW Report

504   No. 268). The JOSIE 2009/2010 ozonesondes were prepared by only three operators, strictly following the same preparation

505   protocols, including the use of purified air from the same cylinders for the ozone-free air source. It can therefore be

506   considered as an ideal data set for well-prepared ozonesondes. All ozonesonde data were processed according to the

507   guidelines of GAW Report No. 268, which we denote as the "conventional" method hereafter. That means: (i) subtracting the

508   constant background current I_{B1}; (ii) correcting the pump flow rate for the moistening effect; (iii) using the empirical

509 effective efficiency tables by Komhyr (1986) and Komhyr et al. (1995) for SPC and EN-SCI ozonesondes respectively; (iv)

510 converting the measured pump temperature to the internal pump body temperature, with an additional small pressure

511 dependent correction (GAW Report No. 268); and (v) no total ozone normalisation. Note also that all simulations were

512 identical in representing a typical mid-latitude ozone profile (Smit et al., 2007).

513 During both campaigns, a total of 26 simulation runs were made, of which all but one had 4 ozonesondes simultaneously in

514 the simulation chamber, giving a total amount of 103 ozonesonde profiles. However, 17 of those profiles were gathered

515 using research-mode SSTs and are not included here. Fourteen simulations were carried out in December 2009, 2 in January

516 2010, and 10 in August 2010.

517 **3.2 Determination of Slow Current $I_S(t)$**

518 **3.2.1 Determination of Stoichiometry S_S**

519 To determine the relative contribution S_S of the slow component in the ECC ozonesonde signal, in other words, the

520 stoichiometry factor of the slow reaction pathway of conversion of O_3 into I_2, the response tests of the JOSIE 2009/2010

521 dataset are used. Four-time response tests are included during these simulations at four different pressure levels, (RT1: 475-

522 375 hPa, RT2: 100-85hPa, RT3: 20-15 hPa, RT4: 6-5 hPa), during which ozone-free air is provided in the simulation

523 chamber for 5 minutes. A typical example of a JOSIE 2009 simulation run is given in Figure 2. After 5 minutes the fast

524 sensor current has declined by more than 16 1/e relaxation times and is negligible. This means that at the end of this time

525 response test, the only contribution to the overall measured current $I_M(t)$, after correction for I_{B0}, comes from the remaining

526 slow current component. At this moment, the fast co-existing OPM data (red in Fig. 2) provide the true value of the

527 ozonesonde signal. The next paragraphs outline the different practical steps.

528 To obtain a direct measure of the true ECC-ozone sensor current, the OPM ozone partial pressure is converted to the generic

529 OPM current (I_{OPM}) for each individual ozonesonde using sonde pump temperature, sonde pump flow rate and true pump

530 efficiency values of JMA (Nakano and Morofuji, 2023, See Table 1), as in Eq. (1).

531

532
$$I_{OPM} = \frac{(\eta_P * \eta_A * \eta_C * \Phi_{P0})}{T_P * 0.043085} * P_{O3,OPM} \tag{14}$$

533

534 In other words, we are calculating the generic sensor current corresponding to the ozone equivalent measured by the OPM,

535 as if it were the true ECC ozone current. This means that the generic I_{OPM} is taken as the actual reference ("true") current for

536 determining the slow stoichiometry factor S_S.

537

538 Additionally, the generic OPM current I_{OPM} (red in Fig. 2) is convolved into $I_{OPM,C}$ with an exponential time response with τ_s

539 = 25 minutes using Eq. 9, to obtain a slow time response into the generic OPM current signal (yellow in Fig. 2).

540
$$I_{OPM,C}(t_k) = I_{OPM}(t_k) - \{I_{OPM}(t_k) - I_{OPM,C}(t_k - 1)\} * X_S \tag{15}$$

541 Finally, the slow stoichiometry factor S_S is obtained by taking the ratio of the remaining ECC sensor current I_M minus the

542 constant background current I_{B0} and the convolved OPM signal ($I_{OPM,C}$), at the end of the time response test intervals RT1,

543 RT2, RT3, RT4, when only the slow component is expected to contribute to the sonde signal, such that

544
$$S_S = \frac{(I_{M(ECC)} - I_{B0})}{I_{OPM,C}} \tag{16}$$

545
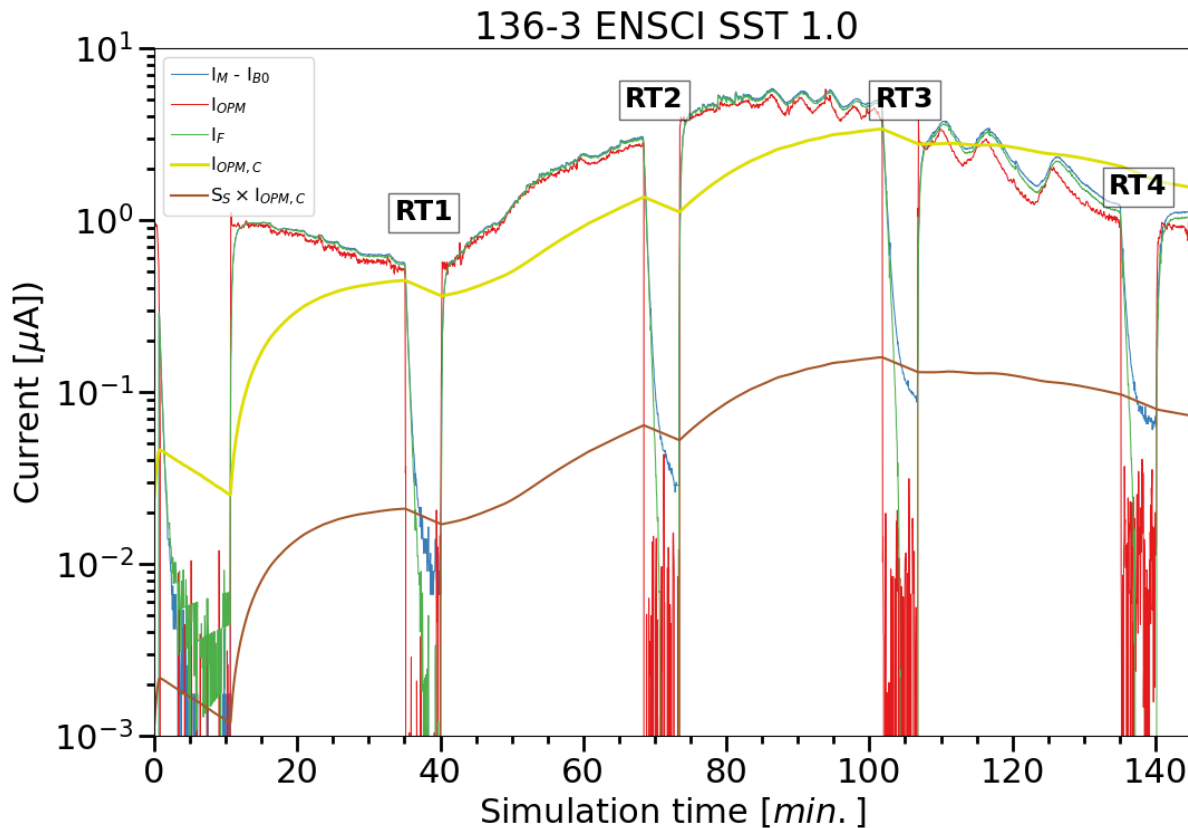
Figure 2. Example of a simulation run during JOSIE 2009 as a function of the simulation time, with the measured ECC current I_M minus I_{B0} (blue line), the generic OPM current I_{OPM} (red line), the 25 min convolved $I_{OPM,C}$ (yellow line) and the 25 min convolved I_{OPM} adapted to I_M-I_{B0} after the determination of the slow stoichiometry factor S_S or slow current I_S (= S_S x $I_{OPM,C}$) (brown line) and the fast sensor current I_F (green line), obtained after correction of the measured sensor current I_M for the constant background current I_{B0} and the slow current contribution I_S

The ratios used to obtain the slow stoichiometry factor (S_S) values are calculated during the final 50 seconds of each time response test, RT1, RT2, RT3, RT4, respectively. Those values, obtained for all ozone profiles within each sonde type and SST combination, are shown in Fig. 3, together with median, 25th and 75th percentile values. The median S_S values and their Median Absolute Deviation (MAD) uncertainties are given in Table 2. Note that the determination of the median S_S values (and their uncertainties) is very robust and does not depend on the time response test interval or the slow time lag constant. We will come back to this in Sect. 6.2. Further it showed that by varying τ_S = 25 min. by ± 5 min. the corresponding S_S values only changed by less than 5%, which is small compared to the MAD uncertainty of S_s (Table 2).

The most striking feature is that S_S only depends on the SST, not on the sonde type. This confirms our hypothesis on the origin of this slow component, as described in Section 2.4. For SST0.5 and SST1.0 there is an almost proportional relation between the magnitude of S_S and the buffer strength. Johnson et al. (2002) have demonstrated that increase of the stoichiometry is primarily caused by the buffer strength with only a minor contribution by the KI-concentration. This result might be explained by the secondary reaction pathway of the reaction mechanism after Saltzman and Gilbert (1959), whereby the extra slow stoichiometry contribution is caused by the buffer (Appendix A). However, a comparable result does not hold for SST0.1 (Table 2). One would expect that for the low buffered case (SST0.1) S_S should be much smaller than for the SST0.5. This is not true; S_S is even slightly larger. It seems that for the SST0.1, other competing reaction mechanisms

16

may occur, which do depend on the KI concentration, and may generate free iodine on a 25-minute time scale. Such a hypothetical mechanism may also explain the fact that for low or no buffered SST we still measure I_{B1} background currents with values of 0.01-0.03 µA larger than I_{B0} as measured in JOSIE 2000 (no buffer SST; Smit and Sträter, 2004b) and JOSIE 2017 (SST0.1; Thompson et al., 2019). A speculative mechanism is that the electronically excited oxygen singlet molecule formed in (R3) of the primary reaction pathway of the O_3+KI chemistry (Appendix A) may, in addition to de-activation in (R4), react with H_2O and produce hydrogen peroxide (H_2O_2) (e.g. Xu et al., 2002). The formed H_2O_2 would oxidize KI to produce free iodine, but on a time scale of 25 minutes which could contribute to the slow current $I_S(t)$. Further studies are required to understand the underlying chemical processes.

Table 2: Median and their Median Absolute Deviation (MAD) uncertainty values of the slow stoichiometry factor S_S obtained from JOSIE 2009 and 2010 for SPC and EN-SCI ozonesondes operated with the sensing solution types SST0.5 and SST1.0. The stoichiometry factor S_S for EN-SCI/SST0.1 has been determined with the same approach but using laboratory measurements at Uccle with an ozone reference instrument (see Appendix B). *: the same value for SPC/SST0.1 has been adopted as for EN-SCI 1.0%-0.1B. N_S is the number of sonde profiles.

Sonde Type	SST1.0	SST0.5	SST0.1
SPC	0.050 ± 0.002 (N_S =16)	0.017 ± 0.004 (N_S =21)	0.023 ± 0.005*
EN-SCI	0.046 ± 0.006 (N_S =23)	0.018 ± 0.004 (N_S =15)	0.023 ± 0.005 (N_S =8)

The stoichiometry factors S_S (Table 2) to determine the slow current $I_S(t)$ are substantially lower than the so-called "steady state bias factors" applied by Vömel et al. (2020). These steady state bias factors were determined as the overall excess stoichiometry to one from laboratory experiments with a fixed ozone exposure during several hours (Figs. 3 & 4 in Vömel and Diaz, 2010). In this study we derived for SST1.0 S_S = 0.046-0.050 which is only half the 0.09 value of Vömel et al. (2020). For SST0.5 and SST0.1, our respective S_S = 0.017-0.018 and 0.023 values are also smaller than their 0.024 and 0.031 steady-state bias factors. Using the same laboratory procedures as Vömel et al. (2010), Johnson et al. (2002) reported an excess overall stoichiometry of ~0.07 for SST1.0. The lower factors obtained in this study, particularly for SST1.0, might also be related to the different methodology followed for determining S_S. Here, S_S values are determined from the response of a downward step under zero-ozone conditions. In Johnson et al. (2002), and Vömel and Diaz (2010) the excess stoichiometry factors were determined from the relatively small differences observed between the ECC sonde and a reference UV-photometer after a 60-min upward step ozone exposure. The latter requires very accurate generation of ozone values with a precision better than 1% to determine the relatively small excess stoichiometry factors involved. Also note that for the earlier studies reference ozone readings are based on older UV absorption cross sections that are now corrected by 1.23% to be compatible with the new UV absorption cross-section applied to the OPM. Accordingly, the steady state bias factors of Johnson et al. (2002) and Vömel et al. (2020) should be decreased by subtracting 0.012. The resulting S_S values would then approach the S_S values obtained here for SST0.1 and SST0.5, and better approximate the SST1.0 S_S values.
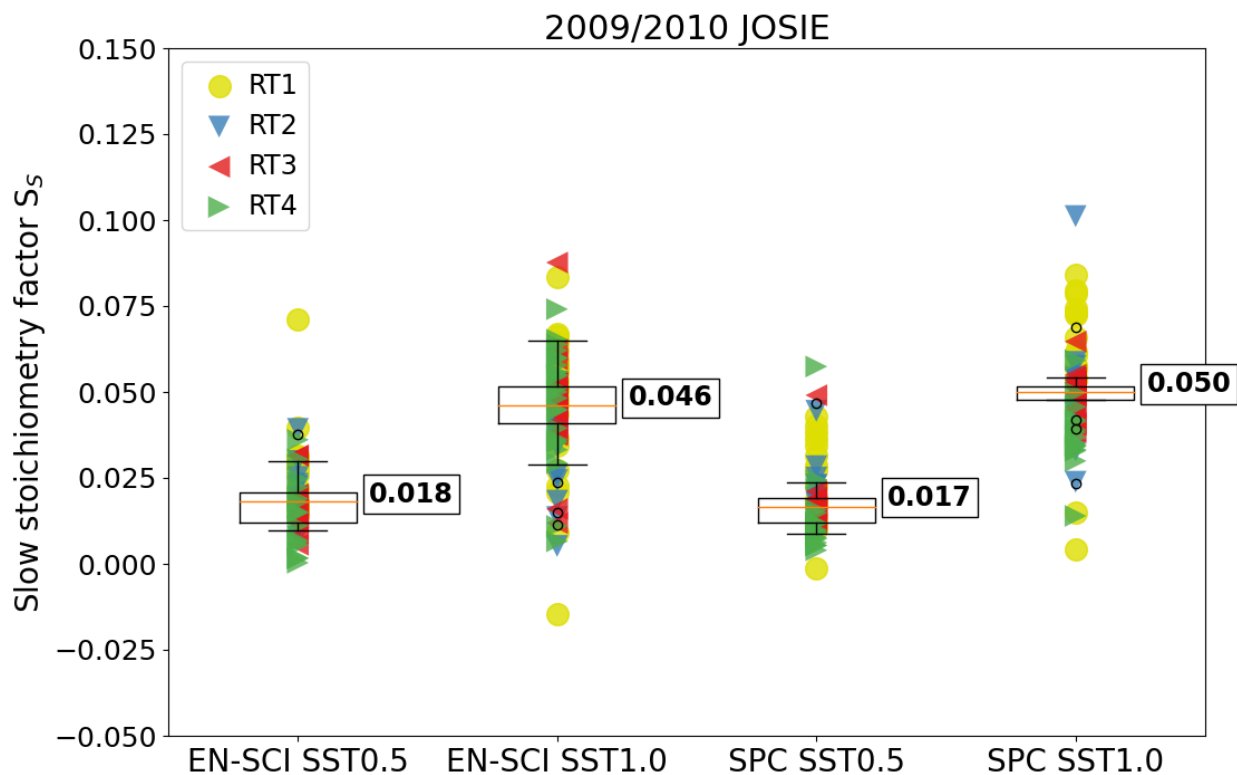
Figure 3. Box-Whisker plots of the slow stoichiometry factor S_S as the ratio of the measured I_M minus I_{B0} to the 25 min convolved OPM current ($I_{OPM,C}$) obtained from JOSIE 2009 and 2010 for EN-SCI and SPC ozonesondes operated with the SST0.5 and SST1.0. The yellow dots and triangle symbols (blue, red and green) represent the individual values obtained from the four response tests RT1, RT2, RT3 and RT4, respectively. Thus, every ozonesonde profile is represented four times in the graph. The Box-Whisker plots are represented by the median plus the 25th and 75th percentiles (respectively, orange and black horizontal lines for each pair of instrument-SST combination).

Another difference between the new methodology and that of Vömel & Diaz (2010) is that we subtract I_{B0} from the ozonesonde signal prior to determining the stoichiometry. However, we also determined the S_S values without correction of I_{B0}; the results appear in Fig. S2 in Supplementary Material. It is noted that these S_S values increase for all sensing solution types by only 0.005-0.009. For SST0.5 and SST0.1, they approach the Vömel & Diaz (2010) values, but the substantially lower S_S values for SST1.0, as derived here (Table 2) cannot be explained exclusively by subtracting I_{B0}. Furthermore, comparing Fig. 3 with Fig. S2, also demonstrates that the subtraction of the I_{B0} value makes the determination of the S_S values even more independent of the selected RT intervals, which is not the case without this prior subtraction (e.g. the RT1 values being significantly larger than the other RT values).

The factors reported by Johnson et al. (2002) and Vömel & Diaz (2010) are based on a limited sample of experiments (three different sondes using three different solutions for a total of 22 runs in Vömel & Diaz, 2010) in contrast to the large statistical sample in this study (Table 2). The difference between the two approaches – in terms of exposure to ozone or not - may be then explained by assuming that when the overall excess stoichiometry originates from the secondary reaction pathway, only half of it contributes to the slow cell current $I_S(t)$ and with the other half contributing to the fast cell current $I_F(t)$. For SST05 and this SST1.0 this can be understood by the type of reaction mechanisms of the secondary reaction pathway as proposed by Saltzman and Gilbert (1959): in this case, about half of the extra stoichiometry caused by the buffer

627 could be still contributing to the relatively fast signal (R7) and the other half to the slow signal (R8) (see Appendix A). This

628 would mean that the stoichiometry of the secondary reaction pathway could be two times the stoichiometry factor S_S of the

629 slow ECC current $I_S(t)$ determined here from the response tests RT1 to RT4 after $I_F(t) = 0$. However, for the S_S values for the

630 SST0.1, even slightly larger than for SST0.5, explanations would be more speculative. More analysis and new JOSIE trials

631 might be required to find the cause of varying factors among the different studies and SSTs.

632

633 **3.2.2 Initial Condition of Slow Current $I_S(t)$**

634 With the derived S_S values, the slow component of the sonde signal (I_S) is computed by convolution with the slow time

635 constant $\tau_s = 25$ min., as in Eq. (10) (brown line in Fig. 2). Note that, in practice, to determine $I_S(t)$, the measured current $I_M(t)$

636 minus I_{B0} can be taken instead of the true generic ozone current $I_{OPM}(t)$, because their differences are rather small (less than

637 5-10%), at the same time the slow stoichiometry factors S_S are also smaller than 0.1. From here on, we will use the measured

638 current $I_M(t)$ minus I_{B0} to determine the slow current $I_S(t)$ along with the S_S values listed in Table 2.

639

640 As Eq. (10) is a recursive expression, the initial conditions of I_S reflect prior ozone exposure during pre-launch preparations,

641 although decaying exponentially in time. Exposure to ozone values during pre-launch will cause non-zero I_S values at the

642 beginning of the simulation, impacting the boundary layer ozone profile (e.g., Fig. 10 in Vömel et al., 2020). Ideally, the

643 convolution of the slow component of the sonde signal is computed taking the pre-launch measurements into account. These

644 pre-launch measurements are available for JOSIE 2009/2010 (as in Fig. 4), but this is often not the case for operational

645 soundings. Using those JOSIE 2009/2010 pre-launch simulation data (with negative simulation times in Fig. 4), we found

646 that the best approximation of the true I_S (red dashed line in Fig. 4, taking all the pre-launch measurements into account) is

647 obtained if $I_S(t_0)$ equals ($I_{B1}-I_{B0}$) multiplied with the exponential decay factor $X_S = \text{Exp}[-\Delta t/\tau_s]$, where Δt is the time interval

648 between the measurement of I_{B1} and the start of the launch (green dashed line in Fig. 4). It is important to mention here the

649 good agreement of the measured I_{B1} value (yellow horizontal line in Fig. 4, subtracted by I_{B0}) with the convolved, pre-

650 launch, slow component I_S (dashed red line) at $t = -2500$ seconds (time mark No.2 in Fig. 4). This reinforces the selection of

651 the $I_{B1} - I_{B0}$ measurement as a good pre-launch representation of the slow component of the ECC signal.

652

653 To apply this method in the ozonesonde network, it is essential to record the time difference between the I_{B1} measurement

654 and the sonde launch. In GAW Report No. 268, the recording of the I_{B1} timestamp is included in the SOP for ozonesonde

655 preparations. For the JOSIE 2009/2010 data, we will use this exponential decay method for the initial condition of the

656 convolved slow component at $t=0$. For the initial condition of the slow component $I_S(t_0)$ we investigated two other

657 alternatives:

- 658 $I_S(t_0) = I_{B1}-I_{B0}$, denoted by the horizontal yellow line in Fig. 4, which results in a slow component I_S marked by the
- 659 purple solid line, which clearly overestimates the true I_S in the beginning of the profile (up to about 3500 s).
- 660 $I_S(t_0) = 0$, for which the corresponding I_S, represented by the brown solid line in Fig. 4, underestimates the true I_S
- 661 up to about a simulation time of 2200s for the JOSIE 2009/2010 representative example here.

662 For stations with a time gap of several hours between the I_{B1} measurement and the launch time, the current will have been

663 fallen back to the I_{B0} (see the Uccle example in Fig. 1), resulting, after subtraction of I_{B0}, in this particular case $I_S(t_0) = 0$.

664

665 A better understanding of the ECC time response provided a justification for quality control indicators on the I_{B0} (< 0.03 µA)

666 and I_{B1} (< 0.07 µA) in GAW Report No. 268. In practice, often higher background currents I_{B0} and I_{B1} are recorded at the

667 sounding sites at the day of the launch. These high background currents are typically caused by the use of an inadequate gas

668 filter in the test unit, e.g. the filter provides ozone free air, but does not trap water vapour and contaminants in the laboratory

669   air that is filtered into the preparation equipment. A poor filter combined with a leaky photolysis cuvette producing ozone by

670   UV-photodissociation of oxygen with a Hg-discharge lamp can contaminate the air flow to produce high background current

671   measurements. It appears that UV irradiation can produce substances that cause reactions similar to KI and O_3. There are

672   some indications (Newton et al., 2016) that high backgrounds may be due to processes with 1/e-decay times ~ 25 minutes

673   like the slow cell current $I_S(t)$. Nevertheless, more research is necessary to investigate the cause and the time behaviour of

674   these high background currents in the course of the sounding in order to correct for this artifact properly. As stated by

675   ASOPOS 2.0 (WMO/GAW Report No. No. 268) the use of proper gas filters to provide ozone free, dry and purified air in

676   practice at the sounding site, is very essential in general, but also when applying the data processing proposed here.
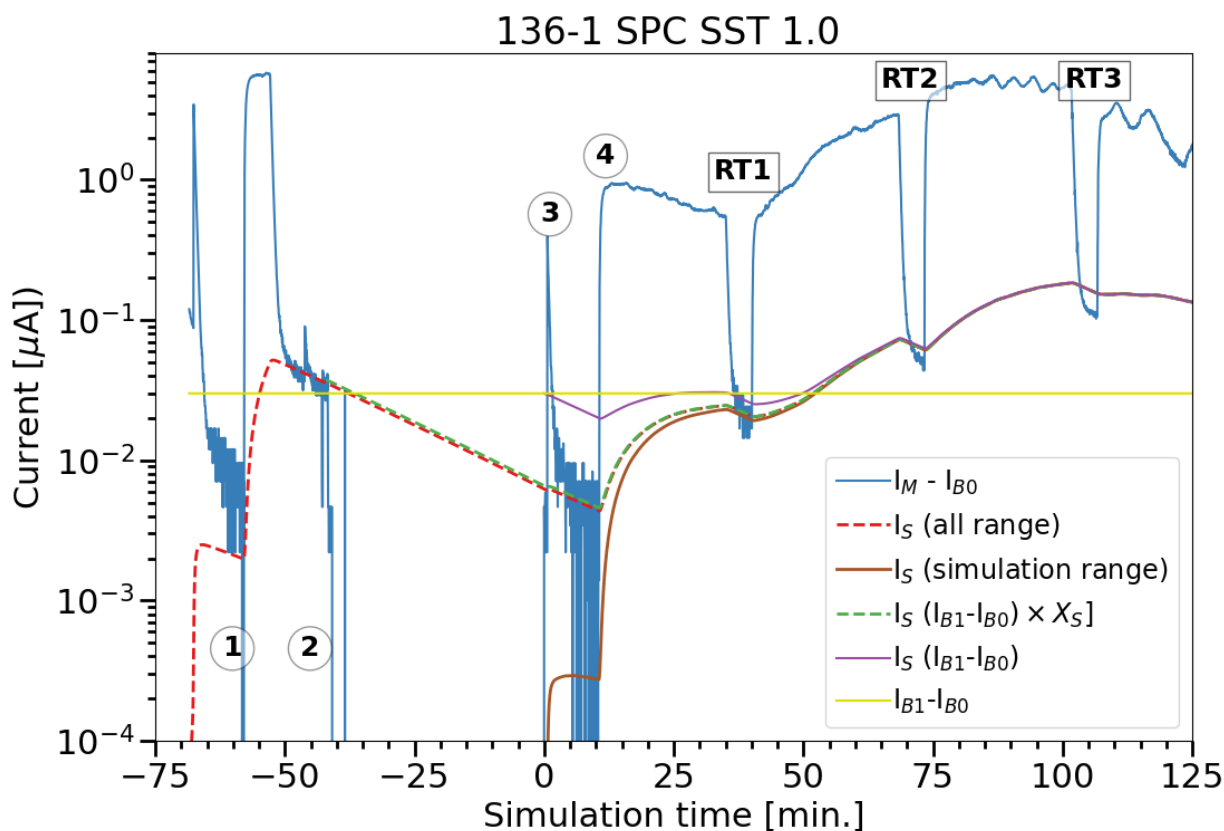
Figure 4. Convolved slow ECC current obtained from different initialization scenarios as function of the simulation time.
(details see text). The dashed red line is the convolved ECC current obtained from the measured I_M minus I_{B0}, hereby
including all pre-launch measurements (with negative simulation times). Time stamps 1-4: 1= record I_{B0}; 2= record I_{B1};
3=turn on pump motor (at simulation time t=0); 4= start ozone profile of simulation. RT1, RT2, RT3 are the first three in-
flight time response tests. Slow current $I_S(t)$ derived with four different start scenarios: (i) all range (I_S =0 at t =-67 min., red
dashed line); (ii) simulation range (I_S =0 at t=0 min., brown solid line); (iii) $I_S = I_{B1}$-I_{B0} at time stamp 2 with 25 min.
exponential decay X_S (green dashed line); (iv) $I_S = I_{B1}$-I_{B0} at time stamp 3 (purple solid line).

3.3 Determination of the Fast ECC Ozone Sensor Current, $I_F(t)$

After determining the slow component of the signal due to the secondary reaction pathway, we can subtract it from the
overall measured current I_M - I_{B0} to end up with the fast component I_F (Eq. 7), as shown by the green line in Fig. 2. From the
fast component $I_F(t)$, we can remove the time lag introduced by the 1/e time response of about 20-30 seconds through
deconvolution of I_F (t) according to Eq. (12). In this paper, we use τ_F = 25 ± 4 seconds for EN-SCI, and τ_F = 21 ± 4 seconds

692   for SPC ozonesondes, which are the average fast time responses determined from all the simulation time response tests (RT1,

693   RT2, RT3, RT4) during JOSIE 2009/2010. The response times of the EN-SCI sondes are typically about 4 seconds larger

694   than the SPC-6A sondes due to the slightly lower pump flow rates and slightly larger volume of the cathode cell of the EN-

695   SCI sondes (Smit and Sträter, 2004a). In general, we found that the fast response times in upward as well as in downward

696   direction agree within 1-2 seconds. Moreover, τ_F only varies marginally in flight with a slight decrease of less than 5-10 %

697   between the surface (RT1) and the upper part of the sounding (RT4). The in-flight τ_F values also agree very well with the τ_F

698   values determined from the response tests made during the pre-flight preparation of the ECC sensor, which confirmed earlier

699   observations made during JOSIE (Smit and Sträter, 2004a). A close-up of the first-time response interval RT1 is provided in

700   Fig. 5, in which also the deconvolved fast component is shown in yellow.
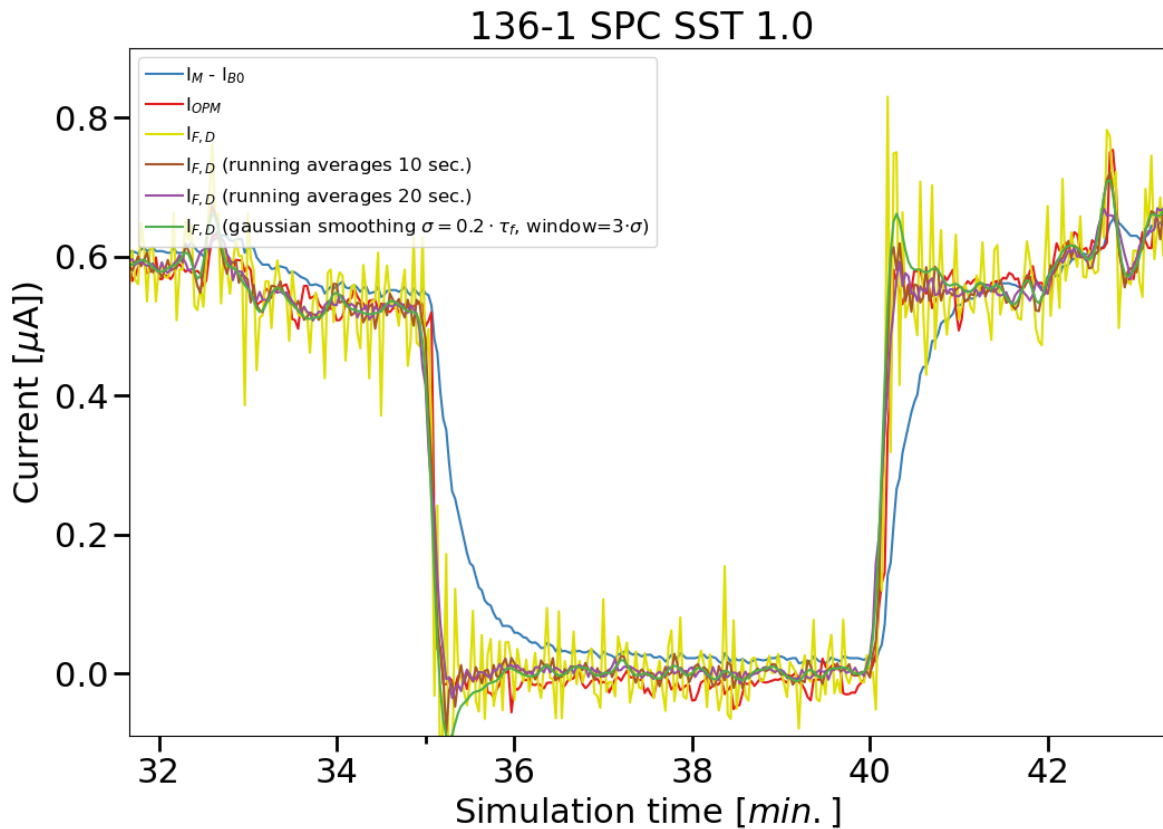
Figure 5. Example of a downward and upward response of a simulation run in the tropospheric part of the vertical profile to show the impact of resolving the fast response effects on the measured cell current I_M minus I_{B0} (I_M-I_{B0}: blue solid line). The fast, deconvolved current $I_{F,D}$, without smoothing, is shown in yellow, and with a moving average smoothing over a time interval of 10 and 20s in brown and purple, respectively. The Gaussian smoothing applied on $I_{F,D}$ and used in this paper is marked by the green line. For reference, the OPM current is shown in red.

709   Note that the deconvolution procedure introduces a substantial amount of noise in the data. To reduce this noise, the

710   deconvolved current signal should be smoothed. We therefore used a smoothing with a Gaussian filter with width equal to

711   20% of the time lag constant τ_F as in Vömel et al. (2020), their equations (10) and (11). Compared to other common

712   smoothing techniques, e.g. running averages with a time window of 10 seconds (see brown line in Fig. 5), this Gaussian

713   filter still has a slight phase shift with respect to the true signal (I_{OPM}, in red in Fig. 5), but outperforms other tested

714   smoothing algorithms in terms of reducing the noise level. The final smoothed deconvolved signal is shown in green in Fig.

715   5. It is obvious that, after correcting for the slow and the fast times responses in the signal, the resulting current better agrees

716 with the OPM current than the original measured current. It even exhibits small-scale features that are also present in the

717 fast(er) response OPM measurements. The remaining small differences indicate that the conversion efficiency, i.e.

718 stoichiometry of the fast reaction, slightly deviates from one.

**4. Comparison of Ozone Profiles Based on the Conventional Versus Updated Time Responses Correction Method**

720 To test the Time Responses Correction (abbreviated here as TRC) methodology as described in the previous section and a

721 first version in Vömel et al. (2020), we apply the methodology on individual ozonesonde profiles of the different JOSIE

722 simulations and compare those corrected profiles with the corresponding OPM measurements. This method involves the use

723 of the stoichiometry factors S_S from Table 2 for the different ozonesonde-SST pairs and the application of the measured true

724 pump efficiency factors of Nakano and Morofuji (2023) (Table 1). In contrast to this TRC method, ozone partial pressures

725 from profiles are determined according to the "conventional method", as recommended in ASOPOS (GAW Report No. 201;

726 GAW Report No. 268), e.g. using the constant background I_{B1} correction with the Komhyr et al. (1986, 1995) empirical

727 effective efficiency factors (Table 1). The comparisons are made for two different JOSIE campaigns: (i) JOSIE 2009/2010

728 with mid-latitude profiles and well-established ozonesonde preparation procedures, and (ii) the JOSIE 2017 campaign with

729 mostly tropical profiles and good ozonesonde preparation procedures.

730 All comparisons of the TRC with the conventional method are processed as a function of flight time. However, to present the

731 results as vertical profiles, they are mapped on a pressure grid with successive pressure levels of $P_i=0.98 \times P_{i-1}$ between 1000

732 and 5-6 hPa. Hereby, all presented JOSIE experiments are based on a pressure, temperature and ozone profile simulating a

733 balloon ascent velocity of about 5 m/s, such that a quasi-realistic linking between the simulated flight time and pressure scale

734 is obtained.

4.1 Ozone Profiles from JOSIE 2009-2010 for SST1.0 and SST0.5

736 In Figure 6, the relative differences with the OPM for the conventionally (left diagrams) and TRC (right diagrams) processed

737 ozonesonde profiles of JOSIE 2009/2010, respectively, are shown for each pair of sonde (SPC6A or EN-SCI) and solution

738 type (SST0.5 or SST1.0), respectively, including the mean (black solid lines) and its 1σ-standard deviation. The absolute

739 ozone partial pressure differences are presented in the supplementary material (Fig. S3).

740
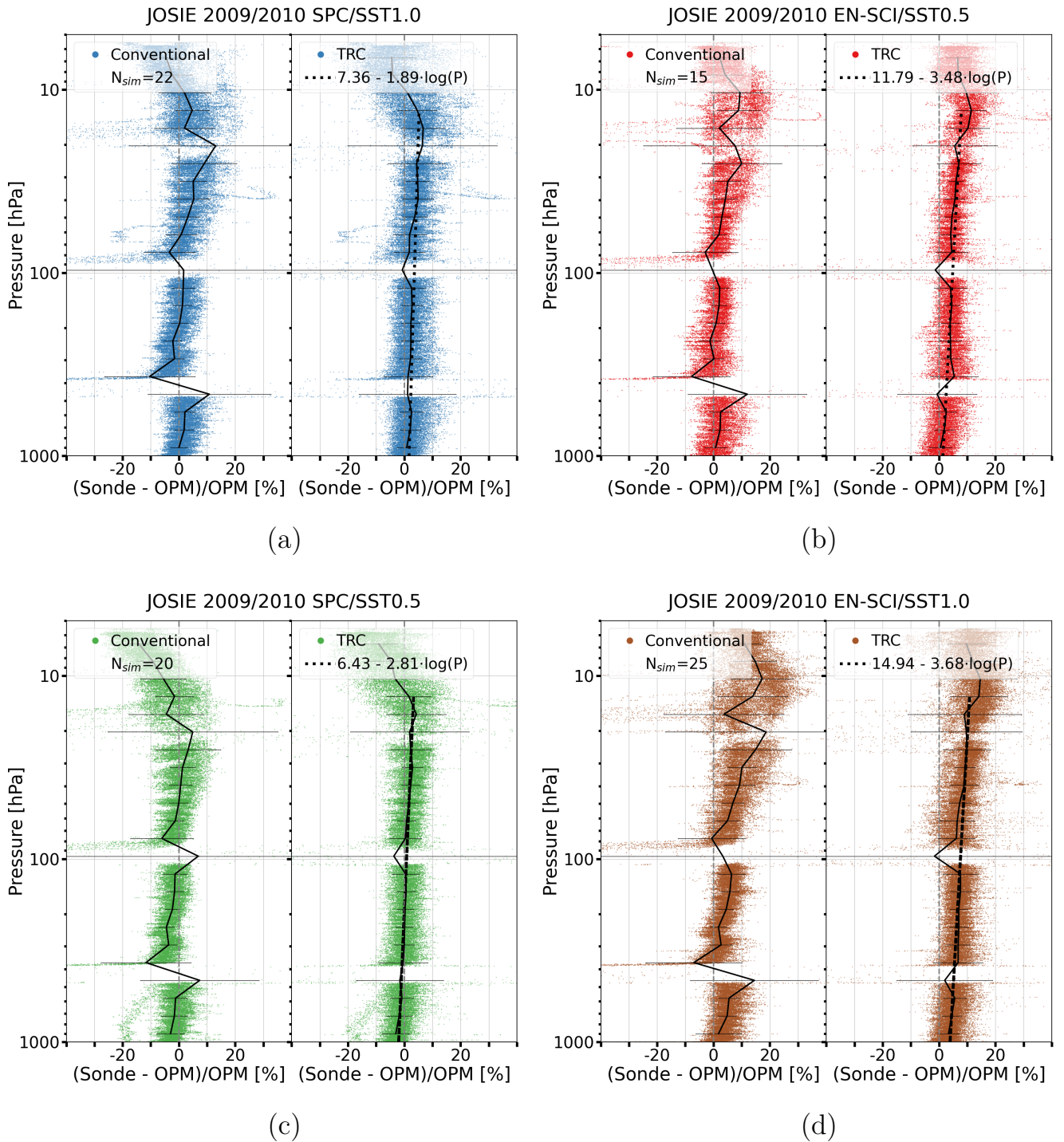
Figure 6 JOSIE 2009/2010: Relative differences with the OPM for the conventional (left diagrams) and TRC (right diagrams) processed ozonesonde profiles for four pairs of sonde type and SST shown as scatter plots in four different colors in the panels a-d: SPC6A/SST1.0 (a: blue dots), EN-SCI/SST0.5 (b: red dots), SPC6A/SST0.5 (c: green dots), and EN-SCI/SST1.0 (d: brown dots), respectively. In each diagram for both methods the mean and 1σ-standard deviation of the relative differences are included (solid black line). The black dashed lines in the TRC-diagrams are the linear regressions of the difference of the ozonesonde to the OPM as function of the pressure (on a ^{10}log scale). A summary plot is provided in Fig. S4, and absolute differences are available in Fig. S3 of the Supplementary material.

For the conventional method, large relative deviations from the OPM exist in the pressure intervals response-time tests (in particular RT1, RT2, RT3) included in a simulation. This can be explained by the difference in response time between the OPM and the ozonesondes and the fact that when ozone concentrations are close to zero, the relative differences will be

23

753   magnified. The TRC method is able to correct well for the time response differences, as illustrated by the small relative
754   differences, although with higher uncertainty (1σ-standard deviation) compared to adjacent pressure levels. A major
755   improvement of the TRC methodology compared to the conventional corrections is the fact that the relative differences with
756   respect to the OPM are almost pressure-independent, hence past ozone exposures. Up to about 13 hPa (Z≈30 km), only a
757   slightly increasing bias with decreasing pressure exists between the overall mean of the TRC-corrected ozonesondes and
758   OPM for the JOSIE 2009/2010 sample (black dashed linear regression lines in Fig. 6).
759
760   At pressures lower than 13 hPa the SPC sondes exhibit a declining behaviour, which is discussed in the next section. Overall,
761   both EN-SCI SST0.5 and SPC SST1.0 agree very well within a few percent, with the TRC methodology using the correct
762   pump efficiencies (see also Fig. S4). Consistent with earlier JOSIE and BESOS campaigns (Smit et al., 2007; Deshler et al.,
763   2008), for both sonde types, SST0.5 gives around 3-5% lower ozonesonde readings than SST1.0, whereas, for both SSTs,
764   SPC ozonesondes read ~ 3-5% lower than EN-SCI.
765

766   **4.2 Ozone Profiles from JOSIE 2017 for SST1.0, SST0.5, and SST0.1**

767   During the JOSIE 2017 campaign, tropical ozone profiles were simulated for three different SSTs: SST1.0, SST0.5 and
768   SST0.1 (Thompson et al., 2019). No time-response tests were performed during these simulations. Therefore, for SST1.0 and
769   SST0.5, the stoichiometry factors, S_S, derived from the JOSIE2009/2010 data have been applied. However, the SST0.1
770   solution was not tested during the JOSIE 2009/2010 campaign. Therefore, for this SST, we determined the stoichiometry
771   factors S_S with the same method as described in Sect. 3.2.1, but with time-response tests during ozonesonde laboratory
772   measurements with a calibrated ozone analyser (details in Appendix B). The derived S_S factor is 0.023 ± 0.005. For the
773   JOSIE 2017 campaign data, the initial value of the slow current component I_S at the start of the simulation at t=0 (Sect.
774   3.2.2) has been chosen to equal 0 (i.e. equal to I_{B0} before subtracting I_{B0}), as there were usually a few hours between the end
775   of the day of launch preparations and the start of the simulation, such that I_{B1} has decayed to I_{B0}.
776

777   The differences of the JOSIE 2017 ozonesonde profiles with the corresponding OPM profile using the conventional and TRC
778   data processing methodologies are shown in Figure 7; the absolute differences appear in Fig. S5. The most prominent feature
779   for the conventional corrections, sonde type-SST combinations, is the dependence of the sonde to OPM differences on
780   pressure or measured ozone amounts: the mean relative differences are largest (as well as the corresponding standard
781   deviations) just below the tropopause at ~(100-200) hPa, where the ozone partial pressures are minimal. The mean relative
782   differences increase with decreasing pressure in both troposphere and stratosphere (also obvious in Fig. S6) and are most
783   pronounced in the Tropics, where the ozone concentrations can be very low near the tropopause. In contrast, when the TRC-
784   method is applied to the data, the pressure/ozone amount dependence of the relative difference almost completely disappears.
785   For the standard EN-SCI/SST0.5 and SPC/SST1.0, there remains a slightly increasing bias with decreasing pressure (black
786   dashed lines), while for the SST0.1 ozonesonde simulations, there is a tendency for decreasing (negative) relative differences
787   with decreasing pressure. For both SPC and EN-SCI, SST0.1 ozone readings are slightly lower than the OPM measured
788   ozone concentrations in the stratosphere, and up to 10% lower than the ozone values measured with the SOP recommended
789   solutions (SPC/SST1.0 and EN-SCI/SST0.5).
790

(a)

(b)

(c)

(d)
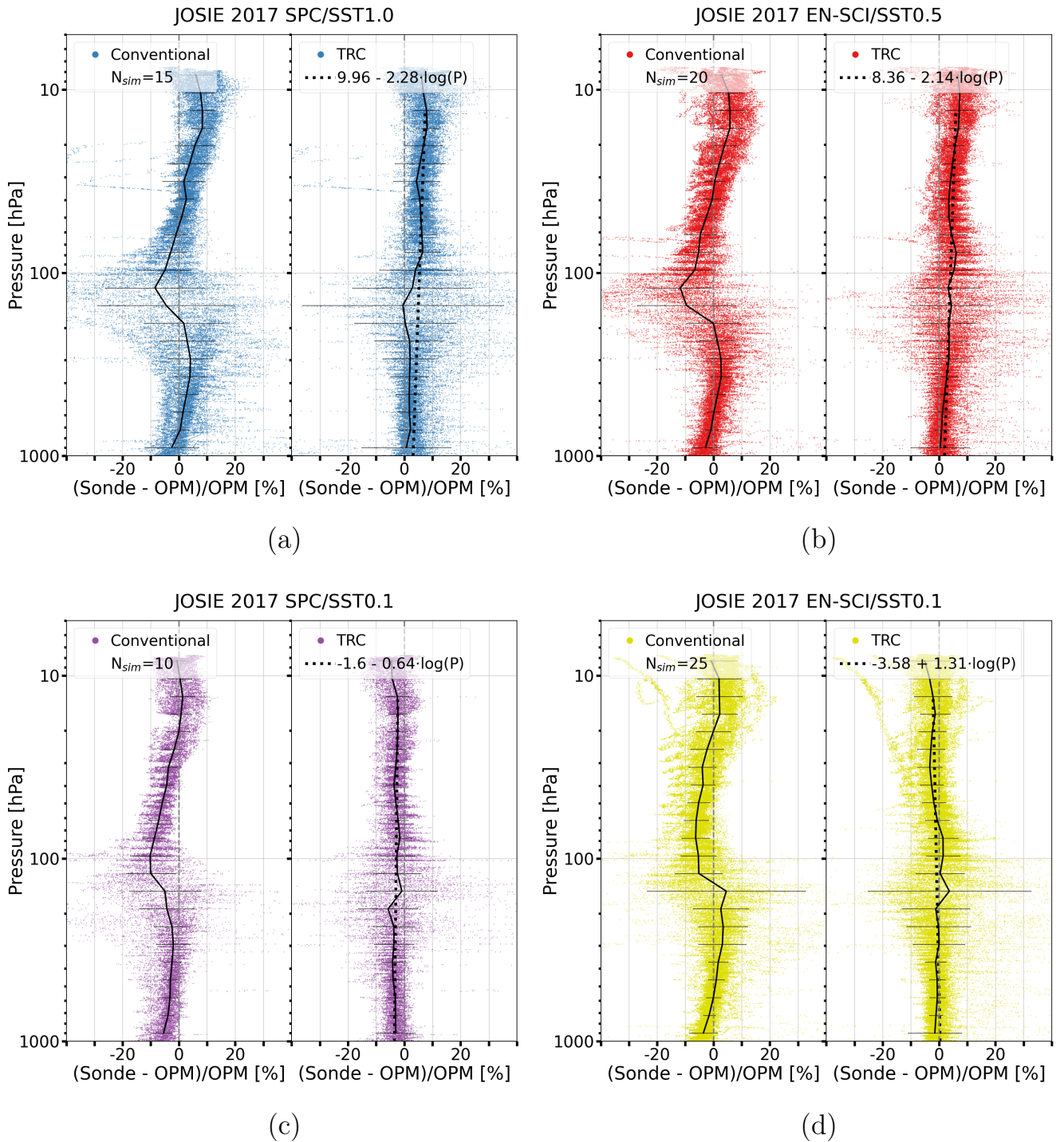
Figure 7. JOSIE 2017: Differences with the OPM for the conventionally (left) and TRC (right) processed ozonesonde profiles for the four sonde-SST pairs as scatter plots: SPC6A/SST1.0 (a: blue dots), EN-SCI/SST0.5 (b: red dots), SPC6A/SST0.1 (c: purple dots), EN-SCI/SST0.1 (d: yellow dots). In each diagram for both methods, mean and 1σ-standard deviations are solid black lines. The black dashed lines in the TRC-diagrams are the linear regressions of the sonde-OPM differences as a function of the pressure on a ^{10}log scale. A summary plot appears in Fig. S6 and absolute differences are in Fig. S5 of Supplementary material.

When comparing the mean relative OPM offsets after processing the ozonesonde measurements with TRC methodology for the two JOSIE campaigns, i.e. Figs. 6 and 7 (also in Figs. S4 and S6), we note that the network standards SPC/SST1.0 and EN-SCI/SST05 are a few percent larger in the stratosphere for the "tropical" JOSIE 2017 campaign. That is, those mean relative differences are manifest in both cases as a slightly decreasing relative bias with increasing pressure during both

25

campaigns. These differences are independent of post-ozone exposure and profile type (mid-latitude or tropical), in contrast to the conventional methodology which exhibits this past ozone memory effect. A striking disagreement between the profile-OPM offsets between JOSIE 2009/2010 and 2017 occurs at the lowest pressure range, lower than ~13 hPa. For the JOSIE 2009/2010 data, the mean relative differences with the OPM display a stronger pressure dependence in this lowest pressure range, distinctly different for both sonde types, in contrast to the JOSIE 2017 mean relative OPM differences. The origin of this different behaviour above 13 hPa lies most likely in pump temperature differences between the simulated profiles. Whereas the mean pump temperature is close to 21°C in this pressure range in JOSIE 2009/2010, it is around 15°C for the tropical profiles in JOSIE 2017. Simultaneous temperature measurements during JOSIE 2017 revealed that the cell temperatures are about 5 to 10°C lower than the corresponding pump temperatures, depending on the sonde type. Specifically, the differences between pump and cell temperature are more at the high-end range of this temperature interval for EN-SCI sondes, and at the low end range for the SPC due to differences in thermal contact between cells and pump. With these cell temperatures and taking the boiling temperatures at those low pressures into account, it turns out that the solutions in the SPC sondes tested in JOSIE 2009/2010 may already start boiling at higher ambient air pressures than during JOSIE 2017. Cell weights were measured before and after all simulations for both campaigns. The weight loss due to evaporation/boiling of the sensing solution was considerably higher during JOSIE 2009/2010 than in JOSIE 2017: about a factor of 2 for EN-SCI/SST0.5 and even a factor of 3 for SPC/SST1.0. Although at these reduced ambient air pressures the absorption efficiency is not critical (Tarasick et al., 2021), the sensing solutions losses of the sondes may have become so large during JOSIE 2009/2010 that the absorption efficiency has non-negligibly declined. This may explain the underestimation of the ozone concentrations at low pressures for the JOSIE 2009/2010 profile simulations, in particular for SPC ozonesondes.

5 Conversion Efficiency of TRC Method Calibrated to OPM

5.1 Differences Between Different Pairs of Sonde Type and SST

In the previous section it was shown that the TRC-method resolves the dependence of the measured ozonesonde profile from the past ozone exposure, whereas the deconvolution of the remaining fast ozone sensor current resolves effectively the impact of gradients in the profile caused by the 20-30 sec time response of the ECC-sensor. The sonde to OPM comparisons presented in section 4 for the mid-latitude profiles of JOSIE 2009/2010 (Fig. 6) and tropical profiles of JOSIE 2017 (Fig. 7) demonstrate that the TRC results are independent of the shape of the simulated ozone profiles, in contrast to the results obtained by the conventional method (e.g. Smit et al., 2007; Deshler et al., 2008, 2017; Thompson et al., 2019).
For each pair of ozone sonde type and SST for JOSIE 2009/2010, JOSIE 2017 and combined JOSIE 2009/2010 and 2017 (for SPC/SST1.0 and EN-SCI/SST0.5) a linear regression has been calculated as a function of pressure on a logarithmic scale for the TRC sonde-OPM relative differences within ±30% for pressures up to 13 hPa. These linear regression lines are shown in Figs. 6 and 7 as black dashed curves in the TRC diagrams for the different sonde-SST pairs; they agree well with the corresponding averages (black solid lines in TRC diagrams). All TRC-sonde/SST pair relative difference scatterplots display variations within 3-7% with altitude between the surface at P=1000 hPa and the upper end of the profile at P=10 hPa, as can be seen in Table 3 that displays the relative sonde-OPM differences at the intercepts P=1000 hPa and P=10 hPa of the linear regression. Table 3 illustrates the same typical differences of 3-5% for the same sonde type but different SST1.0 or SST0.5, as first observed in JOSIE 2000 (Smit et al., 2007). Figures S4 (a & b) and S6 (a and b) show the persistence of these systematic differences in detail for the conventional and TRC method as function of pressure (i.e. altitude). The low buffered (SST0.1) EN-SCI or SPC-6A sondes slightly underestimate ozone by a few percent compared to the OPM. It is noteworthy that the EN-SCI/SST0.1 OPM offsets decrease over the course of the sounding, in contrast to all other sonde-SST pairs for which the relative differences increase (Table 3: last column).

Table 3. Relative differences of the sonde to the OPM at the P= 1000 hPa and P=10 hPa intercepts of the linear regression as a function of $Log_{10}(P)$ obtained from the different JOSIE data sets (Figs. 6-7) and for the sonde pairs SPC-6A and EN-SCI with different sensing solutions SST1.0, STT0.5 and SST0.1. Included are also the relative differences between EN-SCI and SPC6A sondes when operated at the same SST (last three rows).

Data set	Number of Samples	Rel. Differences in % Sonde to OPM at intercept P=1000 hPa	Rel. Differences in % Sonde to OPM at intercept P=10 hPa	Rel. Differences in % Sonde to OPM between P is 1000 and 10 hPa
	SPC-6A /SST1.0			
JOSIE 2009/2010	23	1.69	5.47	3.8
JOSIE 2017	11	3.12	7.68	4.6
JOSIE 2009/2010 + 2017	34	2.26	6.44	4.2
	SPC-6A /SST0.5			
JOSIE 2009/2010	20	-2.0	3.62	5.6
	SPC-6A /SST0.1			
JOSIE 2017	6	-3.52	-2.24	1.8
	EN-SCI /SST1.0			
JOSIE 2009/2010	25	3.89	11.26	7.4
	EN-SCI /SST0.5			
JOSIE 2009/2010	15	1.35	8.30	7.0
JOSIE 2017	20	1.93	6.21	4.3
JOSIE 2009/2010 + 2017	35	1.72	7.02	5.3
	ENSCI /SST0.1			
JOSIE 2017	20	0.35	-2.27	-2.6
SST	EN-SCI – SPC6A			
SST1.0		1.63	4.82	3.2
SST0.5		3.92	3.40	-0.5
SST0.1		3.87	0.03	-3.4

Further, the TRC results show a strong consistency of the mean relative differences with the OPM for the different sonde types-SST combinations across the different (grouped) JOSIE campaigns (see also Figs. S4 and S6). Therefore, those relative mean differences can be characterized by the linear regression curves as a function of $Log^{10}(P)$ in Figs 6-7 and directly linked to the OPM. As such, these linear regression lines (hereafter referred to as "calibration curves") could be applied as the final correction step of the TRCC methodology, tracing the ozonesonde measurements back to the OPM as the reference instrument.

5.2 Parameterisation of the Overall Conversion Efficiency η_C

The linear regressions of the relative differences of the sonde to the OPM (Figs. 6-7) of the TRC method can be interpreted as the correction term of the overall conversion efficiency η_C when deviating from one for each of the different pairs of sonde type and SST. The overall conversion efficiency η_C in Eq. (6) can be expressed as a function of the ambient air pressure of the vertical sounding:

$$\eta_C(P) = 1 + F_C(P) \tag{17}$$

where $F_C(P)$ is the so-called correctional term of η_C as a function of the ambient air pressure P, which is parameterised by the linear regression fit of the relative sonde-OPM deviations as a function of $Log_{10}(P)$ and substituted in Eq. (17). This means that the overall conversion efficiency $\eta_C(P)$, calibrated to the OPM, has the following parameterisation

$$\eta_C(P) = 1 + a + b \cdot Log_{10}(P) \tag{18}$$

The linear regression curves derived for the different pairs of SPC-6A, EN-SCI with SST1.0, SST0.5, or SST0.1 obtained for the different JOSIE campaigns are shown in the TRC diagrams of Figs. 6-7 by the black dashed line. From Fig. 6-7 and Table 3, it is obvious that the relative OPM offsets (and the resulting linear regressions) for the same pairs of sondes and SST05 or SST1.0 are very similar in JOSIE 2009/2010 and JOSIE 2017. Thus, to achieve the best statistics, the results for those campaigns are lumped together in Fig. 8.

The results of the parameterisation of $\eta_C(P)$, i.e. the offset a and the slope b (Eq.18), including their uncertainties Δa and the slope Δb, respectively, are listed for the different pairs of sonde type and SSTs as JOSIE (2009/2010 + 2017) in Table 4. The sonde/SST pairs operated with SST0.5 and SST1.0 cover mid-latitude as well as tropical ozone profile conditions, i.e. the resulting $\eta_C(P)$ functions are independent of the ozone profile. Based on this, we expect that the $\eta_C(P)$ for the SST0.1, which could only be derived in this study for the tropical JOSIE-2017 conditions, can also be applied to non-tropical ozone profiles. Likewise, we expect that the $\eta_C(P)$ determined from JOSIE 2009 only for the SPC/SST0.5 and EN-SCI/SST1.0 pairs are valid for tropical ozone profiles. Of course, the derived linear regression coefficients for the calibration functions are directly linked to the pump efficiency values used, and it is assumed here that the used average pump efficiency values from Nakano and Morofuji (2023) in Table 1 are correct within their uncertainties and representative for this study. However, if these pump efficiency values might change over time (see Nakano and Morofuji, 2023), the calibration functions must be adjusted accordingly.

The calibration functions are presented here (Table 4) as a function of pressure, but this does not mean that they are really pressure dependent. However, the goal is to provide a practical empirical representation of the overall performance of the ozonesonde, ascending with a balloon at ~5m/s. The calibration functions can thus be interpreted as the correction term of the overall conversion efficiency of the ECC sonde when deviating from one, but their origin is still unclear. Most likely this term relates to the unknown stoichiometry of the fast chemical reactions converting ozone into free iodine, in other words, the fast ECC current I_F. This is supported by the shape of the vertical profiles of the absolute P_{O3}-differences of the ECC sonde compared to the OPM for the TRC, shown for the JOSIE 2009/2010, JOSIE 2017 and for the JOSIE 1996-2002 data (described in section 5.3), in the middle diagrams of Figures S3, S5 and S7, respectively. Indeed, in the middle stratosphere, the shapes of the residual currents compared to the OPM are more or less in phase with the simulated ozone profiles. This is most pronounced for the JOSIE-2017 tropical profiles (Fig. S5) and might indicate that these residual currents result from the fast chemical conversion and not from the 25-min delayed slow reaction. In the latter case, a phase shift between the residual currents and the ozone profile would be expected. The observed increase with altitude of typical 3-7% in the calibration functions (Tables 3 & 4) might be explained from a small slightly increasing change of the stoichiometry of the fast O_3 conversion due to an increase of KI concentration and buffer strength caused by evaporation during the sounding.
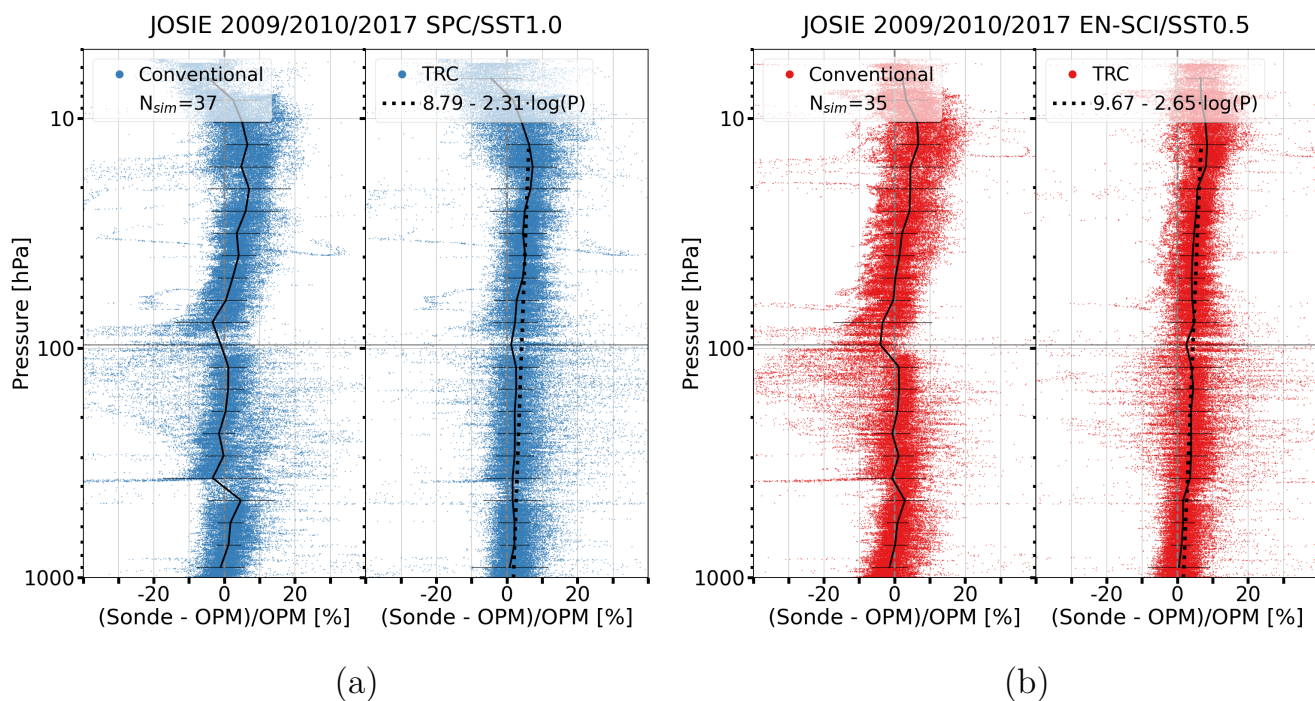
Figure 8. JOSIE 2009/2010 and 2017: Relative differences with the OPM for the conventional (left diagrams of panels (a) and (b)) and TRC (right diagrams of panels (a) and (b)) processed ozonesonde profiles for two pairs of sonde type and SST shown as scatterplots for SPC6A/SST1.0 (a: blue dots) and EN-SCI/SST0.5 (b: red dots), respectively. In each diagram for both methods the mean and 1σ-standard deviation are included (solid black line). The black dashed lines in the TRC-diagrams are the linear regressions of the differences of the ozonesonde to the OPM as function of the pressure (on a ^{10}log scale).

Although the cell temperatures of the ozonesondes (both SPC6A/SST1.0 and EN-SCI/SST0.5) in JOSIE. 2009/2010 were about 10 °C higher than in JOSIE 2017 there are no direct indications that there is any cell temperature dependence of the calibration functions. This is demonstrated by the fact that SPC6A/SST1.0 and EN-SCI/SST0.5 for both campaigns show very similar OPM deviations over the course of the sounding when compared at the intercept points at P=1000 and 10 hPa (Table 3). However, temperature dependence cannot be completely excluded, in as much as the chemical reactions involved in the KI+O_3 chemistry may have significant temperature dependencies. Again, further in-depth investigations are needed.

Table 4. Parameterisation (offset a and slope b) of the calibrated conversion efficiency η_C (P) (Eq. 18) for the different pairs of SPC-6A or ENSCI with SST1.0, SST0.5, or SST01 derived from the results of JOSIE 2009/2010 and JOSIE 2017. Included are the 1σ-uncertainties Δa and Δb of the offset a and slope b in Eq. 18, respectively. The parameterisation of η_C (P) is valid from P=1000 hPa until P=13 hPa (Z≈30 km) for SPC, and for EN-SCI to 10 hPa (Z≈32-33km).

Sonde Type / SST	Number of Samples	TRC-Conversion Efficiency $\eta_C(P) = 1 + a + b \cdot Log_{10}(P)$ Eq. (18)		JOSIE Data Set
		Offset $a \pm \Delta a$	Slope $b \pm \Delta b$	
SPC-6A /SST1.0	37	$(8.79 \pm 0.07) \times 10^{-2}$	$(-2.32 \pm 0.03) \times 10^{-2}$	JOSIE (2009/2010 + 2017)
SPC-6A /SST0.5	20	$(6.43 \pm 0.08) \times 10^{-2}$	$(-2.81 \pm 0.04) \times 10^{-2}$	JOSIE 2009
SPC-6A /SST0.1	10	$(-1.60 \pm 0.12) \times 10^{-2}$	$(-0.64 \pm 0.05) \times 10^{-2}$	JOSIE 2017
EN-SCI /SST1.0	25	$(14.94 \pm 0.07) \times 10^{-2}$	$(-3.68 \pm 0.03) \times 10^{-2}$	JOSIE 2009
EN-SCI /SST0.5	35	$(9.67 \pm 0.06) \times 10^{-2}$	$(-2.65 \pm 0.03) \times 10^{-2}$	JOSIE (2009/2010 + 2017)
EN-SCI /SST0.1	20	$(-3.58 \pm 0.09) \times 10^{-2}$	$(1.31 \pm 0.04) \times 10^{-2}$	JOSIE 2017

5.3 Application to JOSIE 1996 + 1998 + 2000 + 2002 data

The calibrated η_C(P) functions derived from JOSIE 2009/2010 and JOSIE 2017 (Table 4) for the different sonde/SST pairs are applied to TRC processed ozonesonde data of JOSIE 1996 + 1998 + 2000 + 2002, in Figure 9, again as relative differences to the OPM. In the remainder of this paper, we will use the abbreviation TRCC to denote that the TRC method has been applied with additional application of the calibration functions. The JOSIE 1996 + 1998 + 2000 datasets and results were described in detail by Smit and Kley (1998) and Smit and Sträter (2004a, 2004b) and analysed by Smit et al. (2007). For JOSIE 1996, we excluded data from NOAA and CNRS because their operating procedures deviated too greatly from the Komhyr (1986) procedures; JOSIE 2002 was a small campaign in which only 3 simulation runs were made with 10 SPC/SST1.0 sondes. The setup of the earlier campaigns was similar to the JOSIE 2009/2010 or JOSIE 2017 experiments. In the earlier campaigns mostly mid-latitude ozone profiles were simulated with the same four combinations of EN-SCI or SPC with either SST0.5 or SST1.0 (although the sample sizes with SST0.5 were rather small). The largest difference between JOSIE 2009/2010 and the early JOSIE campaigns lies in the preparation of the ozonesondes: in JOSIE 2009/2010, the same SOPs were followed by the three operators; ozonesondes "flown" in the earlier JOSIE-campaigns being prepared by different teams of people with a variety of SOPs.

The comparisons with the OPM in Fig.9 are displayed for the TRC results, hence not calibrated (η_C(P) = 1.00, middle diagrams) and for the TRCC corrections, i.e. calibrated (η_C(P) from Table 4, right diagrams), while the results for the conventional method (left diagrams) are also included. From the figure it is obvious that independent of the sonde type (SPC-6A or EN-SCI) or sensing solution type (SST1.0, SST0.5), after applying η_C(P) the residual average curves (black solid lines) are within less than ±1% deviation from the "zero" over the entire vertical profile until 7-10 hPa. This means that with the TRCC, i.e TRC combined with the use of the specific η_C(P) for the various sonde-SST pairs, there are no longer systematic bias effects in the measured vertical ozonesonde profiles with respect to the OPM as a function of pressure (i.e. altitude). The use of the TRCC can be a powerful tool to homogenize long term ozone records in the global ozonesonde network, so that these are now traceable to one reference standard, i.e. the OPM at the WCCOS. The application of the TRCC with the use of the calibration functions on the JOSIE 2009/2010 and JOSIE 2017 datasets is also illustrated in the figures S3, and S5 in the Supplementary Material, showing the vertical profiles of the absolute differences of the sondes with

30

the OPM for the conventional method, TRC and TRCC. This information is also provided for the absolute differences for the

953 early JOSIE campaigns in Fig. S7.

954

(a)

(b)

(c)

(d)
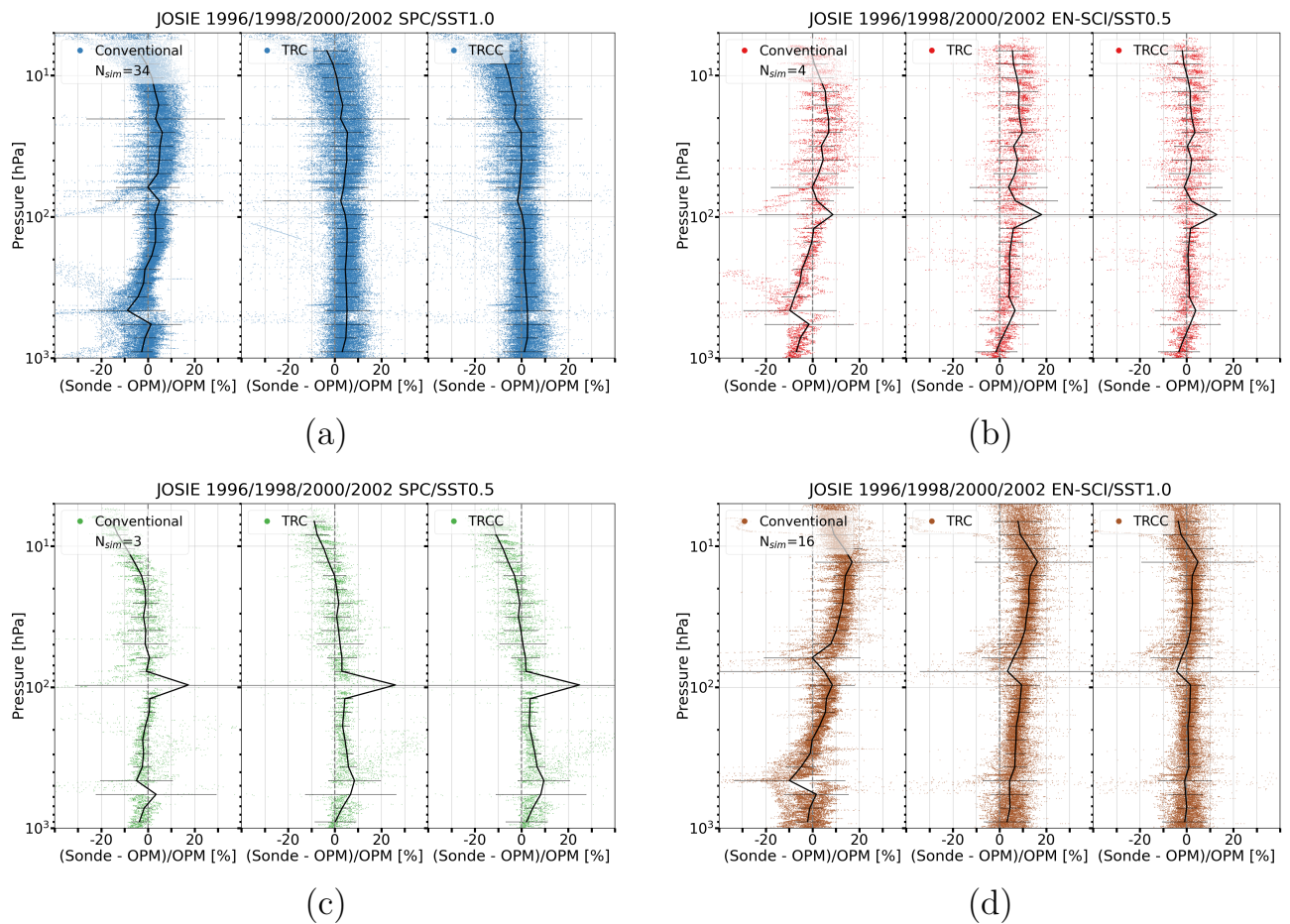
955

956

957 **Figure 9.** JOSIE 1996 +1998 + 2000 + 2002: Relative differences [%] with the OPM for the "conventional" (left diagrams

958 of panels a-d), "TRC" (middle diagrams of panels a-d), and "TRCC " = TRC + application of calibration functions" (right

959 diagrams of panels a-d) processed ozonesonde profiles for four pairs of sonde type and SST, shown as scatter plots in four

960 different colours in the panels a-d: SPC6A/SST1.0 (a: blue dots), EN-SCI/SST0.5 (b: red dots), SPC6A/SST0.5 (c: green

961 dots), and EN-SCI/SST1.0 (d: brown dots), respectively. In each diagram for both methods the mean and 1σ-standard

962 deviation of the relative differences are included (solid black line). The absolute difference plots are available in the

963 Supplementary Material (Fig. S7), and a summary plot of the relative differences in Fig. S8.

964

965

6. Contribution Individual Correction Steps and Uncertainty Budget of the TRCC Method

In this section we quantify the impact of the individual corrections made in the TRCC method and estimate their uncertainty contributions to the overall uncertainty of the ozone partial pressure derived from the measured ECC-ozone sensor current.

6.1 Contribution of Correction Steps of TRC-Method for Mid-Latitude and Tropical Conditions

To derive from the measured cell current I_M the partial ozone pressure in the ambient air the TRCC method includes five different corrections: (i) constant background current I_{B0}; (ii) slow cell current I_S; (iii) time lag of fast current I_F: deconvolved fast cell current (incl. smoothing); (iv) true pump efficiency (Nakano and Morofuji, 2023); (v) calibrated conversion efficiency η_C (P) (Eq. 18 and Table 4). The impact of the different corrections on the measured cell current as a function of pressure (i.e. Log^{10} (P)) is shown in Figure 10 for mid-latitude (JOSIE 2009/2010) and tropical (JOSIE 2017) vertical profile conditions for the standard sonde type –SST pairs, SPC6A/SST1.0 and EN-SCI/SST0.5, respectively; included are in addition examples of the different corrections made using the conventional method for JOSIE 2009/2010 and JOSIE 2017, respectively.

A first, obvious, observation to make is that the corrections for a decreasing pump efficiency are for all sonde type- SST pairs identical and at pressures smaller than 100 hPa increase slowly but significantly from 1 % at P=100 hPa to 12% at P = 10 hPa and to almost 20 % at P = 5 hPa. In the upper part of the profile (above 25 hPa) it is the dominating correction. In the lower part, below 100 hPa , the constant background I_{B0} (brown line) and the past ozone dependent slow cell current I_s (yellow line) are the major corrections, particularly in the upper tropical troposphere, with its very low ozone concentrations (diagrams f and g). Here, those corrections can amount up to about 10-15%, depending on e.g. the amplitude of the measured I_{B0} values. In this context, we also note that, because of the larger S_S values for SPC6A/SST1.0, the past ozone dependent slow current (I_S) correction will be about a factor of 2 larger than the I_S correction for the ENSCI/SST0.5, in all diagrams of Fig. 10. On top of this effect, for SPC6A/SST1.0 JOSIE 2009/2010 (diagram b in Fig. 10), above 10 hPa, the relative I_S correction is even rapidly increasing in absolute value due to the limited performance of the SPC6A sonde due to substantial losses of the sensing solution caused by boiling effects, as explained before in section 4.2. The impact of the time lag correction of the fast current is of the order of $\pm$ 5 %, and of course strongly dependent on the local vertical ozone gradient. Therefore, it can even become the dominant correction in the tropical UTLS region (between 5-10%), with its strong vertical ozone gradient (diagrams f-g). Finally, we mention that very similar results are obtained for the ozonesonde types combined with SST0.1, which are shown in the supplementary material (Fig. S9).

All individual corrections of the TRCC method are based on known physical and chemical processes, with one exception being the remaining conversion efficiency, which was derived from calibration of the TRC-corrected probe readings with the OPM reference instrument. This contrasts with the corrections made in the conventional method (Fig.10-d, g), which were empirically derived to achieve a total ozone normalization factor close to one. Therefore, the following corrections are applied: (i) an empirical effective efficiency function (Fig. 10, blue line in graphs (d) and (g)) that represents the estimation of a decreasing pump efficiency and an increasing conversion efficiency (i.e. increasing stoichiometry of O_3+KI redox reaction (R1) at lower pressures); (ii) a background current I_{B1} correction that compensates for excessive ozone levels near the surface. However, in the tropics the I_{B1} correction is too large (Fig. 10-g: brown line) and leads to significantly too low ozonesonde values in the troposphere (Fig. S9-f in the Supplement).
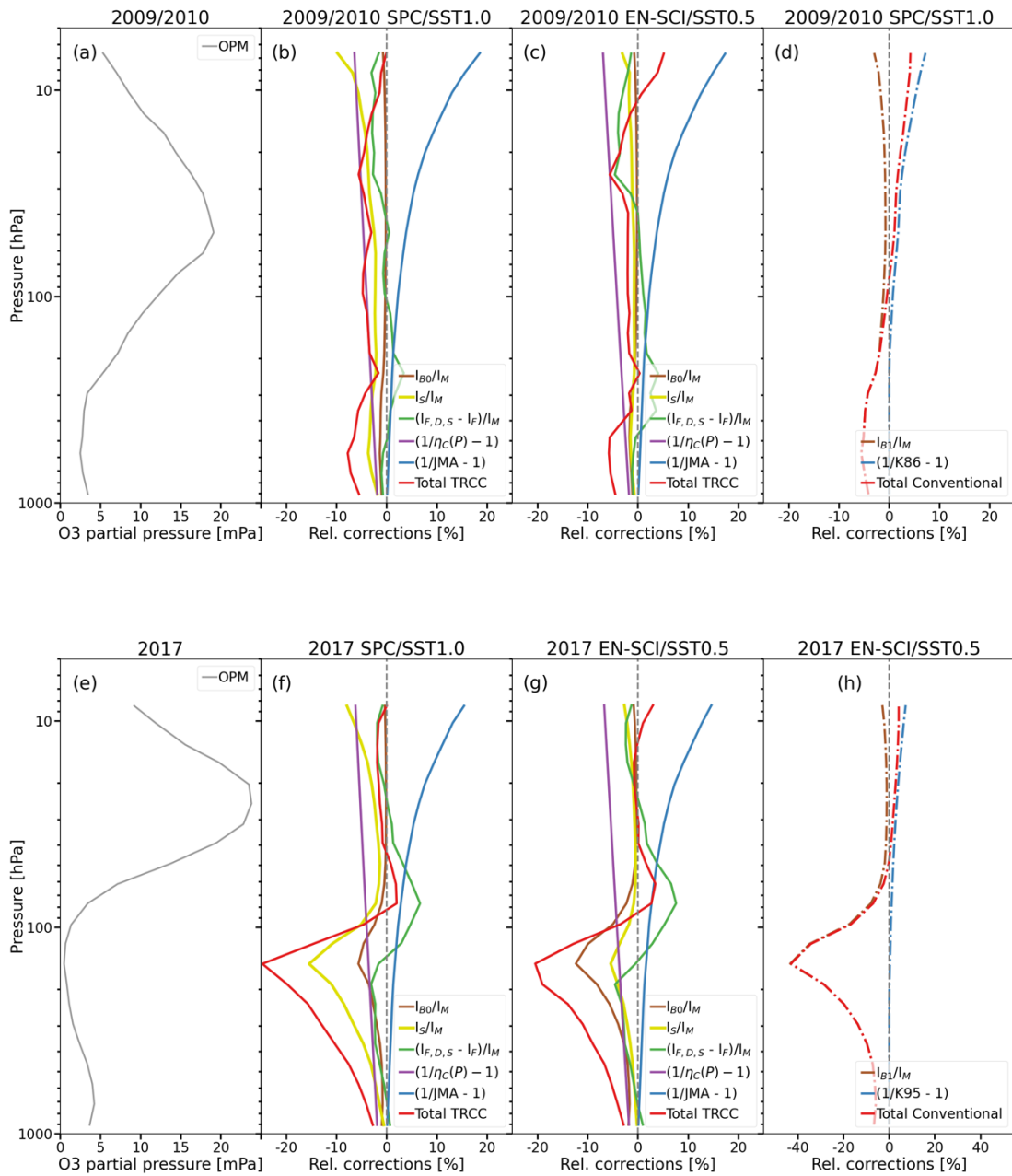
Figure 10. Relative corrections of TRCC method for typical mid-latitude (upper diagrams (a), (b), (c): JOSIE 2009/2010) and tropical (diagrams (e), (f), (g): JOSIE 2017) ozonesonde profiles, respectively, showing the influence of the different correction steps for the new TRCC method for SPC/SST1.0 (diagrams (b) and (f)) and EN-SCI/SST0.5 (diagrams (c) and (g)). The total correction (red line) consists of: (i) I_{B0} (brown line); (ii) I_S (yellow line); (iii) De-convolved and smoothed I_F (green line); (iv) True pump efficiency (blue line: Nakano and Morofuji, 2023); (v) Calibrated conversion efficiency (purple line). Diagrams (d) and (h) show the relative corrections of the conventional method for JOSIE 2009/2010 (SPC/ SST1.0) and JOSIE 2017 (EN-SCI/SST0.5), respectively; total correction (red line) consists of: (i) I_{B1} (brown line); (ii) empirical effective efficiency (blue line: Komhyr (1986) for SPC and Komhyr et al (1995) for EN-SCI, respectively).

6.2 Uncertainty Budget of the TRC Method

For the conventional method a detailed uncertainty budget has been studied by Tarasick et al. (2021) and described in detail in the GAW 268 Report (Eq. E-3-1), together with practical guidelines to determine the overall uncertainty from the individual instrumental and procedural contributions. It is assumed that the uncertainties are random, uncorrelated, and normally distributed and following Gaussian statistics. In case of the TRCC, the overall relative uncertainty of P_{O3} is derived from Eq. (6), which has slightly changed compared to formula E-3-1 in GAW#268 (2021) as follows:

$$\frac{\Delta P_{O3}}{P_{O3}} = \sqrt{\left(\frac{\Delta\eta_P}{\eta_P}\right)^2 + \left(\frac{\Delta\eta_A}{\eta_A}\right)^2 + \left(\frac{\Delta\eta_C}{\eta_C}\right)^2 + \frac{(\Delta I_F)^2}{(I_F)^2} + \left(\frac{\Delta T_P}{T_P}\right)^2 + \left(\frac{\Delta\Phi_{P0}}{\Phi_{P0}}\right)^2 + \sum\varepsilon_i^2} \tag{19}$$

The additional term ε_i represents additional random uncertainties (Tarasick et al., 2021); in case of the TRCC these can be e.g. the relative uncertainty contributions by the used numerical schemes of either the convolution to obtain $I_S(t)$ or the deconvolution of $I_F(t)$ and its additional smoothing.

To determine the uncertainty budget for TRCC in Eq. (19) the uncertainty contributions $\Delta\eta_P$, $\Delta\eta_A$, ΔI_M, ΔI_{B0}, ΔT_P, and $\Delta\Phi_{P0}$ are exactly the same as in GAW Report No. 268 (2021) following the guidelines in its Annex-C. However, the recipes to determine the uncertainty contributions of the time varying $I_F(t)$, and the pressure dependent $\eta_C(P)$ (see Table 4) differ from GAW#268:

Uncertainty contribution ΔI_F:

From Eq. (7) the relative uncertainty of the fast sensor current $I_F(t)$ can be derived:

$$\frac{\Delta I_F(t)}{I_F(t)} = \sqrt{\frac{(\Delta I_M)^2 + (\Delta I_{B0})^2 + (\Delta I_S)^2}{(I_M - I_{B0} - I_S)^2}} \tag{20}$$

Here $\Delta I_{B0} \approx 0.01$ µA, obtained from the I_{B0} time series from Uccle. $I_S(t)$ estimations by varying the slow time constant with $\Delta\tau_S = \pm 5$ minutes has shown that $\Delta\tau_S$ only has a minor contribution to $\Delta I_S(t)$ of less than 1%, while a potential contribution of the numerical convolution scheme itself is vanishing small. It is obvious that $\Delta I_S(t)$ is predominantly determined by the uncertainty ΔS_S of the stoichiometry S_S of the slow reaction path (Table 2) as:

$$\Delta I_S(t) \approx \frac{\Delta S_S(t)}{S_S(t)} \cdot I_S(t) \tag{21}$$

The impact of the slow time constant τ_S on the stoichiometry S_S and its uncertainty ΔS_S is also insignificant, as we assessed by varying $\Delta\tau_S = \pm 5$ minutes. Further, any contribution of the numerical schemes of deconvolution and its additional smoothing to the uncertainty of I_F have been checked and appeared to be vanishingly small (< 0.5%).

Uncertainty contribution $\Delta\eta_C$:

The conversion efficiency $\eta_C(P)$ (Eq. 18) has been calibrated to the OPM such that its uncertainty $\Delta\eta_C(P)$ includes also the uncertainty of the $P_{O3,OPM}$ measurement by the OPM as follows

$$\frac{\Delta\eta_C(P)}{\eta_C(P)} = \sqrt{\frac{(\Delta a)^2 + (Log_{10}(P) \cdot \Delta b)^2}{(\eta_C(P))^2} + \left(\frac{\Delta P_{O3,OPM}(P)}{P_{O3,OPM}(P)}\right)^2} \tag{22}$$

Hereby $\frac{\Delta P_{O3,OPM}(P)}{P_{O3,OPM}(P)}$ is the relative uncertainty of the $P_{O3,OPM}$ measurement of the OPM which is estimated to be better than 2 % at $P > 10$ hPa, and with lower pressures slightly increasing to 3 % until $P = 5$ hPa through potential small wall losses at these pressures. The reported relative uncertainty values here for the OPM are about 1.5 % better than the values mentioned before by Proffitt et al. (1983) because of the seven times smaller uncertainty of the new UV-absorption cross-section (Hodges et al., 2019) compared to the former cross-section (Hearn et al., 1961) that was used before to derive the P_{O3} measurement of the OPM.

The overall uncertainty budget for the TRCC method is summarized in Table 5. Figure 11 shows the contributions of the different uncertainty sources to the uncertainty budgets for the SPC6A/SST1.0 and EN-SCI/SST0.5 when applying the

1059 TRCC method for a typical mid-latitude and tropical ozone profile as used in JOSIE 2009/2010 and JOSIE 2017,

1060 respectively. The results for SPC6A/SST0.5 and EN-SCI/SST1.0 for JOSIE 2009/2010 and the low buffered SPC6A/SST0.1

1061 and EN-SCI/SST0.1 for JOSIE 2017 are shown in Figure S10 in Supplementary Material. For the sake of clarity, the

1062 uncertainty contributions due to (i) ascent rate variation, (ii) pressure uncertainty, (iii) total ozone normalization factor are

1063 not included here, as these are beyond the scope of this study. However, the characteristics of these uncertainty

1064 contributions, as reported by Tarasick et al. (2021) and GAW Report No. 268, would not change the uncertainty budget of

1065 the TRC method itself.

1066

1067 **Table 5.** Sources of ozonesonde profile uncertainty and their estimated magnitudes for the TRCC method. All quoted

1068 uncertainties are one standard deviation (1σ). (*) To approximate ΔS_S as a one standard deviation uncertainty the MAD

1069 values (only covering 25-75 percentiles) in Table 2 have been multiplied by 1.5 to become compatible with the Gaussian

1070 error propagation applied here.

1071

Source	Uncertainty	Reference
Pump flow rate Φ_{P0}	Φ_{P0} [E-3-3] and $\Delta\Phi_{P0}$ [E-3-9]: $\frac{\Delta\phi_{P0}(P)}{\phi_{P0}(P)} = 1\,\%$	GAW Report No. 268 (2021)
Pump temperature T_P	T_P; $\frac{\Delta T_P}{T_P} = 0.25\%$	GAW Report; No. 268 (2021)
Pump efficiency $\eta_P\,(P)$	$\eta_P(P)$ and $\Delta\eta_P(P)$ in Table 1: JMA-efficiency	Nakano and Morofuji (2023)
Absorption efficiency η_A	$\eta_A = 1.00$ and $\Delta\eta_A = 0.01$	GAW Report No. 268 (2021)
Measured cell current $I_M(t)$	$\Delta I_M(t) = \pm\,0.005$ µA. at $I_M(t) < 1.00$µA $\Delta I_M(t) = \pm\,0.5\%$ of $I_M(t)$ at $I_M(t) > 1.00$µA	GAW Report No. 268 (2021)
Background current I_{B0}	$I_{B0} = 0$ to 0.03 µA and $\Delta I_{B0} = 0.01$ µA	GAW Report No. 268 (2021)
Slow cell current $I_S(t)$	Different sonde type and SST: $\Delta I_S(t) = \frac{\Delta S_S(t)}{S_S(t)} \cdot I_S(t)$ from Eq. (21) S_S and ΔS_S from Table 2 [*]	This study
Fast cell current $I_F(t)$	$I_F(t)$ from Eq. (7) and $\frac{\Delta I_F}{I_F}$ from Eq. (20)	This study
Conversion efficiency $\eta_C\,(P)$	Different sonde type and SST: $\eta_C(P)$ from Table 3 and $\frac{\Delta\eta_C(P)}{\eta_C(P)}$ from Eq. (22) $\cong 2\%$	This study
Partial pressure ozone by OPM: $P_{O3,\,OPM}$	$\Delta P_{O3,\,OPM}$: 2 % at $P > 10$ hPa 2 % to 3 % at P from 10 hPa to 5 hPa	This study

1072
1073
1074 In both the mid-latitude and tropical case (Fig. 11) it is seen that the ("background") current in the troposphere and the

1075 conversion efficiency in the stratosphere are the dominant uncertainty sources. For the conventional method the conversion

1076 efficiency assumes that the overall stoichiometry factor is 1.00 with an uncertainty of 0.03 (Dietz et al. 1973), and obviously

1077 also the dominant uncertainty source in the stratosphere. However, in this study we have shown that the overall stoichiometry

1078 can significantly differ from unity, which makes the overall uncertainty for the conventional method rather optimistic. For the

1079 TRCC-method $\Delta\eta_C(P)$ is mostly determined by the 2-3% uncertainty of the OPM as the reference to obtain the $\eta_C(P)$

1080 calibration functions (Table 4). In the troposphere, the contribution of I_S correction in the TRCC method is mostly smaller than

1081 the I_{B1} correction in the conventional method, particularly in the tropics.

35
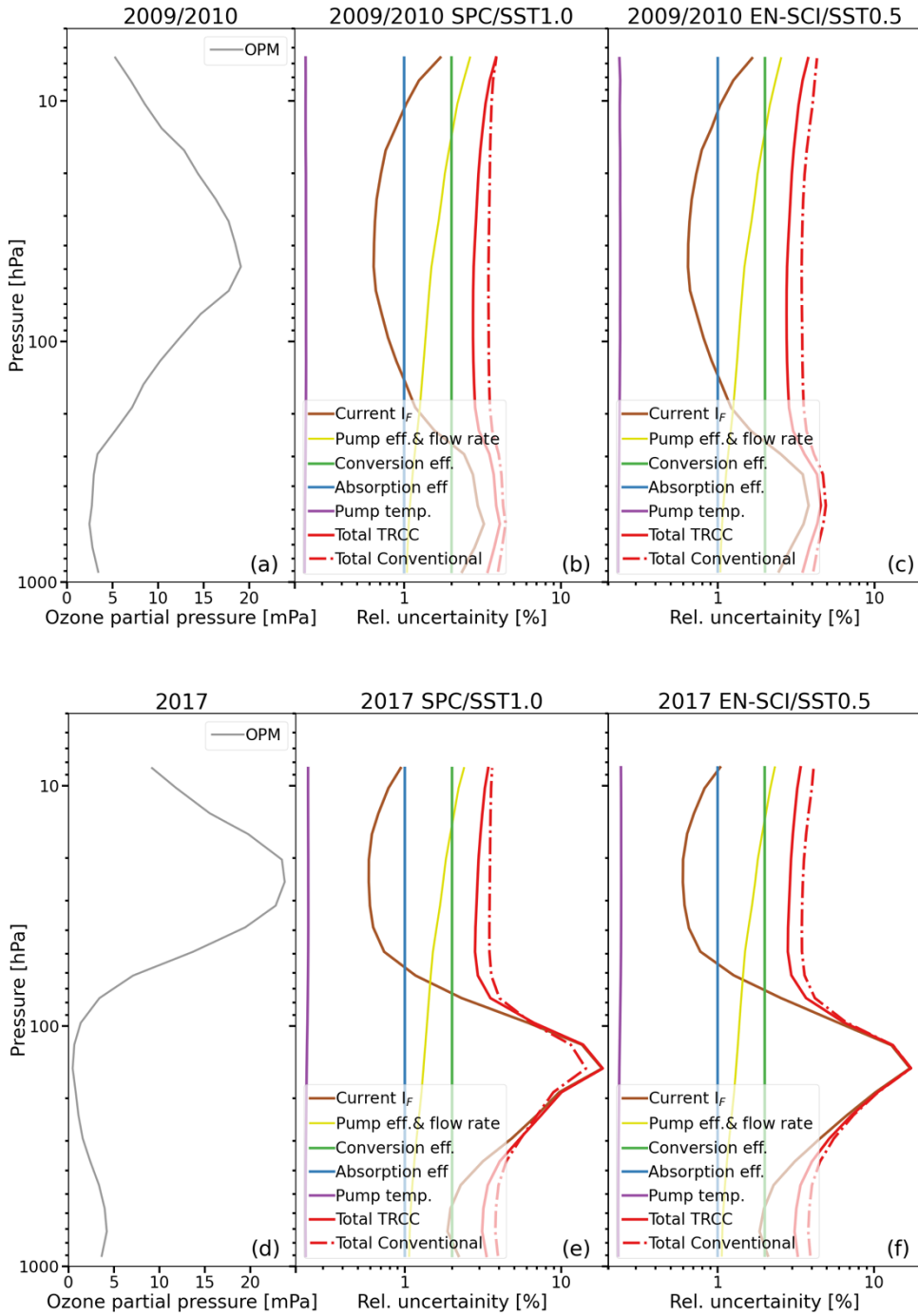
Figure 11. Uncertainty budgets of a mid-latitude (diagrams a, b, c: JOSIE 2009/2010) and tropical (diagrams (d), €, (f): JOSIE 2017) ozonesonde profile, showing the influence of the different uncertainty source terms listed in Table 5 for the TRCC method for SPC/SST1.0 (diagrams (b) and €) and EN-SCI/SST0.5 (diagrams (c) and (f)). Total uncertainty (red solid line) consists of (i) Corrected cell current (brown line: ΔI_{FDS} (TRC)); (ii) Pump efficiency & flow rate (yellow line: $\Delta\eta_c(P)$ & $\Delta\Phi_{P0}$); (iii) Absorption efficiency (blue line: $\Delta\eta_A$,); (iv) Conversion efficiency (green line: $\Delta\eta_c(P)$); (v) Pump temperature (purple line: ΔT_P). In addition, the total uncertainty of the conventional method is shown by the dashed red line.

However, both their contributions to the uncertainty are of the order of 0.01-0.02 μA, but on a relative scale they become strongly dependent on the magnitude of the ozone partial pressures, particularly in the upper tropical troposphere. In the stratosphere the contributions of the different uncertainties do not vary much, and the overall uncertainty stays well below 5%.

It is to be noted that in the remote Tropics in the upper troposphere the partial pressure of ozone P_{O3} can be very low of the order of 0.1-0.3 mPa while the detection limit of the ECC-sensor is of the order of 0.01-0.02 μA, which corresponds to ozone levels of about 0.04-0.08 mPa. It is obvious that at these very low ozone levels the ECC-sonde performance is strongly determined by its detection limit, which of course can have a significant and large impact on the overall uncertainty of the P_{O3} ozonesonde measurements.

7. Implementation of the TRCC Into Field Operation

A detailed procedure for applying the TRCC method in practice is described in Appendix C. In this section, we apply the methodology developed in the previous sections to ozonesonde profile data from three different stations: (i) a mid-latitude site (Uccle); (ii) a tropical station (American Samoa), and (iii) an ozone hole profile from the South Pole station in the Antarctic. At those sites, we selected ascent and the corresponding descent profiles, such that the methodology to resolve time response effects in the ECC signal can be assessed by comparing the ascent and descent profile of the same flight.

For the ozonesonde profiles of the three stations, we first determined the slow component $I_S(t)$ by convolution of the measured cell current $I_M(t)$ with an exponential decay with a time constant $\tau_S = 25$ minutes (Eq. 10) and conversion efficiencies $S_S = 0.018$ for SST0.5 (Uccle) and $S_S = 0.023$ for SST0.1 (Samoa & South Pole). For the I_S at time t = 0 of the launch, (i) zero is used at Uccle, as the last exposure to ozone usually occurs at least one hour prior to launch and the measured value will fall back to I_{B0}, and (ii) we use I_{B1}-I_{B0} multiplied by the exponential decay factor $X_S = \text{Exp}[-\Delta t/\tau_s]$, for the other two stations, with $\tau_s = 25$ min and $\Delta t = 30$ min (South Pole) and 90 min (Samoa). Those time intervals are the typical time differences between the I_{B1} measurement and launch time at those sites. This slow component is then subtracted from the measured cell current I_M, together with the background current I_{B0}. The remaining signal is the fast component, which is deconvolved to correct for the fast time response τ_F. For this latter, the time lag measurements before launch at the stations (e.g. time to drop from 4 to 1.5 μA) are taken. The smoothing of $I_{F,D}$ is done by applying a Gaussian filter prior to the time lag correction using a width equal to 20% of the fast time lag constant (as in Vömel et al., 2020). The final currents are then converted to ozone partial pressures using the calibration functions in Table 4 as conversion efficiency, taking the Nakano and Morofuji (2023) true pump efficiency correction factors into account, correcting the pump temperature and the pump flow rates as in GAW#268 (2021). For the conventional method, the GAW recommendations have been followed rigorously, instead of subtracting I_{B0} (Uccle) and I_{B2} (Samoa and South Pole) as background currents.

In Fig. 12, the profiles corrected with the conventional method are on the left side, while the implementation of the TRCC on the profiles is shown on the right side. It should immediately strike the eye that the agreement between the ascent and descent profiles is much improved after applying in particular the fast time response deconvolution with the new method, and this for the three different sites. But also the profile shape, e.g. around the ozone peak maximum at the Uccle and Samoa profiles, corresponds much better with each other for the ascent and descent profiles for the new method. The slow time response correction contributes to a certain extent as well to this better profile shape agreement.
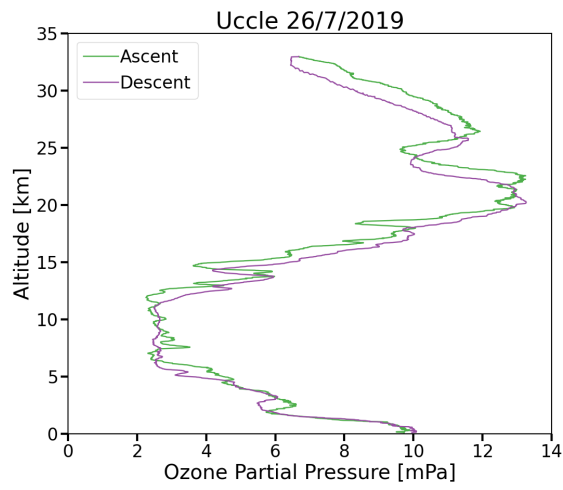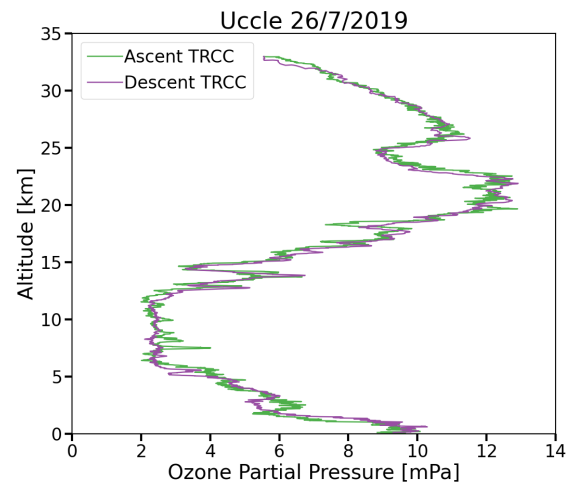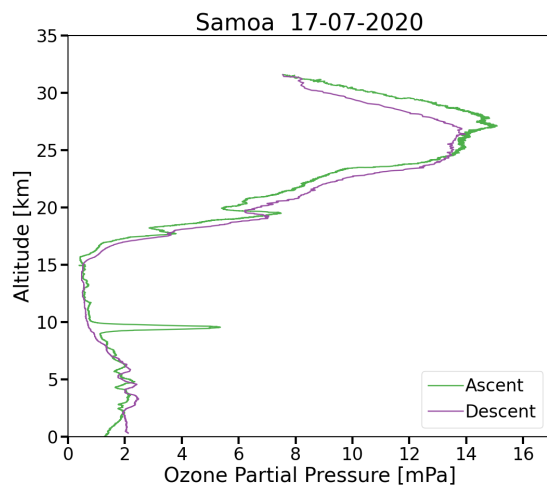
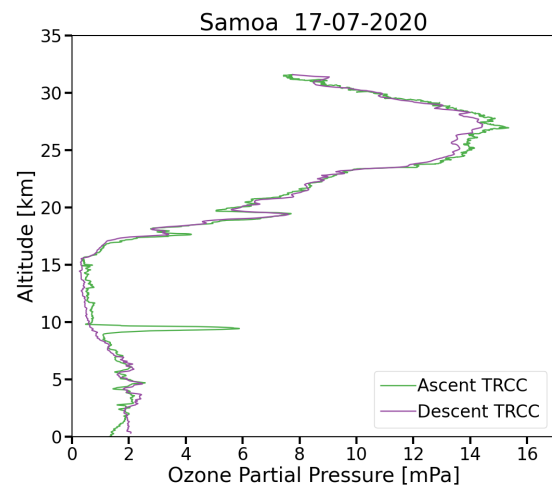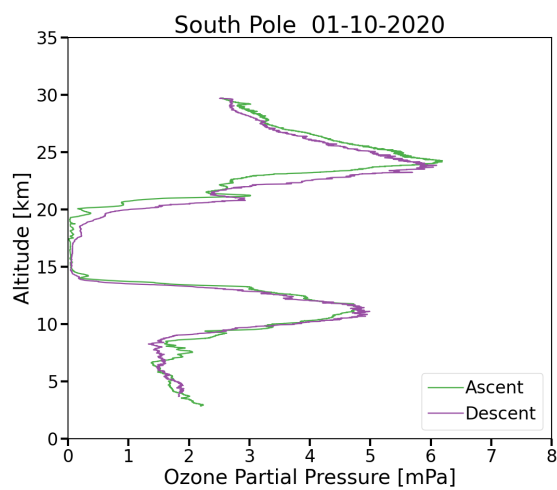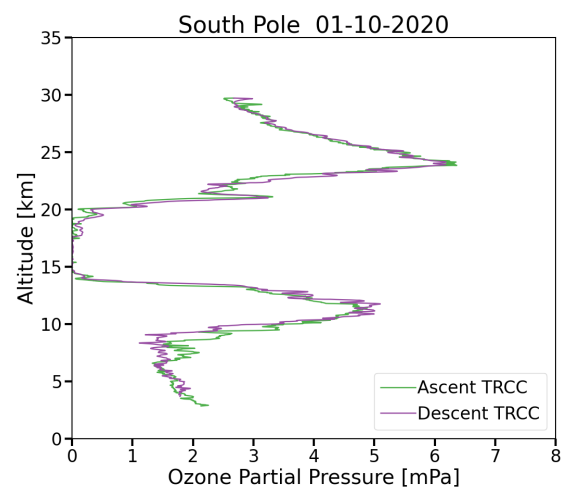**Figure 12.** Comparison of vertical ozone profiles obtained during ascent (green solid line) and descent (purple solid line) at three different ozonesounding stations (Uccle, Samoa, and South Pole) by applying once the conventional method (left diagrams (a), (c), (e)) and the TRCC method (right diagrams (b), (d), (f)).

A nice illustration of the impact of the slow time response correction is also found in the upper troposphere of the Samoa ozone profile. The upper tropospheric ozone concentrations are significantly decreased in both the ascent and descent profiles after applying this correction, while still agreeing very well. The strong reduction of upper-tropospheric ozone concentrations can be ascribed to correct for previous exposure to relatively high ozone amounts from the lower troposphere plus the (artificial) ozone spike for the ascent profile and from the ozone maximum for the descent profile.

The TRCC figures are remarkable in amplifying the features after correcting for the fast time constant. We already observed that the TRCC method is able to resolve some features in the ozonesonde data that were effectively present in the (faster) OPM ozone measurements in the JOSIE simulations. As mentioned by Vömel et al. (2020), the noise amplitude of the fast response time-lag-corrected data is comparable to that of the original data, but its spectral characteristics are different because of the smoothing algorithm. As a result, individual data points are heavily influenced by the noise characteristics of the smoothed data. This is demonstrated by the ozone spike in the Samoa ascent, which has a larger peak amplitude for the TRCC method.

8. Summary and Conclusions

The ECC ozonesonde, in principle an absolute measuring device, encounters in the course of its flight several imperfections, e.g. changing pump and conversion efficiency, that need to be corrected for. In the actual processing chain, the used "empirical effective efficiency" tables (Komhyr 1986, Komhyr et al., 1995) in fact represent an overall correction, empirically tweaked to coincident total ozone measurements, that includes both a measured pump flow efficiency and an estimate of the stoichiometry increase over the flight (GAW Report No.268, 2021). However, the availability of recent measured true ECC pump flow efficiencies (Nakano & Morofuji, 2023), confirming earlier measurements, together with the knowledge that the ECC sonde response (chemical reactions pathways) is driven by a slow and fast component (Vömel et al., 2020, Tarasick et al., 2021), call for a new approach. Vömel et al. (2020) also questioned the term "background current" in the ECC processing.

This study describes the concepts and the development of an updated methodology of ECC sonde data processing that applies a better correction of the ozone exposure dependent stoichiometry of the O_3+KI titration reaction in the electrochemical cell of the ECC-sonde using true pump efficiencies combined with resolving the time responses of the slow ($\cong 25$ min) and fast ($\cong 20$-25 sec) components of the measured ECC-ozone sensor current. Experimental evidence is given to treat the measured ECC-sensor current as the superposition of a (i) dominant fast ozone current I_F ; (ii) slow time-variant, past ozone-exposure dependent, current I_S ; (iii) a constant ozone-independent background current I_{B0} .

The Time Responses Correction plus Calibration (TRCC) method developed here is briefly described in three steps:

    I.   The slow cell current component as a function of flight time is determined from the measured ozone sensor current, after correction for the constant background current I_{B0}, by using a first order numerical convolution scheme (Eq. (10). Hereby, the in-flight time response tests of JOSIE 2009/2010 have been used to quantify the stoichiometry (O_3/I_2) factors S_S (and their uncertainties) of the slow reaction pathways for both sonde types, SPC and EN-SCI, and two different sensing solution types, SST0.5 and SST1.0. In separate laboratory upward and downward response time experiments S_S and ΔS_S of the low buffered combination of EN-SCI with SST0.1 have been determined using the same approach as in JOSIE 2009/2010 (see Appendix B). Depending on the buffer strength the slow current

typically amounts to about 1-4% of measured cell current I_M for SST0.5 or SST0.1 and about 2-8% for SST1.0. However, in regions with very low ozone it can reach up to 10-15 %.

II.   By subtracting the constant background current before exposure of ozone (I_{B0}) and the time variant slow sensor current I_S from the measured ECC-sensor current I_M, the remaining fast sensor current I_F has been resolved from the 20-30 sec. time response by using a first order deconvolution scheme (Eq. 12). Essential for this procedure is that the resulting deconvolved fast current $I_{F,D}$ has to be smoothed adequately to eliminate high frequency noise.

III.   From $I_{F,D,S}$ and using the correct true pump efficiencies (Table 1: Nakano and Morofuji, 2023) the partial pressure of ozone measured by the ECC-sonde is determined (Eq. 6). Additionally, using the conversion efficiency in Table 4 ("calibration functions"), the ozonesonde measurement is referred to the reference of the ozonesonde network, i.e. the photometer in the simulation chamber of the WCCOS in Jülich

Because the numerical convolution scheme used here is a recursive expression, the initial condition of I_S at the launch carries the past ozone exposure of the pre-launch preparations. In laboratory experiments it was shown that after I_{B1} has been recorded during the pre-flight preparation I_S (t) will further decay exponentially at the slow time constant τ_S=25 min. By knowing the time span between recording of I_{B1} and turning-on the pump just before launch I_{B1} can be used to derive the initial value of I_S at the launch. Therefore, it is essential that during the pre-flight preparations both background currents before (I_{B0}) and after (I_{B1}) exposure of ozone are being recorded, including the timestamp at recording I_{B1} and activating the pump just before launch of the sonde. Similarly, our understanding of this slow time constant justifies the use of limiting values for I_{B0} and after I_{B1} in the operational preparation of ozone soundings (see GAW Report No. 268, 2021), with filters providing a good quality zero ozone air source.

The slow stoichiometry factor S_S of the slow background due to the conversion of O_3 into I_2 and their Mean Absolute Deviation (MAD)-uncertainties (Table 2) are each based on a statistically relevant number of samples. S_S depends on the different SSTs used (Table 2), but is not dependent on the sonde type, which indicates that the secondary reaction pathway is not responsible for the systematic 4-5 % relative differences between EN-SCI and SPC when operating with the same SST. However, a direct quantitative relation of the buffer strength and the magnitude of S_S only holds for the full buffered SST1.0 ($S_S \cong 0.046-0.050$) and the half-buffered SST0.5 ($S_S \cong 0.017-0.018$), but not for the low-1/10th buffered SST0.1 ($S_S \cong 0.023$). For SST0.1 significant lower S_S values might be expected, which might indicate that, in lower buffered sensing solutions, another competing chemical reaction scheme may occur that also produce free iodine at a 25-minute time scale and contributes to I_S. This may be the reason that for non-buffered or low-buffered sensing solutions I_{B1} values of 0.01-0.04 µA are still recorded.

S_S values reported in Table 2 are significantly smaller than the so-called "steady bias factor" values applied by Vömel et al. (2020), which are the overall excess stoichiometry derived from steady state experiments under ozone exposure (Vömel and Diaz, 2010). The difference may be explained by the overall excess stoichiometry originating from the secondary reaction pathway that only contributes partly to the slow I_S while the other part still contributes to the fast I_F (Appendix A). Further, in contrast to this study, Vömel et al. (2020) do not correct for I_{B0} before determining I_S and calculating I_F. These two different approaches in the methodology (e.g. I_{B0} subtraction and different stoichiometry factors S_s for the slow current I_S) will of course lead to different results when comparing the sondes to the OPM. To demonstrate the impact of these different assumptions between both correction schemes we have processed the JOSIE 2009/2010 and JOSIE 2017 according to the TRC-scheme used by Vömel et al. (2020). The comparisons are shown in the supplementary material in the figures S4 and S6 for JOSIE 2009/2010 and JOSIE 2017, respectively. The impact of subtracting I_{B0} is generally small and only significant in the upper troposphere in the Tropics, where including subtraction of I_{B0} leads to better agreement with the OPM. The

impact of larger S_S values for SST1.0 and SST0.5 will lower the differences to the OPM above 100 hPa, but there still remains a significant deviation from the OPM. In the upper troposphere, the larger S_S gives negative deviations, particularly in the Tropics.

Different JOSIE data sets (JOSIE 2009/2010, JOSIE 2017, and JOSIE 1996 + 1998 + 2000 + 2002) have been used to compare the relative differences of the sonde to the OPM obtained with the Time Responses Correction (TRC) versus the conventional methodology of post flight data processing (GAW Reports No. 201 and 268). Hereby, it is very important to mention that, in contrast to the conventional methodology, the relative differences obtained with TRC are almost independent of the ozone profile type (e.g. mid-latitude or tropical). In other words, the observed relative differences with TRC are independent of the past ozone exposure and increase only a few percent with altitude (or lower pressure). This is most pronounced in the tropical ozone profiles at 200-100 hPa pressure in the upper troposphere with very low ozone values and the steep vertical ozone gradient when entering the lower stratosphere. The typical systematic relative differences of 3-5% for the same sonde type but different SST1.0 or SST0.5 as observed since JOSIE 2000 are still preserved in the TRC.

The different behavior between JOSIE2009/2010 and JOSIE2017 in the relative differences of the TRC corrected sonde profiles with the OPM for pressures smaller than about 13 hPa is ascribed to different pump temperatures used for the mid-latitude and tropical profiles in the respective campaigns. During JOSIE2009/2010, the higher pump temperatures led to a higher boiling rate in this pressure range, confirmed by the higher solution weight losses.

The TRC mean relative differences of the sonde with the OPM show a strong consistency for the different pairs of sonde type and SST and can be therefore represented by a linear regression as a function of Log_{10} of the pressure. This linear regression can be interpreted as the calibration function for the conversion efficiency which is not quite equal to one (Eq. 18). The calibration functions introduced here for the various sonde-SST combinations, parameterized as a function of ambient air pressure in Table 4, are independent of the ozone exposure, and thus invariant to the measured ozone profile itself. The use of these calibration functions makes the global ozonesonde records traceable to one common standard, i.e. the OPM of the WCCOS. The origin of these calibration functions remains speculative, but there are some experimental indications that they are linked to the unknown stoichiometry of the fast chemical conversion of O_3 into I_2 and not caused by an underestimation of the slow cell current I_S. It is to be noted that the here reported calibration functions are directly linked to the average pump efficiency values from Nakano and Morofuji (2023) as in Table 1, however, if these pump efficiency values might change over time (see Nakano and Morofuji, 2023), the calibration functions must be adjusted accordingly.

The overall uncertainty of combining the TRC with the calibration functions (TRCC) is about 3-4 % throughout the entire ozone profile, except for the upper troposphere, where the overall uncertainty can increase up to 10% for very low ozone amounts, particularly in the tropics. The major uncertainty sources in the upper troposphere are the constant background current I_{B0} and the slow current I_S (i.e. S_S).

The TRCC have been tested in practice (practical guidelines in Appendix C) for three different vertical ozone profiles measured during ascent and descent at a mid-latitude site, a tropical station and during an ozone hole at the South Pole. The resolving power of the fast deconvolution numerical scheme is clearly demonstrated by removing the strong delay shift in the descent ozone profile compared with the ascent ozone profile before and after applying the TRCC. However, the examples also clearly demonstrate the importance of careful and proper smoothing of the deconvolved ozone profile. To apply the TRCC method to the time series of an ozonesonde site, a proper determination of I_{B0} and I_{B1} is required. Imperfect or defective zero ozone air filters might increase those background currents by several orders of magnitude, compromising the subtraction by the (too high) I_{B0} value throughout the entire profile and at the beginning of the profile due to the high

initial value for $I_S(t_0)$. Some more analysis is needed to formulate alternative approaches for these cases. As stated also by ASOPOS 2.0 (GAW Report No. 268) the use of proper gas filters to provide ozone free, dry and purified air in practice at the sounding site, is very essential in general, but also when applying the TRCC data processing.

An important outcome of this study is also that the contribution of the slow current I_S is not as large as previously thought (Vömel et al, 2020), because TRC demonstrates that the secondary pathway involving the buffer can also contribute to the fast stoichiometry factor to increase the fast current I_F so that the uncalibrated conversion efficiency exceeds one, which is most likely the case for SST1.0 and SST0.5. This in contrast to SST0.1, where the slow current has most likely a different chemical origin and not an additional contribution to I_F, so that the fast stoichiometry (i.e. conversion efficiency) does not exceed one and is even a few percent lower. The underlying chemical mechanisms remain speculative in some cases and the stoichiometry of the fast O_3+KI chemistry cannot be quantified explicitly but only expressed implicitly in the conversion efficiency with the introduction of calibration functions (Table 4). These calibration functions can improve the homogenization of long term ozonesonde records of the global network, making the data traceable to one ozone standard, the OPM at the WCCOS at Jülich (Germany). Our OPM reference values have been scaled up 1.23% compared to earlier JOSIE publications because of the revised UV ozone absorption cross-section at 254 nm (BIPM, 2022; Hodges et al., 2019). The latter adjustment is being introduced in the global ozone network in 2024/2025.

Finally, we list some specific recommendations for further research include:

1. Regular JOSIE-campaigns at WCCOS (Jülich, Germany) are essential to check the long-term stability of the calibration functions reported in this study (Table 4) and to guarantee the long-term traceability of global ozonesonde records to the OPM-standard.

2. More research is needed to understand the slow stoichiometry S_S factors in more detail, particularly for the low or no buffered sensing solutions for which the underlying chemical processes are not understood at all. A key question hereby is also the role of KBr in the sensing solutions. This should be in conjunction with understanding the differences observed between the methods to derive S_S from either a zero-ozone or ozone exposure time response experiment. Dedicated laboratory experiments in the WCCOS simulation chamber can accomplish this.

3. More detailed understanding of the chemical reaction mechanisms that are responsible for the fast and slow cell current response of the ECC-sensor, and their interaction. This should include determining the temperature dependency of the KI+O_3 chemistry.

4. Better knowledge of the time behaviour of the high background currents I_{B0} and I_{B1} that are often measured in practice at the sounding sites when not using proper gas filters. Experiments are necessary to describe and eventually correct for this high I_{B0} and I_{B1} caused by using inadequate gas filters. This is essential as re-processing ozonesonde records often goes hand in hand with correcting very high I_{B0} and I_{B1}.

This study did not solve the systematic 3-5% offsets in measured ozone concentrations between EN-SCI and SPC instruments when operating with the same SST. However, we showed that the S_S values are comparable for both sondes with the same SST, which means the differences are not caused by the slow chemistry. More research here is essential.

Both the TRCC and the conventional method are post-flight data processing methods that assume the following three basic QA criteria are met: (i) best operating practices at the ozone monitoring stations in the global network (GAW Report No. 268, 2021) ; (ii) high-quality balloon instruments (e.g. ozone and radiosondes) and ground equipment; (iii) well-trained operators at the sounding site. Even small imperfections in these QA criteria can result in significant degradation in the quality of recorded ozonesonde data, such as the recently observed sudden drop in the total column ozone (TCO) measurements of ozonsondes compared to other TCO-measuring instruments (e.g. satellites) (Stauffer et al., 2020). Neither

1305   the TRCC nor the conventional method can avoid these inconveniences. However, it highlights the future need for QA

1306   monitoring of ozonesonde data in quasi-real time and comparing it with satellite and ground based (e.g. Lidar or

1307   Dobson/Brewer) data to detect potential artifacts (e.g. Stauffer et al. 2022).

1308

Appendix A: KI + O3 Chemistry in Presence of Phosphate-Buffer (NBKI after Saltzman & Gilbert, 1959)

Iodometric determination of ozone and the underlying oxidation of iodide ion by ozone to liberate iodine has long been subject of controversy. The reaction of KI with O_3 may proceed through a variety of chemical pathways strongly depending on pH, KI and O_3 concentrations, whether or not in presence of a pH-buffer. In this study the focus is on the neutral buffered potassium iodide (NBKI) method and its application in the ECC-ozone sensor. Experimentally it was shown by several investigators (e.g. Saltzman and Gilbert, 1959; Flamm and Anderson, 1975) that iodate (IO_3^-) as intermediate can be excluded as long as ozone partial pressures in the air are well below 100 mPa. This makes it most likely that much of the behaviour of the ECC and its slow and fast sensor currents may be explained by the chemical reaction mechanisms for the NBKI and the impact of the phosphate buffer as postulated by Saltzman and Gilbert (1959). It was experimentally shown that the fast and slow reactions increase as KI concentrations increase, whereby the slow reactions increase with the buffer concentration. Buffered solutions with no KI show no evidence of gaseous O_3 uptake into the sensing solution, indicating that the additional reactions with O_3 are secondary reactions after the initial O_3 + KI reaction.

Primary reaction pathway:

(R1) $2KI + H_2O + O_3 \rightarrow 2KOH + I_2 + O_2$

In ion-notation:

(R2) $O_3 + 2H^+ + 2I^- \rightarrow O_2 + I_2 + H_2O$

Or in detail (postulated after Saltzman & Gilbert, 1959) :

(R3) $O_3 + I^- \rightarrow IO^- + O_2^*$ (fast)

(R4) $IO^- + I^- + 2H^+ \rightarrow I_2 + H_2O$ (fast, neutral/acid)

(R5) $O_2^* + M \rightarrow O_2 + M$ (fast)

Losses of IO-, i.e. I_2:

(R6) $IO^- + IO^- \rightarrow 2I^- + O_2$ (slow)
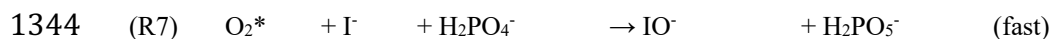
- If all O_3 would be absorbed and react with KI in this primary reaction pathway, it would be expected that the stoichiometry for O_3/IO- i.e. O_3/I_2 in neutral/acid solution is equal to one.
- However, self-reaction of IO^- (R6) can be a loss mechanism, competing with the formation of I_2 (R4).
- In general, loss mechanisms of IO^- might compete with (R4) and then the stoichiometry of the primary reaction pathway is less than one.
- ECC shows for 1% KI and no buffer a stoichiometry less than one (Johnson et al., 2002).
- Dismutation (disproportioning) of IO^- into iodate (IO_3^-) and I^- is extremely slow and is of no importance in case of the ECC-sensor. Iodate-chemistry plays first a role at significantly higher KI or O_3 concentrations than are used in the ECC-sensor or encountered in the atmosphere, respectively.

Secondary Reaction Pathway: Impact of Phosphate Buffer

(R7) $O_2^* + I^- + H_2PO_4^- \rightarrow IO^- + H_2PO_5^-$ (fast)

(R8) $H_2PO_5^- + I^- \rightarrow H_2PO_4^- + IO^-$ (slow)

(R4) $IO^- + I^- + 2H^+ \rightarrow I_2 + H_2O.$ (fast)

But also losses of I_2 iodine (via IO^- losses):

(R9) $H_2PO_5^- + IO^- \rightarrow H_2PO_4^- + I^- + O_2$ (slow)

(R6) $IO^- + IO^- \rightarrow 2I^- + O_2.$ (slow)

- R7 is the key reaction to form extra IO^- that can react via (R4) into I_2 and is contributing in addition to the fast reaction pathway and thus adding to the stoichiometry causing the fast ECC signal.

1352 • $H_2PO_5^-$ can be seen as the interim reactant that is formed fast but via (R8) decaying slowly to form extra IO^-. This latter

1353 can produce in addition extra I_2 which is causing the slow part of the ECC current.

1354 • It is known that $H_2PO_5^-$ reacts similar as H_2O_2 to form IO^-, i.e. I_2 with typical time constant of about 25 minutes: this fits

1355 to the slow, secondary response time of ECC of typical 25 minutes.

1356 **Appendix B: Laboratory Experiments to Determine S_s for EN-SCI SST0.1**

1357 As no time response tests are available during JOSIE campaigns for SST0.1 to determine S_S, we undertook laboratory

1358 measurements under room conditions in Uccle (Belgium). During the experiments, 4 ozonesondes were simultaneously

1359 exposed to ozone amounts generated by a photometric ozone calibrator Teledyne API T703 according to the following

1360 scheme (3 times): 30 minutes of exposure to a value of 450 $\mu g/m^3$ (around 225 ppb) ozone were preceded and succeeded by

1361 10 minutes of ozone-free air, see Fig. B1. The value of 450 $\mu g/m^3$ has been imposed by the upper limit (6.5 μA) of the

1362 microcurrent meters used in the Forschungszentrum Jülich homemade ground calibration box for the 4 ozonesondes. These

1363 microcurrents were read out digitally and, as in the JOSIE experiments, the S_S values were again estimated as the average

1364 over a 50 seconds time interval between 4 and 5 minutes after the end of the ozone exposure. As the time response test

1365 intervals in these laboratory measurements are twice as long (10 minutes) as in the JOSIE 2009/2010 campaigns, we tried

1366 different timings for the determination of the S_S values, but they did not give significantly different results for the slow

1367 stoichiometry coefficients. Again, the differences between the S_S values obtained from the different time response test

1368 intervals RT in one experiment were insignificant as well.
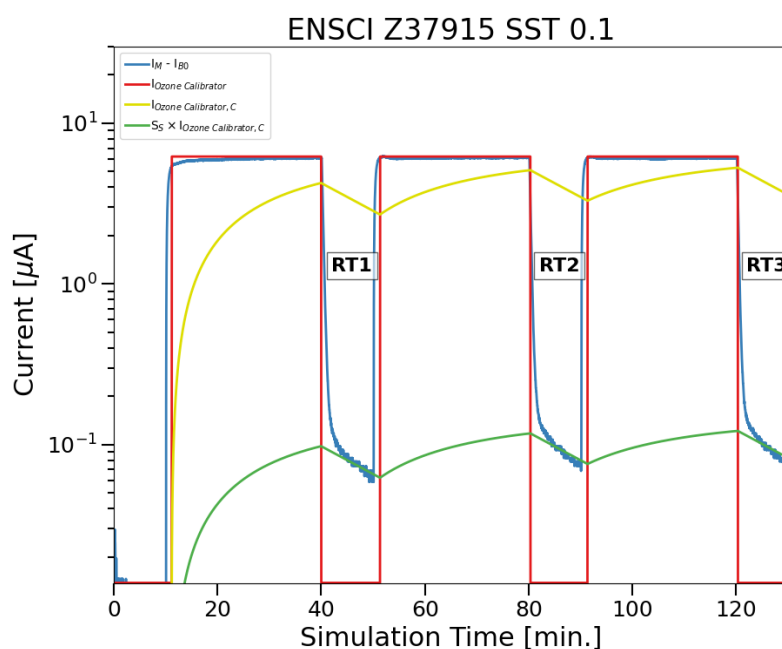
1369

1370 **Figure B1.** Example of a series of three upward and downward ozone steps generated by a photometric ozone calibrator

1371 Teledyne API T703 (represented by the generic $I_{Ozone\ Calibrator}$: red line) and the response of the measured cell current I_M-I_{B0}

1372 (blue line) of an EN-SCI SST01 ozonesonde as function of time, the 25 min convolved $I_{Ozone\ Calibrator,\ C}$ (yellow line) and the

1373 slow current after determination and application of S_S (S_S x $I_{Ozone\ Calibrator,\ C}$: green line).

1374

1375 In total, we have 8 S_S estimations with 4 EN-SCI ozonesondes filled with SST0.1 solutions coming from 3 different

1376 experiment runs: 2 runs with each 2 (new) EN-SCI ozonesondes (with SST0.1), and a run with all 4 (re-used) EN-SCI

1377 ozonesondes involved. These 4 ozonesondes, all with serial numbers Z379xxx, have been prepared by the same person,

1378 according to the SOPs defined in GAW Report No.268, 2021. The median value for S_S for the 8 experiments, each including

1379   three-time intervals, is 0.023 ± 0.005. This value is very close to the value S_S=0.017 found for SST0.5 during the JOSIE

1380   2009/2010 campaign, whereas a smaller value could be expected due to the lower buffer amount in SST0.1 (see Johnson et

1381   al., 2002 and Sect. 3.2). However, the same Uccle experimental setup and method as described here above for EN-SCI

1382   SST0.1 have been used to determine the S_S coefficient for 4 EN-SCI ozonesondes filled with SST0.5 (serial numbers

1383   Z379xxx, but different from those used with SST0.1) during two experimental runs. The resulting median value,

1384   0.022±0.004, is again in close agreement with the value determined for EN-SCI SST0.5 with the JOSIE 2009/2010 (0.018 ±

1385   0.004), confirming the consistency between the two instrumental setups to determine the stoichiometry coefficients.

1386   Nevertheless, a JOSIE campaign is foreseen in 2024 to determine the S_S factors for SST0.1 for both EN-SCI and SPC

1387   ozonesondes, using the same simulation setup as in JOSIE 2009/2010.

1388   **Appendix C: How to use TRCC in practice: Practical Guidelines**

1389   In this appendix, we give a schematic overview of the different steps that need to be taken to implement the TRCC in the

1390   data processing of an ozonesonde time series in practice, displayed schematically in the flow chart in Fig. C1.

1391
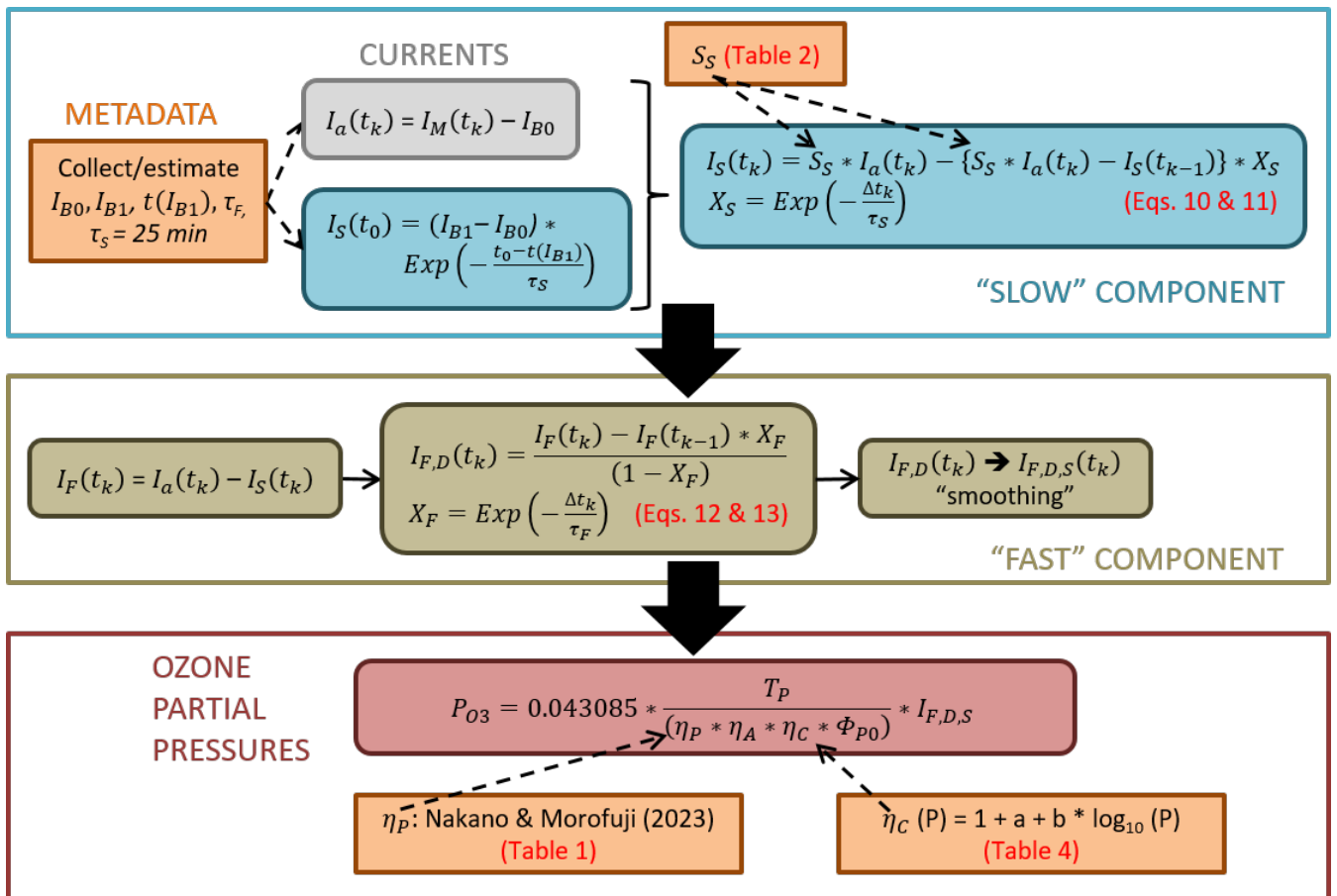
1392
1393
1394   **Figure C1.** Flow chart summarizing the processing steps for the Time Responses Correction & Calibration (TRCC) method

1395   for correcting ozonesonde data. The table and equation numbers in red refer to these in this paper.

1396

1397   First, it should be noted that the TRC is applied on the currents measured by the ozonesonde. Hence, these ozonesonde's raw

1398   measurements should be available. Normally, when a site has been homogenized as part of the O3S-DQA activity, the

1399   currents have been made available or have been converted back from the ozone partial pressures. Secondly, the TRCC

1400   demands the knowledge of some metadata parameters that should have been measured during the preparation of the

46

ozonesonde 0-1 day prior to launch (see also Fig. C1): I_{B0}, I_{B1}, the time of the I_{B1} measurement (relative to the launch time), and the sensor fast response time τ_F, measured as the time to drop from 4.0 to 1.5 μA (after the 5 μA test). If those metadata parameters are missing, these might be estimated as the means over a representative time period, e.g. using the same filter for determining the background currents, or the same batch of ozonesonde serial numbers or sensing solution for the fast response time.

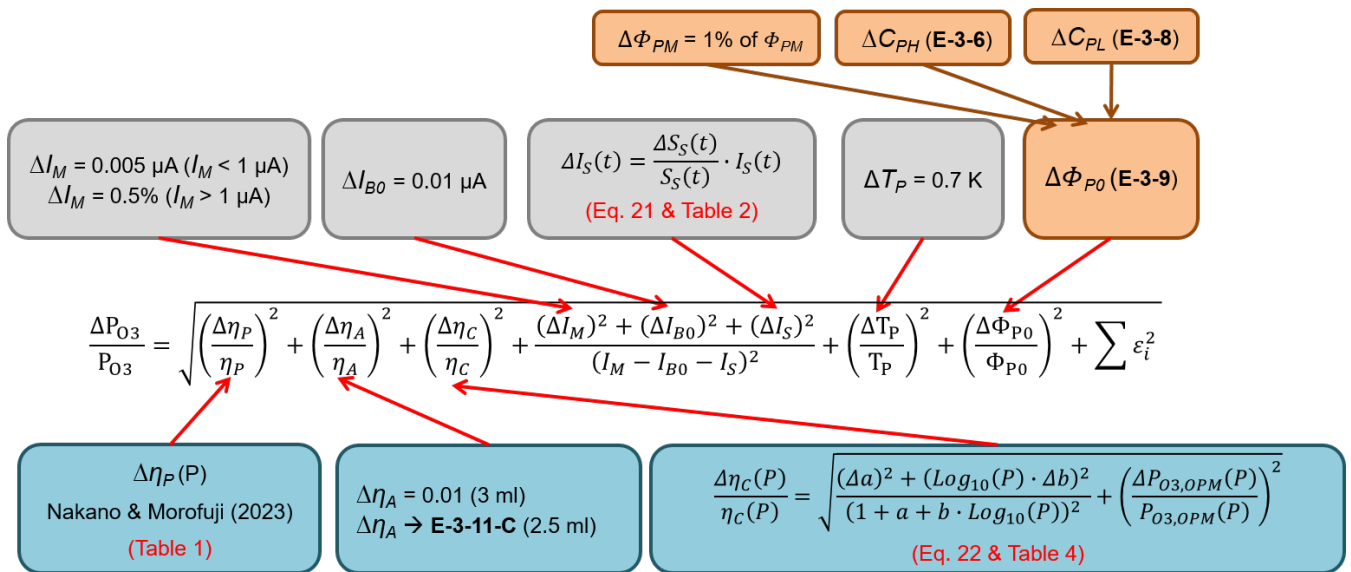In a next step, the I_{B0} value is subtracted from the time series of measured currents of the sounding, resulting in $I_a(t_k)$, and all forthcoming calculations should be done with those currents $I_a(t_k)$. As the calculation for obtaining the slow component of the ECC signal is a recursive equation (Eq. 10), the slow component at launch time should be estimated first. Therefore, it suffices to start from the last measured value of the ozonesonde before launch, the I_{B1}, corrected for (i.e. subtract) the I_{B0} value, and convolve it with an exponential decay function with a slow time constant of 25 minutes. Hereby, the time difference between the I_{B1} measurement and the launch is used. If this time difference is large enough (GAW Report No. 268) recommends a minimum 30-min time window), the exponential decay function will be close to zero, I_{B1} will approach the I_{B0} value, and the slow component at launch time will be zero, which is the allowed lower limit. Now, for every time step, the slow component of the ECC signal can be calculated from equations (10) and (11), using the stoichiometry factor S_S from the sonde–SST combination (see Table 2). This slow component can be seen as a time varying background current and should be subtracted from the currents $I_a(t_k)$, to be left over with the fast component I_F of the ECC signal.

To eliminate the 20 to 25 seconds response delay in the fast component, the latter can be deconvolved (Eqs. 12 and 13), i.e. corrected for the exponential decay of the signal with the fast sensor response time, measured before launch. This deconvolution will introduce a lot of noise in the signal, and therefore, a smoothing of the current, either before or after the deconvolution, will be necessary. Different smoothing algorithms can be considered, with different filter widths and/or time windows (e.g. for running averages). The choice of the smoothing algorithm depends on the application, e.g., to resolve steep vertical gradients, on the profiles (smooth mid-latitude vs. upper-tropospheric tropical profile), as well as on the measurement time interval (10 s versus 1s time resolution). At the end, a compromise between the smoothness of the profile and a full correction for the time response delay around strong vertical gradients should be sought.

The smoothed, deconvolved time series of the fast component $I_{F,D,S}$ of the ECC signal is then used in the basic equation of the ozonesonde signal, converting the current to ozone partial pressure. In this equation, the recommended corrections for T_P, η_A, and ϕ_{P0} in GAW Report No. 268 should be implemented as well: the conversion to the piston pump temperature [E-3-15], a correction for the absorption efficiency if the cathode cell was only filled with 2.5 cm^3 of solution before launch [E-3-11-A&B], and the humidification [E-3-4] and pump temperature [E-3-7] corrections for the pump flow rate at the ground. In comparison with the recommended processing in GAW Report No. 268, the true pump efficiency corrections proposed by Nakano & Morofuji (2023) should now be used for all combinations of sonde type and SSTs, as these are the actual measured ones. The Komhyr (1986) and Komhyr et al. (1995) tables should be discarded, as these are empirical effective efficiency curves, as they actually combine pump efficiency and conversion efficiency. A last difference with the conventional method as proposed in GAW Report No. 268 is the use of the "calibration functions" defined in Sect. 6, Eq. 18: $\eta_C(P) = 1 + a + b * log_{10}(P)$, with the coefficients a and b determined for every sonde type and SST combination separately (see Table 4), for the conversion efficiency, instead of adopting the value $\eta_C(P) = 1.00$. Using the calibration functions, the ozone sounding measurement should be traceable to the common reference of the ozonesonde network, the ozone photometer OPM in the simulation chamber of the World Calibration Centre for Ozonesondes in Jülich.

To calculate the uncertainties associated with the ozone partial pressure measurements of an ozonesonde, corrected with TRCC the uncertainty equation E-3-1 in GAW Report No. 268 (2021) forms the basis. With respect to this formula, the uncertainty equation for the TRC (see also Fig. C2) has one changed term, and the meaning of a couple other terms has changed. We will only describe these 3 terms here.

$$\frac{\Delta P_{O3}}{P_{O3}} = \sqrt{\left(\frac{\Delta\eta_P}{\eta_P}\right)^2 + \left(\frac{\Delta\eta_A}{\eta_A}\right)^2 + \left(\frac{\Delta\eta_C}{\eta_C}\right)^2 + \frac{(\Delta I_M)^2 + (\Delta I_{B0})^2 + (\Delta I_S)^2}{(I_M - I_{B0} - I_S)^2} + \left(\frac{\Delta T_P}{T_P}\right)^2 + \left(\frac{\Delta\Phi_{P0}}{\Phi_{P0}}\right)^2 + \sum \varepsilon_i^2}$$

Figure C2. Overview of the different data processing steps and input to derive the uncertainty of the ozone partial pressure measured with an ozonesonde, using the TRCC. Figure adapted from Fig. C-4 in GAW Report No. 268 (2021). The equation numbers also refer to equations in this GAW report. Table numbers in red refer to tables in the main text of this paper.

First, as both the I_{B0} and slow component I_S are subtracted from the measurement background in the TRC, the uncertainties of the I_{B0} and I_S should be included now. For I_{B0}, the uncertainty is estimated to be 0.01 μA, and the (relative) uncertainty of the slow component is, in a first order approximation, equal to the (relative) uncertainty of the stoichiometric coefficient S_S. The uncertainties of S_S for the different SSTs can be found in Table 2.

For TRCC, the uncertainties of the pump efficiencies $\Delta\eta_P$ (P) are now equal to the standard deviations of the true pump efficiency measurements reported in Nakano & Morofuji (2023), also shown in Table 1. Finally, the uncertainty of the conversion efficiency is no longer estimated as a fixed value $\Delta\eta_C$ $(P) = 0.03$, but should take into account the uncertainty of the derived calibration functions $\eta_C(P) = 1 + a + b * log_{10}(P)$ in Sect. 6 (see Table 4 for the uncertainties on the linear regression coefficients a and b for the different combinations of sonde type and SST), as well as the uncertainty of the photometer (OPM) to which the ozonesonde measurements are traced back. This latter (relative) uncertainty $\frac{\Delta P_{O3,OPM}(P)}{P_{O3,OPM}(P)}$ is estimated to be around 2%.

Appendix D: Nomenclature of parameters

1464	**Appendix D: Nomenclature of parameters**	
1465	I_{B0}	Background Current before exposure with ozone (after 10 min flushing cathode cell with "zero" air)
1466	I_{B1}	Background Current after exposure with ozone (after 10 min flushing cathode cell with "zero" air)
1467	I_{B2}	Background Current at launch site just before flight
1468	I_B	Background Current used in data processing in Eq. (1).
1469	I_M	Measured (cathode) cell current
1470	I_{OPM}	Ozone equivalent ECC current at time t derived from OPM
1471	I_F	Fast cell current
1472	$I_{F,D}$	Fast cell current, deconvolved
1473	$I_{F,D,S}$	Fast cell current, deconvolved, smoothed
1474	I_S	Slow cell current
1475	S_F	Stoichiometry factor of fast reaction pathway of conversion of O_3 into I_2
1476	S_S	Stoichiometry factor of slow reaction pathway of conversion of O_3 into I_2
1477	P_{O3}	Ozone partial pressure
1478	R	Universal gas constant
1479	F	Faraday constant
1480	T_P	Pump temperature
1481	Φ_{P0}	Pump flowrate
1482	η_A	Absorption efficiency
1483	η_P	Pump efficiency
1484	η_C	Conversion efficiency
1485	η_T	Total (overall) efficiency
1486	τ_F	Response time of fast reaction pathway of conversion of O_3 into fast cell current component
1487	τ_S	Response time of slow reaction pathway of conversion of O_3 into slow cell current component
1488	**RT1, RT2, RT3, RT4**	Response time tests in vertical ozone profile
1489		
1490		

Appendix D: Nomenclature of parameters

Line	Symbol	Definition
1465	I_{B0}	Background Current before exposure with ozone (after 10 min flushing cathode cell with "zero" air)
1466	I_{B1}	Background Current after exposure with ozone (after 10 min flushing cathode cell with "zero" air)
1467	I_{B2}	Background Current at launch site just before flight
1468	I_B	Background Current used in data processing in Eq. (1).
1469	I_M	Measured (cathode) cell current
1470	I_{OPM}	Ozone equivalent ECC current at time t derived from OPM
1471	I_F	Fast cell current
1472	$I_{F,D}$	Fast cell current, deconvolved
1473	$I_{F,D,S}$	Fast cell current, deconvolved, smoothed
1474	I_S	Slow cell current
1475	S_F	Stoichiometry factor of fast reaction pathway of conversion of O_3 into I_2
1476	S_S	Stoichiometry factor of slow reaction pathway of conversion of O_3 into I_2
1477	P_{O3}	Ozone partial pressure
1478	R	Universal gas constant
1479	F	Faraday constant
1480	T_P	Pump temperature
1481	Φ_{P0}	Pump flowrate
1482	η_A	Absorption efficiency
1483	η_P	Pump efficiency
1484	η_C	Conversion efficiency
1485	η_T	Total (overall) efficiency
1486	τ_F	Response time of fast reaction pathway of conversion of O_3 into fast cell current component
1487	τ_S	Response time of slow reaction pathway of conversion of O_3 into slow cell current component
1488	**RT1, RT2, RT3, RT4**	Response time tests in vertical ozone profile

Appendix E: List of Abbreviations

1491	**Appendix E: List of Abbreviations**	
1492	**ASOPOS**	Assessment of Standard Operating Procedures for OzoneSondes
1493	**BESOS**	Balloon Experiment on Standards for OzoneSondes
1494	**CMDL**	Climate Monitoring and Diagnostics Lab (formerly called GMD, now GML)
1495	**ECC**	Electrochemical Concentration Cell
1496	**EN-SCI**	Environmental Science Corporation; ECC ozonesonde manufacturer
1497	**ESRL**	Earth System Research Laboratories
1498	**FZJ**	ForschungsZentrum Jülich
1499	**GAW**	Global Atmosphere Watch
1500	**GML**	Global Monitoring Laboratory (division of NOAA's ESRL; formerly GMD)
1501	**H_2O_2**	Hydrogen peroxide
1502	**IAP**	Institute of Atmospheric Physics, Beijing, China
1503	IGACO	Integrated Global Atmospheric Chemistry Observations
1504	IOC	International Ozone Commission
1505	**IPCC**	Intergovernmental Panel on Climate Change
1506	**JMA**	Japanese Meteorological Agency
1507	**JOSIE**	Jülich OzoneSonde Intercomparison Experiment
1508	**KI**	Potassium Iodide
1509	**NASA**	National Aeronautics and Space Administration
1510	**NBKI**	Neutral-Buffered Potassium Iodide
1511	**NDACC**	Network for the Detection of Atmospheric Composition Change
1512	**NOAA**	National Oceanic and Atmospheric Administration
1513	**NO_x**	Nitrogen Oxides
1514	**O3S-DQA**	OzoneSonde-Data Quality Assessment
1515	**OPM**	Ozone PhotoMeter instrument (used as ozone UV-photometer reference at WCCOS)
1516	**SHADOZ**	Southern Hemisphere ADditional OZonesonde
1517	**SI^2N**	Ozone trend assessment study supported by SPARC, IOC, IGACO, and NDACC
1518	**SOP**	Standard Operating Procedure
1519	**SPARC**	Stratosphere-troposphere Processes And their Role in Climate
1520	**SPC**	Science Pump Corporation; ECC ozonesonde manufacturer
1521	**SST**	Sensing Solution Type
1522	**SST0.1**	1.0% KI & 1/10th buffer solution
1523	**SST0.5**	0.5% KI & half pH-buffer solution
1524	**SST1.0**	1.0% KI & full pH-buffer solution
1525	**SST2.0**	2.0% KI & non-pH-buffered solution with no KBr
1526	**STP**	Standard Temperature (=273.15 K) and Pressure (=1013.25 hPa) conditions
1527	**TOAR**	Tropospheric Ozone Assessment Report
1528	**TRC**	Time Responses Correction
1529	TRCC	TRC + Calibration
1530	**UNEP**	United Nations Environment Programme
1531	**UV**	Ultraviolet
1532	**UWYO**	University of Wyoming
1533	**VOC**	Volatile Organic Compound

1534   **WCCOS**   World Calibration Centre for OzoneSondes

1535   **WMO**   World Meteorological Organization

1536

1537

Code availability: All software code can be provided on request by Roeland Van Malderen.

Code and Data availability: All the JOSIE data used in this study is available at the WOUDC-data archive.
Note: DOI and https-link are both in preparation and will be available in course of Nov.2023 to be included in this publication).

Interactive computing environment: N/A.

Sample availability: N/A.

Video supplement: N/A.

Supplement link: *(will be included by Copernicus).*

Team list: N/A.

Author contribution: (i) the very first idea of resolving the slow and fast response times was proposed by DWT and the ASOPOS panel; (ii) the concept of this study was developed and worked out by HGJS and RVM; (iii) data processing by DP; (iv) data analysis by HGJS, RVM and DP; (v) preparation of the manuscript has been led by HGJS and RVM with the support of all co-authors. Data provision by HGJS (JOSIE campaign data) and RVM (Uccle-ground check and -laboratory data).

Competing interests: Roeland Van Malderen is a member of the editorial board of Atmospheric Measurement Techniques. The peer review process has been guided by an independent editor. The authors have no other competing interests to declare.

Disclaimer: N/A.

Special issue statement: Atmospheric ozone and related species in the early 2020s: latest results and trends (ACP/AMT inter-journal SI).

Review statement: This paper was edited by Birgit Hassler and reviewed by two anonymous referees.

References

Ancellet, G., Godin-Beekmann, S., Smit, H. G. J., Stauffer, R. M., Van Malderen, R., Bodichon, R., and Pazmiño, A.: Homogenization of the Observatoire de Haute Provence electrochemical concentration cell (ECC) ozonesonde data record: comparison with lidar and satellite observations, Atmos. Meas. Tech., 15, 3105–3120, https://doi.org/10.5194/amt-15-3105-2022, 2022.

BIPM, 2022: https://www.bipm.org/documents/20126/27085544/RapportBIPM-2022-02.pdf/f93def70-2544-ff13-ae63-3bc73f36688e .

Crutzen, P.J.: The influence of nitrogen oxides on the atmospheric ozone content, Quart. J. Roy. Met. Soc., 96, No. 408, 320–325, https://doi.org/10.1002/qj.49709640815, 1970.

Davies, J., McElroy, C.T., Tarasick, D.W., and Wardle, D.I.: Ozone capture efficiency in ECC ozonesondes: Measurements made in the laboratory and during balloon flights, EAE03-A-13703, in Geophysical Research Abstracts, Vol. 5, 13703, EGS-AGU-EUG Joint Assembly, Nice, France, 6–11 April 2003, 2003.

De Muer, D., & Malcorps, H.: The frequency response of an electrochemical ozone sonde and its application to the deconvolution of ozone profiles, J. Geophys. Res., 89, 1361–1372, 1984.

Deshler, T., Mercer J., Smit, H.G.J., Stübi, R., Levrat, G., Johnson, B.J., Oltmans, S.J., Kivi, R., Davies, J., Thompson, A.M., Witte, J., Schmidlin, F.J., Brothers, G., Sasaki, T.: Atmospheric comparison of electrochemical cell ozonesondes from different manufacturers, and with different cathode solution strengths: The Balloon Experiment on Standards for Ozonesondes, J. Geophys. Res., 113, D04307, https://doi.org/10.1029/2007JD008975, 2008.

Deshler, T., Stübi, R., Schmidlin, F. J., Mercer, J. L., Smit, H.G.J., Johnson, B.J., Kivi, R. and Nardi, B., 2017: Methods to homogenize ECC ozonesonde measurements across changes in sensing solution concentration or ozonesonde manufacturer, Atm. Meas. Tech., 10, 2012–2043, doi:10.5194/amt-10–2021–2017, 2017.

Dietz, R. N., Pruzansky, J., & Smith, J. D.: Effect of pH on the stoichiometry of the iodometric determination of ozone. Anal. Chem., 45, 402–404, 1973.

Farman, J.C., Gardener, B.G., and Shanklin, J.D.: Large Losses of total ozone in Antartica reveal seasonal ClOX/NOX interaction, Nature, 315, 207-210, 1985.

Garner, G. G., and Thompson, A. M.: Ensemble statistical post-processing of the National Air Quality Forecast Capability: Enhancing ozone forecasts in Baltimore, Maryland. Atmos. Environ., **81**, 517–522, doi:10.1016/j.atmosenv.2013.09.020, 2013.

GAW Report No. 104: Report of the Fourth WMO Meeting of Experts on the Quality Assurance/Science Activity Centres (QA/SACs) of the Global Atmosphere Watch, WMO Global Atmosphere Watch Report Series, No. 104, World Meteorological Organization, Geneva, 1995.

GAW Report No. 201, Smit, H.G.J., and the ASOPOS Panel: Quality Assurance and Quality Control for Ozonesonde Measurements in GAW, WMO Global Atmosphere Watch Report Series, No. 201, World Meteorological Organization, Geneva, [Available online at https://library.wmo.int/doc_num.php?explnum_id=7167], 2014.

GAW Report No. 268, Smit, H.G.J., Thompson, A.M., and the ASOPOS 2.0 Panel: Ozonesonde Measurement Principles and Best Operational Practices, WMO Global Atmosphere Watch Report Series, No. 268, World Meteorological Organization, Geneva, [Available online at https://library.wmo.int/doc_num.php?explnum_id=10884], 2021.

Haagen-Smit, A.J.: Chemistry and physiology of Los Angeles smog, Indust.Eng. Chem., 44, 1342-1346, 1952.

Hearn, A.G.: Absorption of ozone in ultraviolet and visible regions of spectrum, Proc. Phys. Soc., 78, 932–940, 1961.

Hodges, J.T., Viallon, J., Brewer, P.J., Drouin, B.J., Gorshelev, V., Janssen, C., Lee, S., Possolo, A., Smith, M.A.H., Walden, J., Wielgosz, R.I.: Recommendation of a consensus value of the ozone absorption cross-section at 253.65 nm based on a literature review, Metrologia. 56: 034001. https://iopscience.iop.org/article/10.1088/1681-7575/ab0bdd, 2019.

Huang, L.J., Chen, M.J., Lai, C.H., Hsu, H.T. and Lin, C.H.: New Data Processing Equation to Improve the Response Time of an Electrochemical Concentration Cell (ECC) Ozonesonde. *Aerosol Air Qual. Res.* 15: 935-944. https://doi.org/10.4209/aaqr.2014.05.0097, 2015.

Imai, K., Fujiwara, M., Inai, Y., Manago, N., Suzuki, M., Sano, T., Mitsuda, C., Naito, Y., Hasebe, F., Koide, T., Shiotani, M.: Comparison of ozone profiles between Superconducting Submillimeter-Wave Limb-Emission Sounder and worldwide ozonesonde measurements, *J. Geophys. Res. Atmos.*, 118, 12,755– 12,765, doi:10.1002/2013JD021094, 2013.

IPCC-Climate Change 2013: The Physical Science Basis. Contribution of Working Group I to the Fifth Assessment Report of the Intergovernmental Panel on Climate Change [Stocker, T.F., Qin, D. , Plattner, G.-K., Tignor, M., Allen, S.K., Boschung, J., Nauels, A., Xia, Y., Bex, V. and Midgley, P.M. (eds.)]. Cambridge University Press, Cambridge, United Kingdom and New York, NY, USA, 1535 pp, 2013.

IPCC-Climate Change 2021: The Physical Science Basis. Contribution of Working Group I to the Sixth Assessment Report of the Intergovernmental Panel on Climate Change [Masson-Delmotte, V., Zhai, P., Pirani, A., Connors, S.L., Péan, C., Berger, S., Caud, N., Chen, Y., Goldfarb, L., Gomis, M.I., Huang, M., Leitzell, K., Lonnoy, E., Matthews, J.B.R., Maycock, T.K., Waterfield, T., Yelekçi, O., Yu, R., and Zhou, B. (eds.)]. Cambridge University Press, Cambridge, United Kingdom and New York, NY, USA, In press, doi:10.1017/9781009157896, 2022.

Johnson, B.J., S.J. Oltmans, Vömel, H., Smit, H.G.J., Deshler, T. and Kroeger, C.: ECC Ozonesonde pump efficiency measurements and tests on the sensitivity to ozone of buffered and unbuffered ECC sensor cathode solutions, Journal of Geophysical Research, 107, D19, https://doi.org/10.1029/2001JD000557, 2002.

Komhyr, W.D.: Nonreactive gas sampling pump, Rev. Sci. Instr., 38, 981–983, 1967.

Komhyr, W.D.: Electrochemical concentration cells for gas analysis, Ann. Geoph., 25, 203–210, 1969

Komhyr, W.D. and T.B. Harris: Development of an ECC Ozonesonde, NOAA Technical Report, ERL 200-APCL 18, 1971.

Komhyr, W.D.: Operations handbook - Ozone measurements to 40 km altitude with model 4A-ECC ozone sondes, NOAA Technical Memorandum, ERL-ARL-149, 1986.

Komhyr, W.D., Barnes, R.A., Brothers, G.B., Lathrop, J.A. and Opperman, D.P.: Electrochemical concentration cell ozonesonde performance evaluation during STOIC 1989, J. Geophys. Res., 100, 9231–9244, 1995.

Lovelock, J.E., Maggs, R.J., Wade, R.J.: Halogenated Hydrocarbons in and over the Atlantic, Nature, 241, 194-196, https://doi.org/10.1038/241194a0, 1973.

Miloshevich, L. M., Paukkunen, A., Vomel, H., and Oltmans, S. J.: Development and validation of a time lag correction for Vaisala radiosonde humidity measurements, J. Atm. Ocean. Tech., 21, 1305-1327, 2004.

Mills, G, Pleijel, H., Malley, C.S., Sinha, B., Cooper, O.R., Schultz, M.G., Neufeld, H.S., Simpson, D., Sharps, K., Feng, Z., Gerosa, G., Harmens, H., Kobayashi, K., Saxena, P., Paoletti, E., Sinha, V. and Xu, X.: Tropospheric Ozone Assessment Report: Present-day tropospheric ozone distribution and trends relevant to vegetation. Elem Sci Anth, 6: 47. DOI: https://doi.org/10.1525/elementa.302, 2018.

Molina, M., Rowland, F. Stratospheric sink for chlorofluoromethanes: chlorine atom-catalysed destruction of ozone. Nature 249, 810–812, https://doi.org/10.1038/249810a0, 1974.

Nakano, T. and Morofuji, T.: Development of an automated pump-efficiency measuring system for ozonesondes utilizing an airbag-type flowmeter, Atm. Meas. Tech., 16, 1583–1595, https://doi.org/10.5194/amt-16-1583-2023, 2023.

Newton, R., Vaughan, G., Ricketts, H.M.A., Pan, L.L., Weinheimer, A. J. and Chemel, C., 2016: Ozonesonde profiles from the West Pacific Warm Pool: Measurements and validation, Atm. Chem. Phys., 619–634, doi:10.5194/acp-16–619–201, 2016.

Proffitt, M.H. and McLaughlin, R.J.: Fast response dual-beam UV-absorption photometer suitable for use on stratospheric balloons, Rev. Sci. Instr., 54, 1719–1728, 1983.

Reid, S.J., Vaughan, G., Marsh, A.R. and Smit, H.G.J.: Intercomparison of ozone measurements by ECC sondes and BENDIX chemiluminescent analyser, J. Atmos. Chem., 25, 215–226, 1996.

Saltzman, B.E. and Gilbert, N.: Iodometric micro-determination of organic oxidants and ozone, resolution of mixtures by kinetic colorimetry, Anal. Chem., 31, 1914–1920, 1959.

Seinfeld, J.H., Pandis, S.N.: Atmospheric Chemistry and Physics (From Air Pollution to Climate Change, 3rd Edition, 1152 pp., ISBN-13: 978-111894740, John Wiley and Sons, Inc., New York, 2016.

Smit, H.G.J., Sträter, W., Kley, D. and Profitt, M.H.: The evaluation of ECC ozonesondes under quasi flight conditions in the environmental simulation chamber at Jülich, in Proceedings of Eurotrac symposium 1994, edited by P.M. Borell et al., SPB Academic Publishing B.V., The Hague, The Netherlands, 349–353, 1994.

Smit H.G.J and Kley, D.: JOSIE: The 1996 WMO International Intercomparison of Ozonesondes Under Quasi Flight Conditions in the Environmental Simulation Chamber at Jülich, WMO Global Atmosphere Watch Report Series, No. 130, WMO/TD No. 926, World Meteorological Organization, Geneva, 1998.

Smit H.G.J., Sträter, W., Helten, M. and Kley, D.: Environmental Simulation Facility to Calibrate Airborne Ozone and Humidity Sensors. Jül Berichte, No. 3796, Forschungszentrum Jülich, 2000.

Smit, H.G.J.: Ozonesondes, in Encyclopedia of Atmospheric Sciences, Second Edition, edited by G.R. North, J.A. Pyle, and F. Zhang, Vol 1, pp. 372–378, Academic Press, London, 2014.

Smit, H.G.J., and Sträter, W.: JOSIE-1998, Performance of ECC Ozone Sondes of SPC-6A and ENSCI-Z Type, WMO Global Atmosphere Watch Report Series, No. 157, WMO/TD No. 1218, World Meteorological Organization, Geneva, 2004a.

Smit, H.G.J., and Sträter, W.: JOSIE-2000, Jülich Ozone Sonde Intercomparison Experiment 2000, The 2000 WMO International Intercomparison of Operating Procedures for ECC Ozonesondes at the Environmental Simulation Facility at Jülich, WMO Global Atmosphere Watch Report Series, No. 158, WMO TD No. 1225, World Meteorological Organization, Geneva, 2004b.

Smit, H.G.J.: Tropospheric Ozone as a Tracer to Investigate Deep Convection and its Influence on the Humidity in the Marine Tropics, PhD Thesis, University of Wuppertal, [on-line available: https://elekpub.bib.uni-wuppertal.de/ubwhsmig/content/titleinfo/3555358], 2004c.

Smit, H.G.J., Sträter, W., Johnson, B.J., Oltmans, S.J., Davies, J., Tarasick, D.W., Högger, B., Stübi, R., Schmidlin, F.J., Northam, T., Thompson, A.M., Witte, J.C., Boyd, I. and Posny, F.: Assessment of the performance of ECC ozonesondes under quasi-flight conditions in the environmental simulation chamber: Insights from the Jülich Ozone Sonde Intercomparison Experiment (JOSIE), Journal of Geophysical Research, 112, D19306, doi:10.1029/2006JD007308, 2007.

Smit, H.G.J., and O3S-DQA Panel: Guidelines for Homogenization of Ozonesonde Data, SI2N/O3S-DQA Activity as part of "Past Changes in the Vertical Distribution of Ozone Assessment", available at https://www.wccos-josie.org/en/o3s-dqa/, 2012.

Stauffer, R.M., Thompson, A.M., Kollonige, D.E., Tarasick, D.W., Van Malderen, R., Smit, H.G.J.: An examination of the recent stability of ozonesonde global network data. Earth and Space Science, 9, e2022EA002459. https://doi.org/10.1029/2022EA002459, 2022.

Steinbrecht W., Schwartz, R. and Claude, H.: New pump correction for the Brewer-Mast ozone sonde: Determination from experiment and instrument intercomparisons, J. Atm. Ocean. Tech., 15, 144–156, 1998.

Sterling, C.W., Johnson, B.J., Oltmans, S.J., Smit, H.G.J., Jordan, A.F., Cullis, P.D., Hall, E.G., Thompson, A.M. and Witte, J.C.: Homogenizing and estimating the uncertainty in NOAA's long-term vertical ozone profile records measured with the electrochemical concentration cell ozonesonde, Atm. Meas. Tech., 11, 3661–3687, https://doi.org/10.5194/amt-11–3661–2018, 2018.

Stolarski, R. S. and Cicerone, R. J.: Stratospheric Chlorine: a Possible Sink for Ozone, Can. J. Chem., 1610-1615, https://doi.org/10.1139/v74-233, 1974.

Tarasick, D.W., Jin, J.J., Fioletov, V.E., Liu, G., Thompson, A.M., Oltmans, S.J., Liu, J., Sioris, C.E., Liu, X., Cooper, O.R., Dann, T. and Thouret, V.: High-resolution tropospheric ozone fields for INTEX and ARCTAS from IONS ozonesondes, J. Geophys. Res., 115, D20301, https://doi.org/10.1029/2009JD012918, 2010.

Tarasick, D.W., Davies, J., Smit, H.G.J. and Oltmans, S.J.: A re-evaluated Canadian ozonesonde record: measurements of the vertical distribution of ozone over Canada from 1966 to 2013, Atm. Meas. Tech., 9, 195–214, doi:10.5194/amt-9–195–2016, 2016.

Tarasick, D., Galbally, I.E., Cooper, O.R., Schultz, M.G., Ancellet, G., Leblan, T., Wallington, T.J., Ziemke, J., Liu, X., Steinbacher, M., Staehelin, J., Vigouroux, C., Hannigan, J.W., García, O., Foret, G., Zanis, P., Weatherhead, E., Petropavlovskikh, I., Worden, H., Osman, M., Liu, J., Chang, K.-L., Gaudel, A., Lin, M., Granados-Muñoz, M., Thompson, A.M., Oltmans, S.J., Cuesta, J., Dufour, G., Thouret, V., Hassler, B., Trickl, T. and Neu, J.L.: Tropospheric Ozone Assessment Report: Tropospheric ozone from 1877 to 2016, observed levels, trends and uncertainties. Elementa: Science of the Anthropocene, 7:39. https://doi.org/10.1525/elementa.376, 2019.

Tarasick, D.W., Smit, H.G.J., Thompson, A.M., Morris, G.A., Witte, J.C., Davies, J., Nakano, T., Van Malderen, R., Stauffer, R.M., Deshler, T., Johnson, B.J., Stübi, R., Oltmans, S.J. and Vömel, H., 2021: Improving ECC ozonesonde data quality: Assessment of current methods and outstanding issues, Earth and Space Science, 8, e2019EA000914, https://doi.org/10.1029/2019EA000914, 2021.

Thompson, A.M.: The oxidizing capacity of the Earth's atmosphere: Probable past and future changes. Science, 256, 1157–1165, https://doi.org/10.1126/science.256.5060.1157 ,1992.

Thompson, A.M., Stone, J.B., Witte, J.C., Miller, S.K., Pierce, R.B., Chatfield, R.B., Oltmans, S.J., Cooper, O.R., Loucks, A.L., Taubman, B.F., Johnson, B.J., Joseph, E., Kucsera, T.L., Merrill, J.T., Morris, G.A., Hersey, S., Forbes, G., Newchurch, M.J., Schmidlin, F.J., Tarasick, D.W., Thouret, V. and Cammas, J.-P.: Intercontinental Chemical Transport Experiment Ozonesonde Network Study (IONS) 2004: 1 Summertime upper troposphere/lower stratosphere ozone over northeastern North America, J. Geophys. Res., 112, D12S12, doi:10.1029/2006JD007441, 2007a.

Thompson, A.M., Witte, J.C., Smit, H.G.J., Oltmans, S.J., Johnson, B.J., Kirchhoff, V.W.J.H. and Schmidlin, F.J.: Southern Hemisphere Additional Ozonesondes (SHADOZ) 1998–2004 tropical ozone climatology: 3. Instrumentation, station-to-

station variability, and evaluation with simulated flight profiles, J. Geophys. Res., 112, D03304, doi:10.1029/2005JD007042, 2007b.

Thompson, A.M., Oltmans, S.J., Tarasick, D.W., von der Gathen, P., Smit, H.G.J. and Witte, J.C.: Strategic ozone sounding networks: Review of design and accomplishments, Atm. Env., 45, 2145–2163, doi:10.1016/j.atmosenv.2010.05.002, 2011.

Thompson, A.M., Witte, J.C., Sterling, C., Jordan, A., Johnson, B.J., Oltmans, S.J., Fujiwara, M., Vömel, H., Allaart, M., Piters, A., Coetzee, G.J.R., Posny, F., Corrales, E., Andres Diaz, J., Félix, C., Komala, N., Lai, N., Maata, M., Mani, F., Zainal, Z., Ogino, S.-Y., Paredes, F., Luiz Bezerra Penha, T., da Silva, F.R., Sallons-Mitro, S., Selkirk, H.B., Schmidlin, F.J., Stübi, R. and Thiongo, K.: First reprocessing of Southern Hemisphere Additional Ozonesondes (SHADOZ) ozone profiles (1998–2016). 2. Comparisons with satellites and ground-based instruments, J. Geophys. Res., 122, https://doi.org/10.1002/2013JD019771, 2017.

Thompson, A.M., Smit, H.G.J., Witte, J.C., Stauffer, R.M., Johnson, B.J., Morris, G.A., von der Gathen, P., Van Malderen, R., Davies, J., Piters, A., Allaart, M., Posny, F., Kivi, R., Cullis, P., Nguyen T.H. Ahn, Corrales, E., Machinini, T., DaSilva, F.R., Paiman, G., Thiong'o, K., Zainal, A., Brothers, G.B., Wolff, K.R., Nakano, T., Stübi, R., Romanens, G., Coetzee, G.J.R., Diaz, J.A., Mitro, S., 'bt Mohamad, M. and Ogino, S.-Y.: Ozonesonde quality assurance: The JOSIE-SHADOZ (2017) experience, Bull. Amer. Met. Soc., 100, https://pubmed.ncbi.nlm.nih.gov/33005057/, 2019.

Thompson, A.M., Stauffer, R.M., Wargan, K., Witte, J.C., Kollonige, D.E., and Ziemke, J.R.: Regional and Seasonal Trends in Tropical Ozone From SHADOZ Profiles: Reference for Models and Satellite Products, J. Geophys. Res., 126, https://doi.org/10.1029/2021JD03469, 2021.

Thompson, A.M., Smit, H.G.J., Kollonige, D.E., Stauffer, R.M.: Ozonesondes: Instrumentation and Data Application, In: Field Measurements for Passive Environmental Remote Sensing (Ed. Nalli, N.R.), 458 pp., 1st Edition, ISBN 13- 978- 0128239537, Elsevier, Amsterdam, 2022.

Thornton, D.C., and Niazy, N.: Sources of background current in the ECC ozonesonde: Implication for total ozone measurements, J. Geophys. Res., 87, 8943–8950, 1982.

Thornton, D.C. and Niazy, N.: Effects of solution mass transport on the ECC ozonesonde background current, Geophys. Res. Lett., 10, 148–15, 1983.

UNEP-Ozone Secretariat, Handbook for the Montreal Protocol on Substances that Deplete the Ozone Layer, 14th Edition, ISBN: 978-9966-076-79-3, [on-line available https://ozone.unep.org/sites/default/files/Handbooks/MP-Handbook-2020-English.pdf], 2020.

Van Malderen, R., Allaart, M.A.F., De Backer, H., Smit, H.G.J., De Muer, D.: On instrumental errors and related correction strategies of ozonesondes: possible effect on calculated ozone trends for the nearby sites Uccle and De Bilt, Atm. Meas. Tech., 9, 3793–3816, doi:10.5194/amt-9–3793–2016/, 2016.

Vömel, H. and Diaz, K.: Ozone sonde cell current measurements and implications for observations of near-zero ozone concentrations in the tropical upper troposphere, Atm. Meas. Tech., 3, 495–505, doi:10.5194/amt-3–495–2010, http://www.atmos-meas-tech.net/3/495/2010/, 2010.

Vömel, H., Smit, H.G.J., Tarasick, D.W., Johnson, B.J., Oltmans, S.J., Selkirk, H.B., Thompson, A.M., Stauffer, R.M., Witte, J.C., Davies, J., Van Malderen, R., Morris, G.A., Nakano, T. and Stübi, R.: A new method to correct the ECC ozone sonde time response and its implications for "background current" and pump efficiency, Atm. Meas. Tech., 13, 5667–5680, https://amt.copernicus.org/articles/13/5667/2020/, 2020.

Wang, H. J. R., Damadeo, R., Flittner, D., Kramarova, N., Taha, G., Davis, S., Thompson, A.M., Strahan, S., Wang, Y., Froidevaux, L., Degenstein, D., Bourassa, A., Steinbrecht, W., Walker, K.A., Querel, R., Leblanc, T., Godin-Beekmann, S., Hurst, D., Hall, E.: Validation of SAGE III/ISS solar occultation ozone products with correlative satellite and ground based measurements, J. Geophys. Res., 125, e2020JD032430, https://doi.org/10.1029/2020JD032430, 2020.

Witte, J.C., Thompson, A.M., Smit, H.G.J., Fujiwara, M., Posny, F. , Coetzee, G.J.R., Northam, E.T., Johnson, B.J., Sterling, C.W., Mohamad, M., Ogino, S.-Y., Jordan, A. and da Silva, F.R.: First reprocessing of Southern Hemisphere Additional Ozonesondes (SHADOZ) profile records (1998–2015): 1. Methodology and evaluation, J. Geophys. Res., 122, 6611–6636, https://doi.org/10.1002/2016JD026403, 2017.

Witte, J.C., Thompson, A.M., Smit, H.G.J., Vömel, H., Posny, F. and Stübi, R.: First reprocessing of Southern Hemisphere Additional Ozonesondes profile records: 3. Uncertainty in ozone profile and total column. J. Geophys. Res., 123, 3243–3268. https://doi.org/10.1002/2017JD027791, 2018.

Witte, J.C., Thompson, A.M., Schmidlin, F.J., Northam, E.T., Wolff, K.R. and Brothers, G.B.: The NASA Wallops Flight Facility digital ozonesonde record: Reprocessing, uncertainties, and dual launches. J. Geophys. Res., 124, 3565–3582, doi:10.1029/2018JD030098, 2019.

WMO/UNEP: Scientific Assessment of Ozone Depletion: 2022, Ozone Research and Monitoring – GAW Report No. 278, World Meteorological Organization, Geneva, 2023.

Xu, X., Muller, R.P., Goddard, W.A.: The gas phase reaction of singlet dioxygen with water: A water-catalyzed mechanism, PNAS, 99 (6), 3376-3381, https://doi.org/10.1073/pnas.052710099, 2002.

Zhang, J., Xuan, Y., Yan, X., Liu, M., Tian, H., Xia, X., Pang, L. and Zheng, X.: Development and preliminary evaluation of a double-cell ozonesonde, Adv. Atm. Sci., 31, 938–947, 2014a.

Zhang, J.-Q., Xuan, Y.-J., Xia, X,-A, Liu, M.-Y., Yan, X.-L., Pang, L., Bai, Z.-X., and Wan, X.-W.: Performance evaluation of a self-developed ozonesonde and its application in an intensive observational campaign, Atm. Ocean. Sci. Lett., 7, 175–179, https://doi.org/10.3878/j.issn.1674-2834.13.0089, 2014b.